

Energy Research and Development Division  
FINAL PROJECT REPORT

**IMPROVING EFFICIENCY OF SPARK -  
IGNITED, STOICHIOMETRICALLY  
OPERATED NATURAL GAS ENGINES**

Prepared for: California Energy Commission  
Prepared by: Sturman Industries



MARCH 2013  
CEC-500-2013-103

**PREPARED BY:**

***Primary Author(s):***

Dan Giordano, Program Manager  
Marc Henderson, Development Engineer  
Jeff Rogers, Analysis Engineer  
Jeff Stewart, Controls Engineer  
Evelyn Vance, Analysis Engineer

Sturman Industries  
One Innovation Way  
Woodland Park, Colorado 80863

***Contract Number: PIR-08-023***

***Prepared for:***

**California Energy Commission**

Pablo Gutierrez  
***Contract Manager***

Linda Spiegel  
***Office Manager***  
***Energy Generation Research Office***

Laurie ten Hope  
***Deputy Director***  
***ENERGY RESEARCH AND DEVELOPMENT DIVISION***

Robert P. Oglesby  
***Executive Director***

**DISCLAIMER**

This report was prepared as the result of work sponsored by the California Energy Commission. It does not necessarily represent the views of the Energy Commission, its employees or the State of California. The Energy Commission, the State of California, its employees, contractors and subcontractors make no warranty, express or implied, and assume no legal liability for the information in this report; nor does any party represent that the uses of this information will not infringe upon privately owned rights. This report has not been approved or disapproved by the California Energy Commission nor has the California Energy Commission passed upon the accuracy or adequacy of the information in this report.

## PREFACE

The California Energy Commission Energy Research and Development Division supports public interest energy research and development that will help improve the quality of life in California by bringing environmentally safe, affordable, and reliable energy services and products to the marketplace.

The Energy Research and Development Division conducts public interest research, development, and demonstration (RD&D) projects to benefit California.

The Energy Research and Development Division strives to conduct the most promising public interest energy research by partnering with RD&D entities, including individuals, businesses, utilities, and public or private research institutions.

Energy Research and Development Division funding efforts are focused on the following RD&D program areas:

- Buildings End-Use Energy Efficiency
- Energy Innovations Small Grants
- Energy-Related Environmental Research
- Energy Systems Integration
- Environmentally Preferred Advanced Generation
- Industrial/Agricultural/Water End-Use Energy Efficiency
- Renewable Energy Technologies
- Transportation

*Improving Efficiency of Spark-Ignited, Stoichiometrically Operated Natural Gas Engines* is the final report for the Improving Efficiency Of Spark-Ignited, Stoichiometric Operated Natural Gas Engine project (Grant number PIR-08-023) conducted by Sturman Industries. The information from this project contributes to Energy Research and Development Division's Environmentally Preferred Advanced Generation Program.

For more information about the Energy Research and Development Division, please visit the Energy Commission's website at [www.energy.ca.gov/research/](http://www.energy.ca.gov/research/) or contact the Energy Commission at 916-327-1551.

## ABSTRACT

Applying digital hydraulic valve actuation to high-volume transportation engines offers the opportunity to meet strict emission and fuel consumption requirements in both mobility and stationary power applications without the need for dedicated and expensive mechanical engine systems. This system offers the potential to enhance engine operation through simple and cost-effective engine tuning. The engine selected for this program was an on-highway Cummins ISX15, rated at 298 kilowatts on diesel fuel. This engine used a mechanical valve train with bridged intake and exhaust valve components.

The application of a fully flexible engine valve train was necessary to realize the emission and thermal efficiency requirements of this project. This report documented the design, development, fabrication, and testing of a digital hydraulic valve actuation system for the Cummins ISX15 natural gas engine.

The digital hydraulic valve actuation system provided independent control of valve timing and duration combined with cylinder de-activation capability. Engine testing was conducted for both lug-line and 13-mode test cycles to determine the composite emission results for baseline and enhanced conditions. The test results showed improved efficiency by enhancing the valve train timing with a composite brake thermal efficiency result of 38.13 percent. In addition, the 13-mode composite emissions met the 2007 California Air Resources Board requirements with combined heat and power credit.

**Keywords:** Hydraulic valve actuation, camless, natural gas engine, Cummins ISX

Please use the following citation for this report:

Giordano, Dan; Henderson, Marc; Rogers, Jeff; Stewart, Jeff; Vance, Evelyn (Sturman Industries). 2013. *Improving Efficiency of Spark-Ignited, Stoichiometrically Operated Natural Gas Engines*. California Energy Commission. Publication number: CEC-500-2013-103.

# TABLE OF CONTENTS

PREFACE .....	i
ABSTRACT .....	ii
TABLE OF CONTENTS.....	iii
LIST OF FIGURES.....	vi
LIST OF TABLES .....	ix
<b>EXECUTIVE SUMMARY .....</b>	<b>1</b>
Purpose.....	1
Project Objectives .....	<b>Error! Bookmark not defined.</b>
Project Outcomes .....	2
Conclusions and Recommendations .....	<b>Error! Bookmark not defined.</b>
<b>CHAPTER 1: Introduction.....</b>	<b>5</b>
<b>CHAPTER 2: Overview of Modeling Approach .....</b>	<b>6</b>
2.1 Model Description.....	6
2.2 Engine Valve Profile Description.....	8
2.3 Model Results .....	10
2.3.1 Cylinder Model Validation.....	10
2.3.2 HVA-D Valve Motion versus System Supply Pressure .....	12
2.3.3 HVA-D System Performance at Specified Operating Conditions.....	16
2.3.4 HVA-D System Power Consumption .....	20
<b>CHAPTER 3: HVA-D Design Summary.....</b>	<b>22</b>
3.1 System Overview .....	22
3.2 HVA-D System Design.....	23
3.3 HVA-D System Structural Analysis .....	28
<b>CHAPTER 4: Hydraulic Supply System Design.....</b>	<b>31</b>
4.1 System Overview .....	31
4.2 Analytical Hydraulic Supply System Predictions .....	32
4.3 Hydraulic Pump Overview and Mounting.....	33

<b>CHAPTER 5: Controls Components Overview .....</b>	<b>35</b>
5.1 Interface Requirements .....	35
<b>CHAPTER 6: Fuel System Control for a Natural Gas Engine .....</b>	<b>37</b>
<b>CHAPTER 7: Hydraulic Valve Actuation (HVA) System Control for a Natural Gas Engine ..</b>	<b>39</b>
<b>CHAPTER 8: Engine Control of a Natural Gas Engine .....</b>	<b>41</b>
8.1 Overall Structure of the STEC Control Code .....	41
8.2 Periodic Functions.....	41
8.2.1 Throttle Control.....	43
8.2.2 Calibration Table Look-ups .....	43
8.2.3 Modifications to Intake Valve Close (IVC) Timing .....	44
8.2.4 Mass Airflow (MAF) Sensor processing .....	44
8.2.5 Fuel Enable determination.....	44
8.2.6 Piston Position Update .....	45
8.3 Synchronous Functions .....	45
8.4 Instructions to Operate the Code .....	46
<b>CHAPTER 9: HVA Components Overview and Validation.....</b>	<b>48</b>
9.1 HVA System Validation.....	48
9.2 HVA System Assembly .....	49
9.3 Single Valve Testing .....	52
9.4 Multi Cylinder Assembly.....	55
9.5 Multi Cylinder Testing .....	59
9.6 Multi Cylinder Validation Testing .....	60
<b>CHAPTER 10: Natural Gas System Components Bench Testing .....</b>	<b>63</b>
<b>CHAPTER 11: Dynamometer Test of Engine Platform .....</b>	<b>64</b>
11.1 Overview of Sturman Test Facility .....	64
11.1.1 Emissions Measurement Equipment.....	64
11.1.2 CNG Flow Measurement Equipment.....	65
11.1.3 Pressure and Temperature Measurement .....	65

11.2	Test Plan Overview .....	65
11.3	Discussion of CNG Quality .....	66
11.3.1	Background .....	66
11.3.2	Natural Gas Properties .....	67
11.4	Engine Hardware Modifications.....	69
11.4.1	Piston Design .....	69
11.5	Engine Start-up and System Validation.....	69
11.5.1	EGR System Improvements.....	71
11.6	Baseline Results (No Catalyst) .....	74
11.7	Baseline Results (With Catalyst) .....	78
11.8	Optimized Results (With Catalyst).....	79
11.8.1	Catalyst Sensitivity to Air/Fuel Ratio .....	82
11.8.2	Optimized Cylinder Pressure Coefficient of Variation.....	83
11.8.3	Effects of Late Intake Valve Closing.....	83
11.8.4	Optimized Idle Condition.....	88
11.8.5	Three Cylinder Operation at A25, B25, C25 .....	88
11.8.6	Optimized Comparison to Baseline.....	91
<b>CHAPTER 12: Conclusions and Recommendations.....</b>		<b>96</b>
12.1	Conclusions.....	96
12.2	Commercialization Potential .....	96
12.2.1	Regulatory and Institutional Factors.....	96
12.2.2	Required Business and Commercial Relationships.....	97
12.2.3	Economic Market Potential.....	98
12.3	Recommendations.....	98
12.4	Benefits to California .....	99
12.4.1	Background of California’s Energy Problem .....	99
12.4.2	Assumptions used in Calculations of Energy Savings .....	100
12.4.3	Expected Benefits (Energy and Savings to Ratepayers) .....	100

<b>GLOSSARY</b> .....	<b>101</b>
<b>Appendix A: Multi Cylinder Validation Test Results</b> .....	<b>A-1</b>
<b>Appendix B: Dyno Testing Cylinder Pressure &amp; Heat Release Results - Baseline</b> .....	<b>B-1</b>
<b>Appendix C: Dyno Testing Cylinder Pressure &amp; Heat Release Results - Optimized</b> .....	<b>C-1</b>
<b>Appendix D: Peripheral Data for Baseline and Optimized Tests</b> .....	<b>D-1</b>
<b>Appendix E: Optimization Sweep Results</b> .....	<b>E-1</b>

## **LIST OF FIGURES**

Figure 1: Cummins ISX15 at Sturman Facility .....	5
Figure 2: MATLAB/Simulink Dynamic Model of HVA-D System .....	7
Figure 3: Details of HVA-D Model in MATLAB/Simulink Dynamic Model .....	8
Figure 4: HVA-D Valve Profile Definition .....	9
Figure 5: Stock Camshaft Valve Profiles for Cummins ISX15 Engine .....	10
Figure 6: Measured and Predicted Cylinder Pressures for Peak Torque on Cummins ISX-15L Engine .....	11
Figure 7: Measured and Predicted Cylinder Pressures for the Rated Condition on Cummins ISX15 Engine .....	12
Figure 8: Predicted Max Lift Seating Velocity and Valve Seating Velocity for Both Exhaust and Intake Valves .....	14
Figure 9: Predicted Flank Velocities for Both Exhaust and Intake Valves .....	15
Figure 10: Predicted HVA-D Valve Profiles at Engine Idle Operating Conditions .....	17
Figure 11: Predicted HVA-D Valve Profiles at Low speed, 50% Load Operating Conditions .....	18
Figure 12: Predicted HVA-D Valve Profiles at Peak Torque Operating Conditions .....	18
Figure 13: Predicted HVA-D Valve Profiles at High Speed, Full Load Operating Conditions .....	19
Figure 14: Predicted HVA-D Valve Profiles at Rated Power Operating Conditions .....	19
Figure 15: Predicted HVA-D Valve Profiles at Max Speed Operating Conditions .....	20
Figure 16: Power Consumption of HVA-D System for 13 Mode Operating Points .....	21
Figure 17: Final Schematic of HVA System for Natural Gas Engine .....	22
Figure 18: ISX15 Head with HVA Packaging .....	24
Figure 19: HVA Packaging Overview .....	25
Figure 20: Baseline ISX15 Cylinder Head .....	25
Figure 21: ISX15 Head Modifications .....	26
Figure 22: Top View Single Cylinder Detail .....	27
Figure 23: HVA Actuator Module Overview .....	27
Figure 24: Hydraulic Rail FEA Overview .....	28
Figure 25: ISX15 Stock Engine Valve Tip FEA Overview .....	29
Figure 26: HVA Control Valve Bore Distortion .....	29
Figure 27: HVA Valve Housing Stress Analysis Results .....	30
Figure 28: Hydraulic Supply System Schematic .....	31
Figure 29: High Pressure Rail Transient Prediction .....	32

Figure 30: Back Pressure Rail Performance .....	33
Figure 31: Representative Hydraulic Pump Location (Front of Engine).....	34
Figure 32: Model of Hydraulic Pump Mounting.....	34
Figure 33: Electronics Interface Diagram for PIR-08-023.....	36
Figure 34: The Omnitek ECM-66A .....	37
Figure 35: Example: User Interface for the Omnitek Fuel Controller.....	38
Figure 36: Condor Controller (Shown with Lid Removed) .....	39
Figure 37: Condor’s SCALE User Interface (Typical) .....	40
Figure 38: STEC Controller (Shown with Lid Removed) .....	41
Figure 39: Illustration of the Top-Level Simulink Model in the Periodic Execution Unit Showing I/O for the Unit .....	42
Figure 40: Illustration of the Functional Level Model in the Periodic Unit Showing Many of the Algorithms Contained Within the Unit .....	43
Figure 41: Intake Valve Close Adjustment Algorithms.....	44
Figure 42: Preparation of CAN C Miscellaneous Data .....	45
Figure 43: Top Level Synchronous Control Model (Developed Outside of PIR-08-023).....	46
Figure 44: SCALE Help Table of Contents .....	47
Figure 45: HVA Actuator Modules.....	49
Figure 46: Valve Tip Protrusion Measurement Setup and Assembled Exhaust Module with Calibration Fixture.....	50
Figure 47: HVA Valve Position Sensor Calibration Example .....	51
Figure 48: Electronics Rack .....	51
Figure 49: Single Exhaust Valve Test Setup .....	52
Figure 50: Valve Motion of Single Exhaust Valve .....	53
Figure 51: Valve Motion of Single Intake Valve .....	53
Figure 52: Hydraulic Rail Assembly .....	55
Figure 53: Transfer Plate and Hydraulic Rail Assembly .....	56
Figure 54: Spark Plug Sleeves.....	57
Figure 55: Transfer Plate Assembly Installed.....	57
Figure 56: Head Assembly without Valve Cover.....	58
Figure 57: Head Assembled in Test Cell.....	58
Figure 58: Cylinder Head Assembly Bench Testing .....	59
Figure 59: Multi Cylinder Valve Traces Example.....	60
Figure 60: Multi Cylinder Processed Data Example .....	61
Figure 61: Multi Cylinder Cycle by Cycle Review .....	62
Figure 62: Natural Gas System Component Bench Testing .....	63
Figure 63: Sturman Industries' Dynamometer Facility.....	64
Figure 64: Methane Number vs. HHV for Various Natural Gas Sources around the World .....	67
Figure 65: Modified ISX vs. IPD Cast Piston.....	69
Figure 66: Engine During De-greening Process.....	70
Figure 67: Intake Configuration Comparison .....	72
Figure 68: Replacement Electronic Pressure Regulating Valve.....	73
Figure 69: Baseline Valve Trace Example (unthrottled) .....	75

Figure 70: Lug Line Comparison .....	76
Figure 71: Baseline Valve Trace Example .....	77
Figure 72: P-V Diagram for Throttled Operation at A25.....	81
Figure 72: P-V Diagram for Unthrottled Operation at A25.....	81
Figure 73: Sweep of Commanded Lambda at C50 Test Point .....	82
Figure 74: Omnitek Data for C50 Commanded Lambda Sweep.....	83
Figure 75: %COV vs. 13 Mode Test Point.....	83
Figure 76: Optimized Volumetric CR and Effective CR Based on IVC Seating Angle .....	85
Figure 77: 50% Heat Release Timing vs. 13 Mode Test Point .....	86
Figure 78: Cylinder Pressure Comparison at A50 Operating Condition .....	86
Figure 79: Heat Release Comparison at A50 Operating Condition .....	87
Figure 80: Effective Compression Ratio vs. 13 Mode Test Point Baseline and Optimized.....	87
Figure 81: Fuel Use Optimization at Idle.....	88
Figure 82: A25_3Cyl Valve Trace Example .....	89
Figure 83: A25_3Cyl Cylinder Pressure Example .....	89
Figure 84: Optimized BTE Summary .....	91
Figure 85: Optimized and Baseline 13-Mode BTE Comparison.....	92
Figure 86: 13-Mode Composite BTE Comparison .....	92
Figure 87: Optimized vs. Baseline BSFC Improvement.....	93
Figure 88: Throttle $\Delta P$ vs. BSFC Improvement.....	94
Figure 89: TP01 Cylinder 1 Overlay .....	A-1
Figure 90: TP01 Cylinder 2 Overlay .....	A-1
Figure 91: TP01 Cylinder 3 Overlay .....	A-1
Figure 92: TP01 Cylinder 4 Overlay .....	A-2
Figure 93: TP01 Cylinder 5 Overlay .....	A-2
Figure 94: TP01 Cylinder 6 Overlay .....	A-3
Figure 95: TP01 Cylinder 1 by Cycle .....	A-4
Figure 96: TP01 Cylinder 2 by Cycle .....	A-4
Figure 97: TP01 Cylinder 3 by Cycle .....	A-5
Figure 98: TP01 Cylinder 4 by Cycle .....	A-5
Figure 99: TP01 Cylinder 5 by Cycle .....	A-6
Figure 100: TP01 Cylinder 6 by Cycle .....	A-6
Figure 101: TP02 Cylinder 1 Overlay .....	A-7
Figure 102: TP02 Cylinder 2 Overlay .....	A-7
Figure 103: TP02 Cylinder 3 Overlay .....	A-8
Figure 104: TP02 Cylinder 4 Overlay .....	A-8
Figure 105: TP02 Cylinder 5 Overlay .....	A-9
Figure 106: TP02 Cylinder 6 Overlay .....	A-9
Figure 107: TP02 Cylinder 1 by Cycle .....	A-10
Figure 108: TP02 Cylinder 2 by Cycle .....	A-10
Figure 109: TP02 Cylinder 3 by Cycle .....	A-11
Figure 110: TP02 Cylinder 4 by Cycle .....	A-11
Figure 111: TP02 Cylinder 5 by Cycle .....	A-12

Figure 112: TP02 Cylinder 6 by Cycle .....	A-12
Figure 113: Baseline – Idle Test Point .....	B-1
Figure 114: Baseline - A25 Test Point .....	B-2
Figure 115: Baseline – A50 Test Point.....	B-3
Figure 116: Baseline – A75 Test Point.....	B-4
Figure 117: Baseline – A100 Test Point.....	B-5
Figure 118: Baseline - B25 Test Point .....	B-6
Figure 119: Baseline – B50 Test Point .....	B-7
Figure 120: Baseline – B75 Test Point .....	B-8
Figure 121: Baseline – B100 Test Point .....	B-9
Figure 122: Baseline - C25 Test Point.....	B-10
Figure 123: Baseline – C50 Test Point .....	B-11
Figure 124: Baseline – C75 Test Point .....	B-12
Figure 125: Baseline – C100 Test Point.....	B-13
Figure 126: Optimized – Idle Test Point .....	C-1
Figure 127: Optimized - A25 Test Point.....	C-2
Figure 128: Optimized – A50 Test Point .....	C-3
Figure 129: Optimized – A75 Test Point .....	C-4
Figure 130: Optimized – A100 Test Point .....	C-5
Figure 131: Optimized - B25 Test Point.....	C-6
Figure 132: Optimized – B50 Test Point.....	C-7
Figure 133: Optimized – B75 Test Point.....	C-8
Figure 134: Optimized – B100 Test Point.....	C-9
Figure 135: Optimized - C25 Test Point .....	C-10
Figure 136: Optimized – C50 Test Point .....	C-11
Figure 137: Optimized – C75 Test Point .....	C-12
Figure 138: Optimized – C100 Test Point .....	C-13
Figure 139: Peripheral Data for Baseline and Optimized Tests.....	D-1
Figure 140: Optimized (A25, B25, C25 3-Cylinder) BTE vs. Test Point .....	1
Figure 141: Optimized (A25, B25, C25 3-Cylinder) BSFC vs. Test Point.....	1
Figure 142: Optimized (A25, B25, C25 3-Cylinder) BSNOx vs. Test Point .....	1
Figure 143: Optimized (A25, B25, C25 3-Cylinder) BSCO vs. Test Point .....	2
Figure 144: Optimized (A25, B25, C25 3-Cylinder) BSNMHC vs. Test Point.....	2

## LIST OF TABLES

Table 1: Calculated Flank Velocities for Camshaft Valve Profiles for Cummins ISX15 Engine ...	15
Table 2: Engine Operating Conditions for HVA-D Dynamic Model Predictions.....	16
Table 3: Engine Operating Conditions for 13-Mode Points .....	21
Table 4: HVA System Validation Test Plan.....	48
Table 5: Simulated vs. Measured Exhaust Valve Flank Velocity .....	54
Table 6: Simulated vs. Measured Intake Valve Flank Velocity .....	55

Table 7: HVA System Validation Test Points Matrix.....	60
Table 8: Test Plan Overview .....	65
Table 9: Natural Gas Composition for Engine Testing.....	68
Table 10: Natural Gas Properties for Engine Testing.....	68
Table 11: Break-in Cycle for Cummins ISX engine .....	71
Table 12: Dyno Test Configuration Summary .....	73
Table 13: Predicted and Measured HVA Pump Power.....	74
Table 14: Emissions Limits for Exhaust Components.....	77
Table 15: Baseline 13-Mode Results (No Catalyst) .....	78
Table 16: Baseline 13-Mode Results (With Catalyst).....	79
Table 17: Optimized 13-Mode Results (6 Cylinder Operation) .....	80
Table 18: Effective Compression Ratio and Heat Release Results .....	84
Table 19: Optimized 13-Mode Results (3 Cylinder Operation at A25, B25, and C25).....	90
Table 20: 13-Mode Composite Comparison .....	95

# EXECUTIVE SUMMARY

## Introduction

California intends to install up to 4,000 megawatts (MW) of new power generating capacity over the next decade. Implementing distributed power generation is of great interest and is the only practical way to fully utilize the potential of combined heat and power (CHP) systems. Power generation at the point of use allows for the practical recovery of low quality waste heat for industrial processing, hot water, and space heating. CHP systems offer up to 80 percent overall efficiency, effectively doubling the efficiency of today's simple power generating units without heat recovery. Distributed power systems can be implemented at small as well as large scale using reciprocating piston internal combustion engines, which are large scale installations making use of multiple engines. By turning engines on and off in order to match supply and demand, peak efficiencies can be achieved nearly all of the time, avoiding the poor efficiencies associated with part load operation. Reciprocating piston engines are the most responsive power generating systems, making them ideally suited to respond to fluctuating loads and the intermittency of wind and solar generation.

## Project Purpose

The goal of this project was to use a fully flexible digital hydraulic valve actuation (HVA-D) system and closed-loop engine controls to improve the thermal efficiency of a spark-ignited, stoichiometric operated, heavy-duty, on-highway, natural gas engine for use in stationary power generation applications with or without CHP systems. The addition of hydraulic valve actuation differentiated this approach from other more standard techniques. Although a cam driven system may have some flexibility, the application of a fully flexible camless system allows improved adjustment for a larger range of fuel qualities as well as aggressive transient control. The valve actuation system should reduce pumping losses at light loads through an early intake valve closing or late intake valve closing (Miller cycle). It also had the ability to deactivate cylinders. This approach still allowed for a high expansion ratio to increase the engine efficiency. The effective compression ratio could be varied to account for different natural gas qualities using intake valve close timing instead of throttling, which resulted in improved engine efficiency. The camless system therefore allowed for effective compression ratio adjustments without increasing the pumping losses due to throttling.

The objectives of this project were to realize a flexible and common engine architecture that could maximize efficiency in both mobile and stationary applications. The engine would specifically run on natural gas. The intent was to demonstrate a natural gas engine for distributed energy resources that was compliant with California Air Resources Board (ARB) 2007 emissions standards while showing a peak engine brake thermal efficiency of better than 40 percent. This would be demonstrated during steady-state dynamometer testing utilizing a 13-mode composite test procedure. Implementation of a common platform lends itself to substantially reducing engine cost by taking advantage of higher production volumes. The improved engine efficiency combined with low emissions should increase the market

penetration of natural gas engines, improving air quality and reducing United States dependence on foreign oil.

## Project Results

The hydraulic valve actuation system was designed and implemented to meet the technical requirements of this project. The system provided independent control of each engine valve by using custom electro-hydraulic actuators. Each actuator provided valve duration and timing control along with deactivation potential. In addition, the system was designed to be installed on the head before final engine assembly. An engine mounted hydraulic supply system was also designed for this application. The supply system consisted of a hydraulic pump, regulators for pressure control, and rails necessary to capture the high and low pressure fluid for proper system operation. The hydraulic valve actuation system was packaged to be fully assembled off of the engine as a modular unit to allow direct installation on the engine short block.

Optimized 13-mode testing using late intake valve close timing with a mid-loaded three-way-catalyst and high pressure exhaust gas recirculation demonstrated compliance with ARB's 2007 emissions regulations using CHP credits. Optimized testing also showed two operating modes with greater than 40 percent brake thermal efficiency. Optimized test results showed brake specific fuel consumption improvements over the baseline ranging from two percent to 18 percent over the 13-mode test and a composite improvement of 4.8 percent. The baseline used for comparison consisted of the results obtained during throttled operation with this engine platform. These results included the losses associated with the hydraulic system and were obtained even though the natural gas supplied to the dynamometer facility was of low quality (low methane number). The composition of the natural gas supply was tested and used to calculate the methane number. The calculated methane number for the natural gas used in the engine was 67.7 and it had a lower heating value of 41.87 megajoules per kilogram (MJ/kg). This left the engine highly susceptible to engine knock with a static compression ratio of 14:1.

The lug line generated for this engine was slightly reduced compared to the diesel variant due to the knock limitation attributed to the low methane number natural gas and the temperature limitations of the variable geometry turbocharger.

This report documented the design of a digital hydraulic valve actuation (HVA) system for the Cummins ISX15 for use with natural gas. Analysis, simulation, and testing showed that the HVA system met the technical requirements for this project. The valve actuation system consisted of a single-lift actuator for each engine valve combined with a transfer plate and rail assembly. The modular design allowed the system to be installed on the head and tested before installation on the engine. In addition, the hydraulic simulation showed acceptable system response with an engine mounted pump.

Steady-state 13-mode testing showed excellent results for both engine efficiency and emissions with the available natural gas supply. Further testing should be conducted with various other compositions of natural gas.

The turbocharger included in the base engine limited the maximum lug line generated due to the turbine inlet temperature limit. Changing this unit to a waste gated version better matched to the setup would allow for improved lug line performance.

The high pressure exhaust gas recirculation system proved adequate for this project, but additional efficiency gains may be achieved by implementing a low pressure exhaust gas recirculation system. This would reduce pumping losses by lowering the exhaust backpressure that is required to drive high pressure exhaust gas as well as lower the intake charge temperature. This could also increase the knock limit threshold.

Cylinder deactivation showed efficiency gains for light engine loads and required further testing. Controls development was recommended to further explore transient operation and strategies for operation on varying qualities of natural gas for both optimized performance and knock mitigation. Some of this development might include cylinder-to-cylinder air/fuel ratio balancing as well as individual cylinder load control.

### **Project Benefits**

Using the hydraulic valve actuation system could result in reduced fuel consumption equaling 6.8 thousand cubic feet (MCF) per year or 205 billion MCF over the 30-year life of the engines. The reduction in fuel consumption could increase dramatically to 31 billion MCF per year and 914 billion MCF over 30 years if CHP systems are enabled by the distributed power approach. The reduction in fuel consumption triggered by the efficiency gains could also result in a fuel cost savings of \$27 billion per year and \$820 billion over 30 years (in today's dollars) for California's rate payers. In the context of CHP systems, the savings could increase substantially to \$122 billion per year or \$3.7 trillion over 30 years (in today's dollars.) In addition, the hydraulic valve actuation system could help to improve air quality and reduce United States dependence on foreign oil.



# CHAPTER 1: Introduction

The goal of this project was to use Sturman's fully flexible digital hydraulic valve actuation (HVA) system and closed-loop engine controls to improve the thermal efficiency of a spark-ignited stoichiometric (SIS<sub>t</sub>) operated, heavy-duty, on-highway, natural gas engine for use in stationary power generation applications with or without combined heat and power (CHP) systems. To meet this goal, a chemically correct combustion (stoichiometric) natural gas engine with exhaust gas recirculation (EGR) and a three way catalyst (TWC) was used. In addition, the application of a fully-flexible engine valve train was a necessary component to realize the emission and thermal efficiency requirements of this program. This report documents the design of a digital hydraulic valve actuation (HVA-D) system for the Cummins ISX15 engine. This system provided independent control of valve timing and duration combined with cylinder de-activation capability. In addition, the system was designed to be fully contained on the engine with the installation of an engine mounted pump.

## 1.1. Engine Platform

The engine platform for the HVA system was a stock, Cummins ISX15 diesel engine as shown in Figure 1. The engine configuration as delivered is rated at 298 kW (400 HP). This engine utilizes dual-overhead camshafts and has four valves per cylinder.

**Figure 1: Cummins ISX15 at Sturman Facility**



Source: Sturman Industries

## **CHAPTER 2:**

# **Overview of Modeling Approach**

Dynamic analysis of the HVA-D design was performed using a hydraulic system model created in MATLAB/Simulink. The analysis was used to help size hydraulic components like actuators, control valves and flow orifices. The final model was then used to predict general performance of the system over the hydraulic supply pressure range, system performance at specified operating conditions and power consumption of the system on the engine.

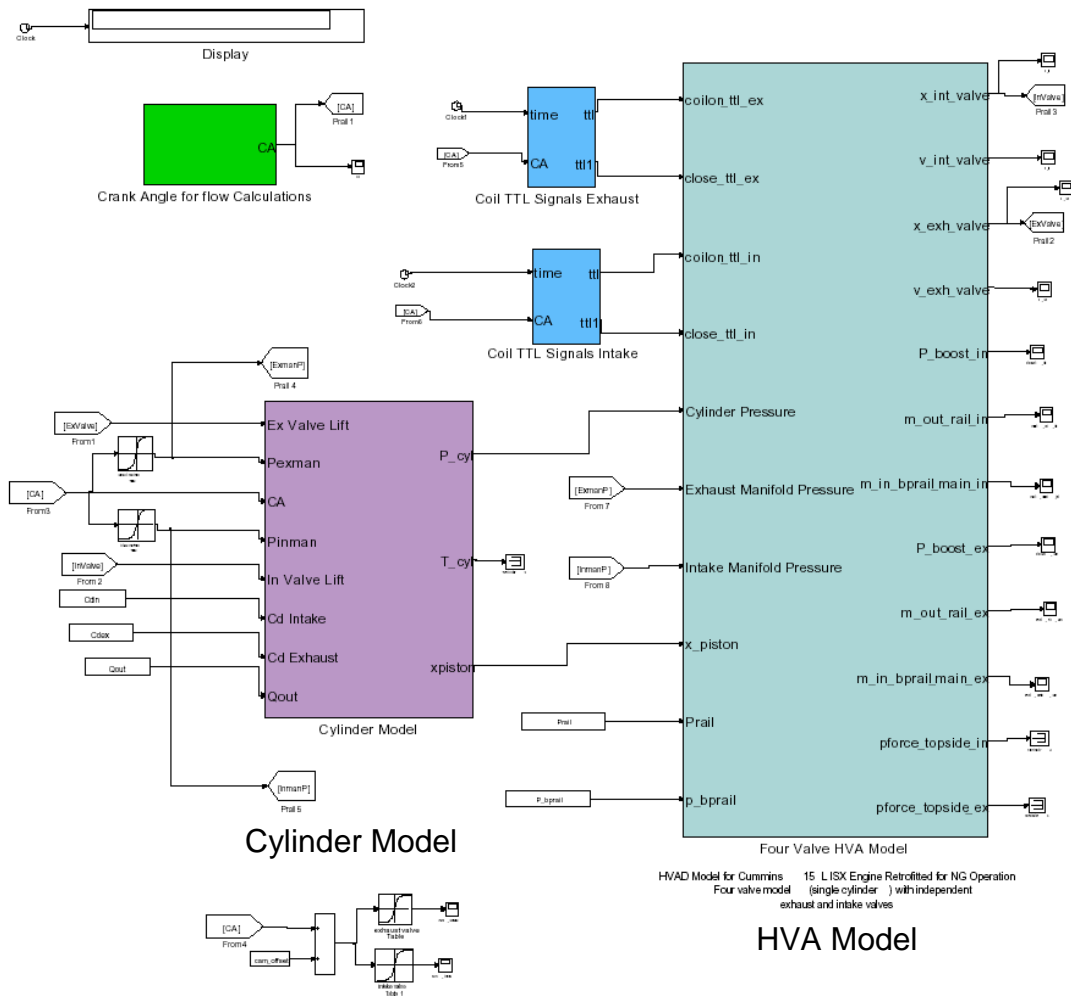
### **2.1 Model Description**

The MATLAB/Simulink model of the HVA-D system was built using hydraulic and dynamic components from a library developed by STURMAN over the last 10 years. These components represent solid bodies, springs, fuel lines, orifices, fluid volumes and so forth. Special contact elements provide realistic modeling of impacts and compressions under pressure of the above solid parts. The hydraulic fluid used to operate the HVA-D system is a compressible media and thus full dynamic wave modeling (acoustic modeling) is used throughout the model for accurate representation of the fluid physics. Hydraulic fluids are considered slightly compressible; their compressibility is defined by the bulk modulus of the fluid. Components for simulating annular sleeve leakages and squeeze film effects are also available in the library. These basic components are then used to build sub-models, a magnetically operated spool valve for example. The sub-model can then be independently validated with test data and placed in the component library as a Simulink block for use in a system model like the dynamic model of the HVA-D design for this project.

The top level of the dynamic system model used for this analysis is shown in Figure 2. It consists of the HVA-D model and the cylinder model. It should be noted that the hydraulic rails and supply pump were not part of this model. Those systems were modeled separately and are discussed in Section 4. The cylinder model provides accurate representation of the cylinder pressure as a function of time in order to accurately represent the in-cylinder forces the engine valves have to open against at any time during the engine cycle. The cylinder model was validated by using measured cylinder pressure traces on this engine with standard camshaft based engine valve motion. The validation cases are discussed in the model results section (section 0). The HVA section of the dynamic model is shown in more detail in Figure 2. Both the intake and exhaust valve components are modeled and the model is separated into the mechanical components and the hydraulic components. Mechanical components are the moving masses like the boost and drive pins in the main engine valve actuator. The mechanical model includes the boost pin, boost hard stop, drive pin, hydraulic return/push plate, full lift hard stop, engine valve and engine valve seat. The hydraulic components are the volumes and lines that contain hydraulic fluid and the components that control the flow like control valves and orifices. The hydraulic model includes the

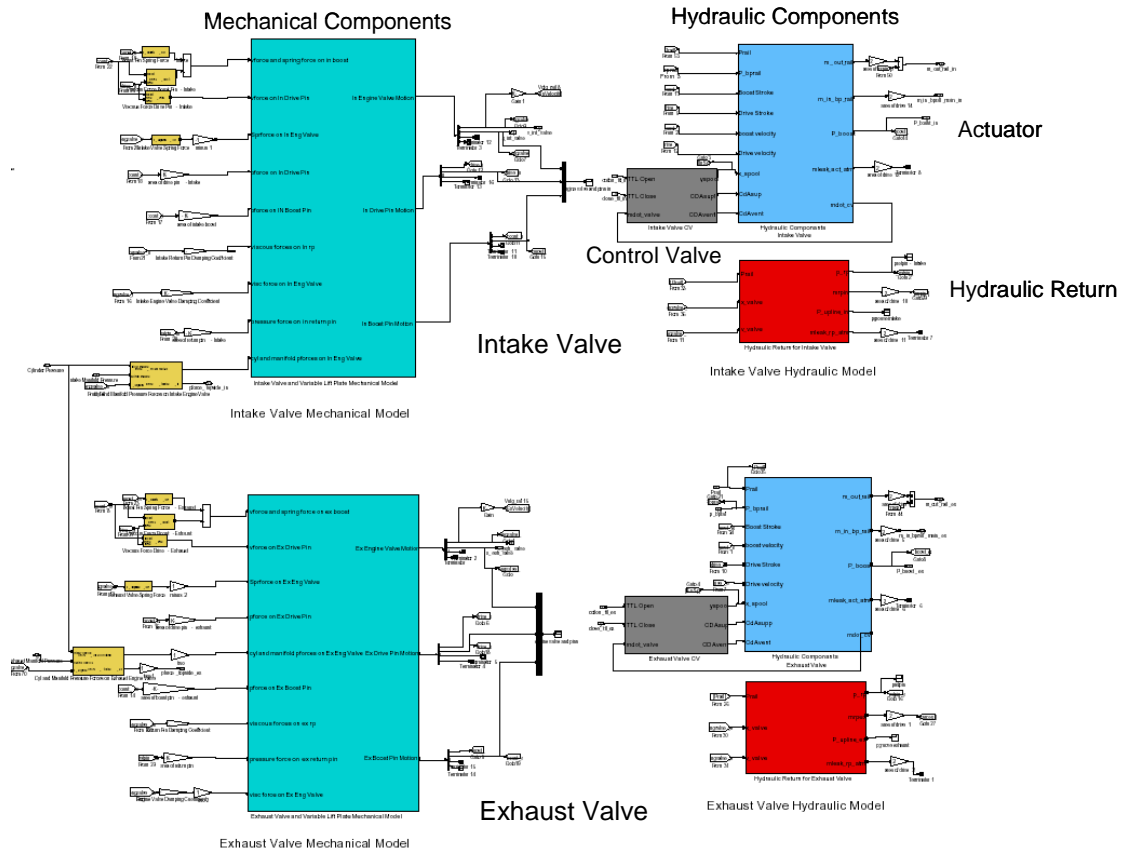
actuator control valve, the actuator volume and the hydraulic return volume. It also includes all the drillings and lines connecting the volumes to the hydraulic supply, all flow control orifices and all hydraulic fluid leak paths. The mechanical and hydraulic components are coupled through the dynamics of the actuator parts. The pressures in the actuator volumes create forces that move the actuator pistons and engine valve. In turn, the motion of the actuator piston results in pressure changes in the actuator volume. The differential equations that control both the motion of the parts and the fluid flows and pressures in the system are integrated and solved in the time domain by Simulink.

**Figure 2: MATLAB/Simulink Dynamic Model of HVA-D System**



Source: Sturman Industries

**Figure 3: Details of HVA-D Model in MATLAB/Simulink Dynamic Model**



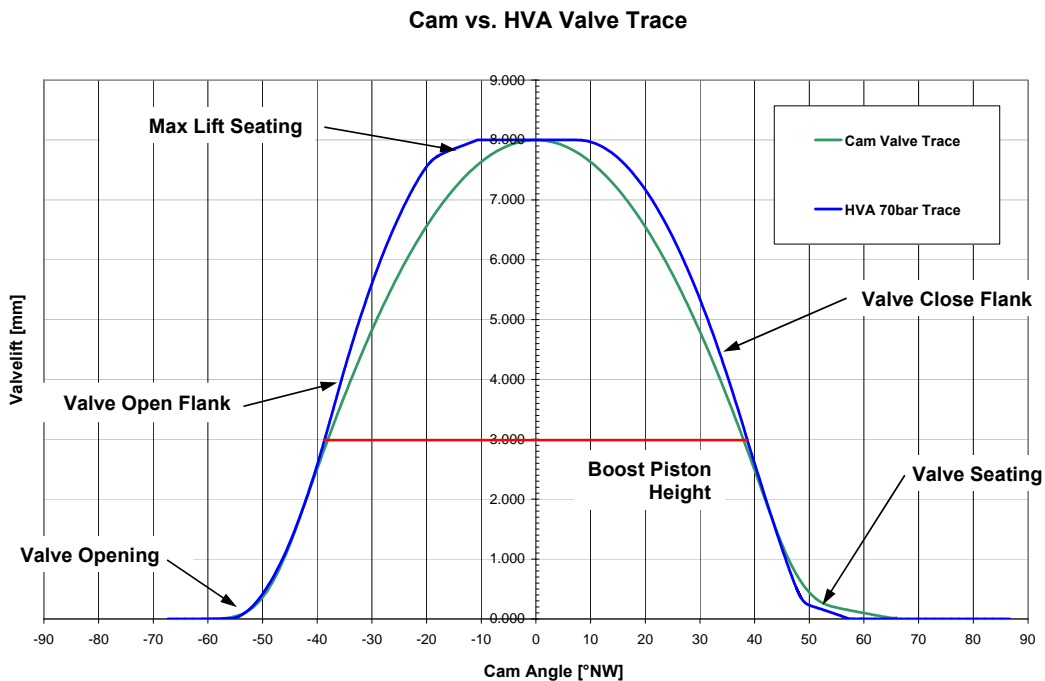
Source: Sturman Industries

## 2.2 Engine Valve Profile Description

The timings of the opening and closing of the engine valves are controlled by the timing of the opening and closing of the digital control valves that supply flow to the engine valve actuators. However, the valve motion profile is controlled by the actuator sizes, the supply pressure, the size and location of specified flow control orifices, and to a lesser extent by the digital valve flow area. A typical HVA-D valve profile is shown with a typical camshaft profile in Figure 3. The important aspects of the HVA-D valve profile are called out in the figure. The valve opening is controlled by engaging a flow control orifice for a specified amount of lift. As soon as the valve lift is above a set point, the valve opening orifice is bypassed. Often times, no orifice is engaged during the valve opening to facilitate a fast opening. The valve open flank is controlled by the actuator size and supply pressure. Care is taken not to limit the motion of the valve in this region by restricting flow to the actuator. The max lift seating velocity is controlled by orificing the flow from the hydraulic return at specified lifts in the valve profile. A graduated flow restriction is created by engaging progressively smaller orifices as the valve nears full lift and the mechanical hard stop for the actuator. The velocity at which the valve

impacts the max lift hard stop is kept below 0.6 m/s to reduce noise and structural issues associated with high velocity impacts. The valve close flank is primarily controlled by the vent flow area on the digital control valve. If the vent flow was not restricted during closing, the closing flank would be much faster than the opening flank, giving rise to asymmetric valve profiles (which may be acceptable) and difficulty seating the valve in a reliable manner at an acceptable velocity. The valve seating is controlled by engaging a flow control orifice at a specified valve lift until the valve has seated. The size of this orifice, in conjunction with the actuator size, controls the seating velocity. If the engine valve is travelling too fast when the valve seating orifice engages, the engine valve can “bounce” on the very high pressure that is generated in the actuator volume at the time the flow is restricted. This bounce can lead to variability in the seating timing and velocity and excessive hydraulic noise during seating.

**Figure 4: HVA-D Valve Profile Definition**



Source: Sturman Industries

The MATLAB/Simulink dynamic model was used in the design process to optimize the valve profile over the operating range by sizing the actuators, and determining the size and location of the flow control orifices that control the valve profile.

## 2.3 Model Results

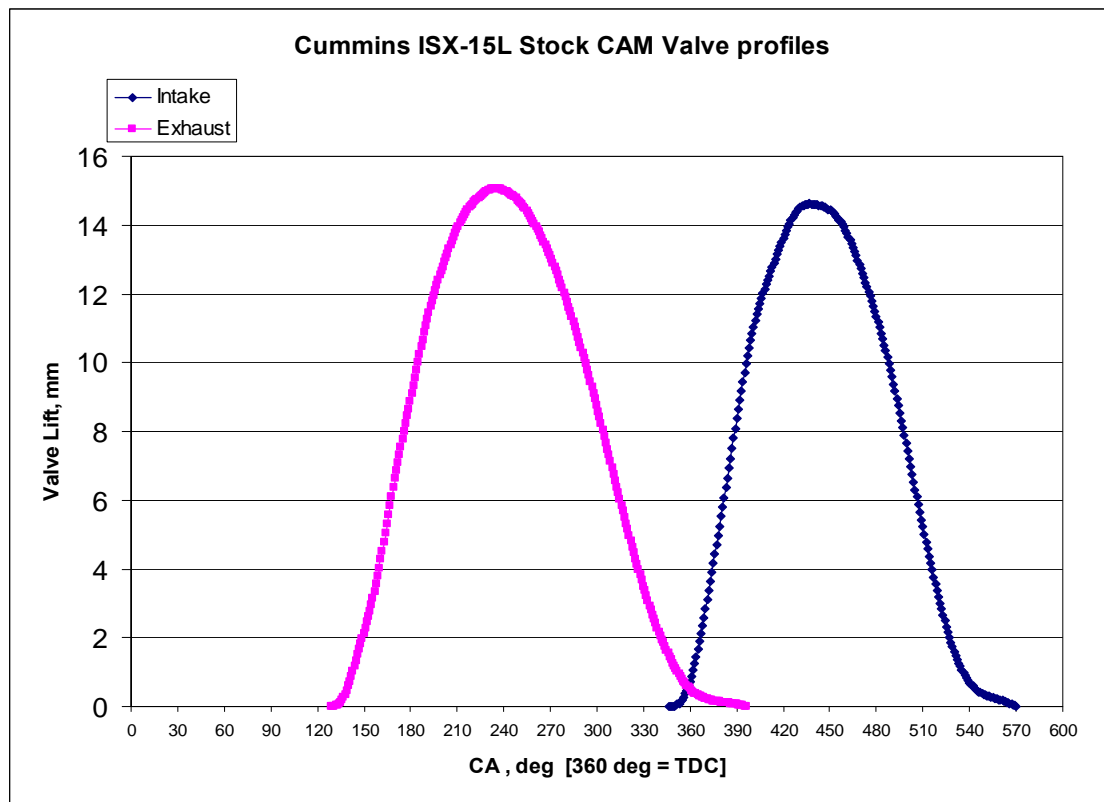
The results from the dynamic model used during the system design phase are discussed in this section. The results are broken down into four subsections:

1. Cylinder model validation using engine blow down data.
2. General valve motion performance as a function of system supply pressure.
3. System performance at specified operating conditions.
4. System power consumption.

### 2.3.1 Cylinder Model Validation

Cylinder pressure data as a function of crank angle from a Cummins ISX15 600 HP diesel engine operated as a dual-fuel lean burn natural gas engine was obtained and used to validate the cylinder model for predicting cylinder pressure during the exhaust and intake valve events. The data was taken with a stock camshaft controlling the valve motion. The measured valve profiles from the stock camshaft were also provided and are shown in Figure 5.

**Figure 5: Stock Camshaft Valve Profiles for Cummins ISX15 Engine**



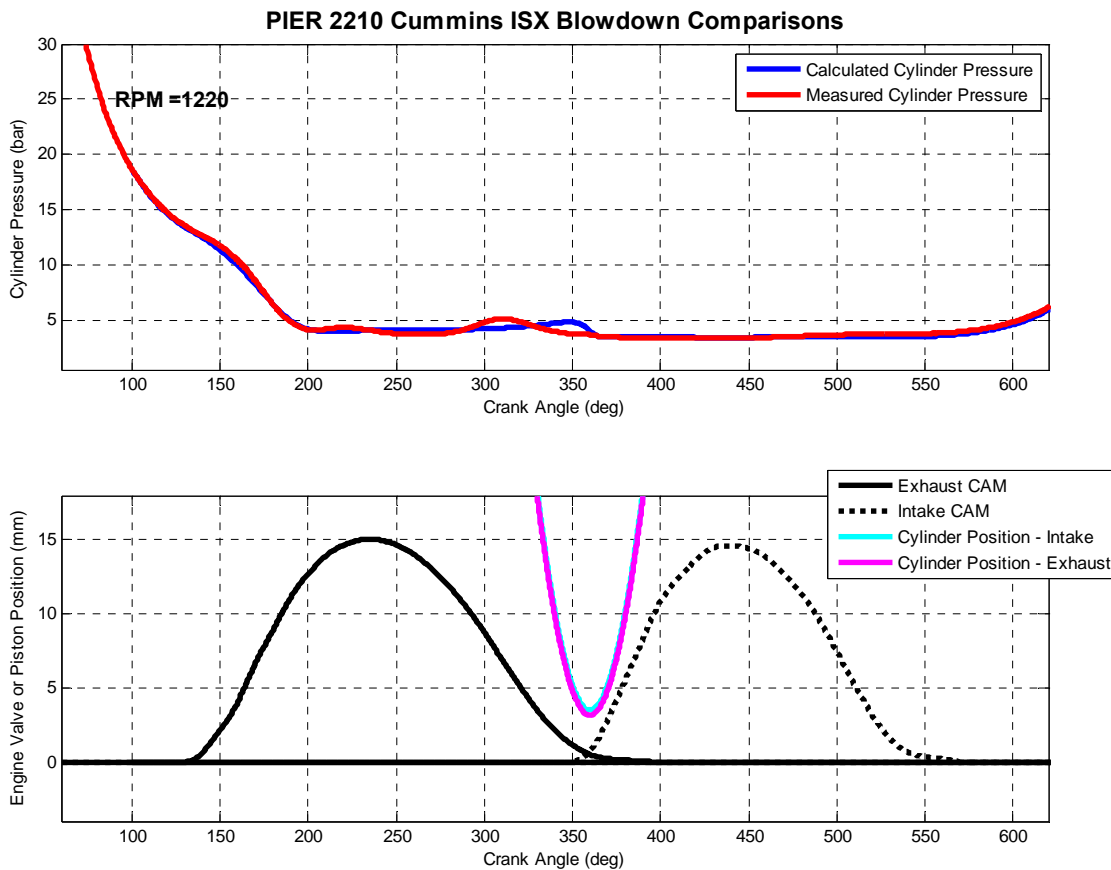
Source: Sturman Industries

Two cases were validated with the model, the peak torque point and the rated power point. The cylinder model was initialized with the average measured cylinder pressure and temperature and average measured intake and exhaust manifold pressures and

temperatures at 100 CA degrees. The simulation was then run using the measured camshaft valve profiles as input into the cylinder model and the measured and simulated cylinder pressures were compared.

The results from the peak torque point comparison are shown in Figure 6. The top graph shows the measured cylinder pressure (red) and predicted cylinder pressure (blue) for crank angles between 100 and 600 degrees. The cylinder model accurately predicts the cylinder pressure during the cylinder blow down. There is some discrepancy between the two curves between 300 and 350 degrees which is probably due to dynamics in the exhaust manifold that were not modeled.

**Figure 6: Measured and Predicted Cylinder Pressures for Peak Torque on Cummins ISX-15L Engine**

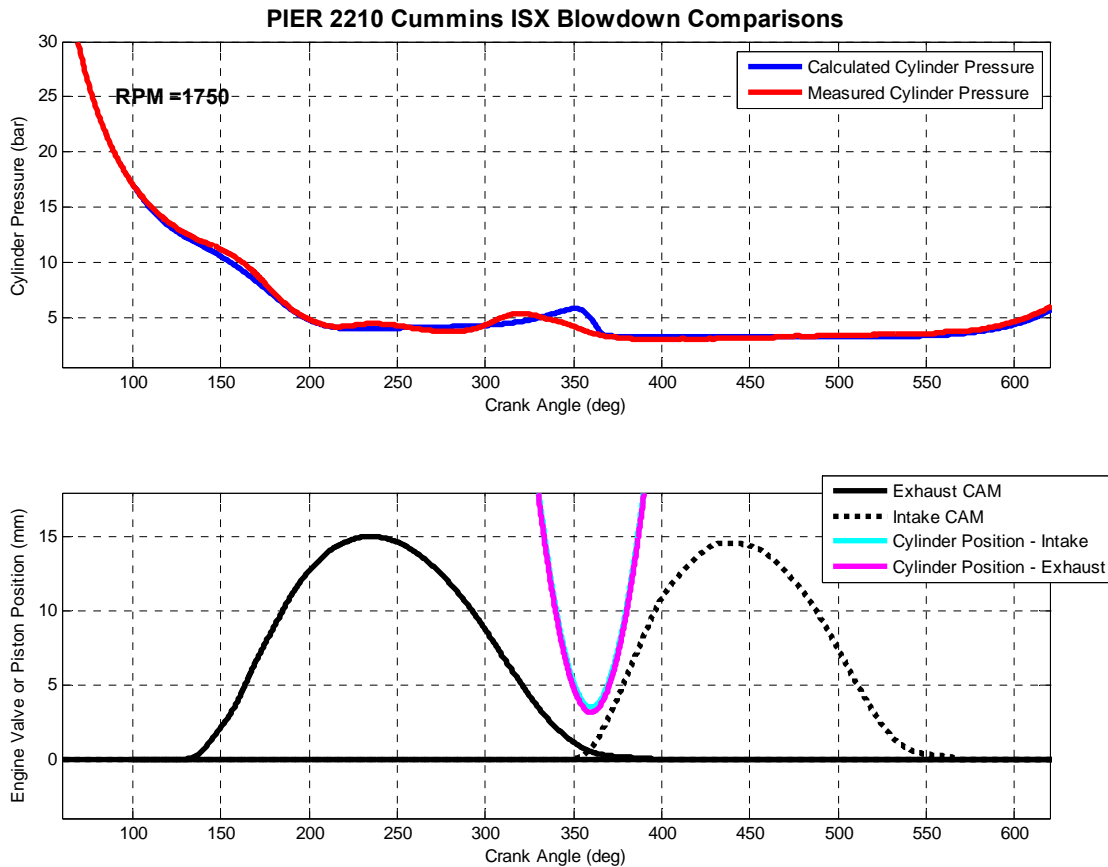


Source: Sturman Industries

The results from the rated power point comparison are shown in Figure 6. The top graph shows the measured cylinder pressure (red) and predicted cylinder pressure (blue) for crank angles between 100 and 600 degrees. The cylinder model shows slightly lower pressure than the data around 160 CA degrees, but it is small (~ 0.5 bar). There is also some discrepancy between the two curves between 300 and 350 degrees, the same as

was seen for the peak torque point, which is probably due to dynamics in the exhaust manifold that were not modeled.

**Figure 7: Measured and Predicted Cylinder Pressures for the Rated Condition on Cummins ISX15 Engine**



Source: Sturman Industries

In general the cylinder model did a good job of predicting the cylinder pressure during the exhaust and intake valve events and thus should yield accurate cylinder pressure predictions for the HVA-D generated valve profiles.

### 2.3.2 HVA-D Valve Motion versus System Supply Pressure

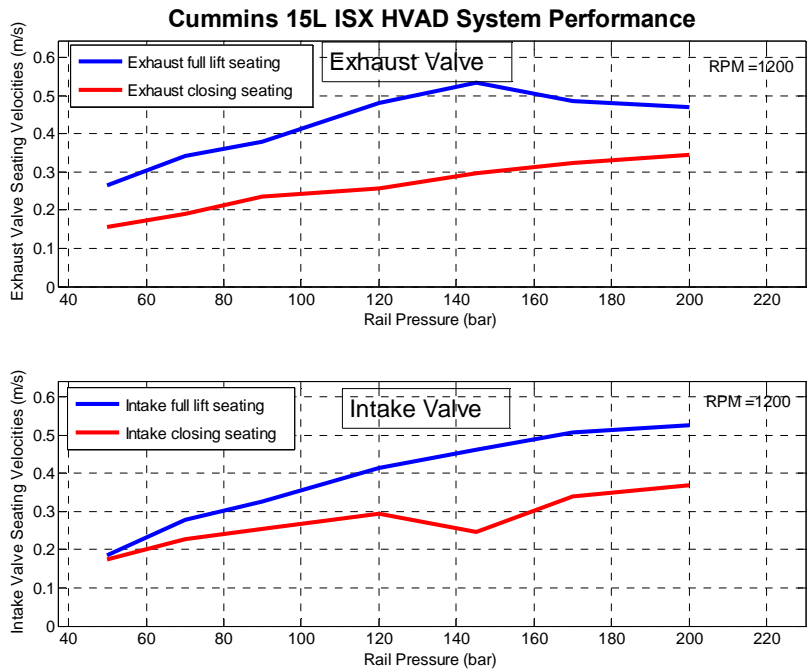
The HVA-D system was designed to operate with supply pressures ranging from 50 bar (725 psi) to 200 bar (2900 psi). The actual supply pressure for an operating condition will be determined by the HVA-D controller and will depend on the engine speed, engine load and desired valve timing. In general, supply pressure increases with increasing engine load, increasing engine speed and earlier exhaust valve opening timing. The HVA-D system must have flank and seating velocities that meet the valve profile specifications over the entire supply pressure operating range. The valve profile specifications were as follows:

- Valve seating targets are from 0.1 m/s to 0.4 m/s. Seating velocity should not exceed 0.45 m/s.
- Max lift seating velocity targets are from 0.3 m/s to 0.6 m/s. Max lift seating velocity should not exceed 1 m/s
- Open and close flank velocities should allow HVA valve profile to be outside the camshaft valve profile during opening and closing of the valve. Average flank rate should never be slower than the camshaft.

The HVA-D dynamic system model was run for system pressures varying from 50 bar (725 psi) to 200 bar (2900 psi) at 1200 RPM and 2 bar (29 psi) initial pressure in the cylinder @ 100 CA degrees and the max lift seating velocities, average and maximum open and close flank velocities and seating velocities were predicted at each system pressure for both the intake and exhaust valve. The average flank velocity was calculated between 1 mm lift and 14 mm lift to avoid the max lift seating and valve close seating areas of the valve profiles.

The predicted max lift seating velocities and valve seating velocities as a function of the system supply (rail) pressure for both the exhaust and intake valve on the HVA-D system are shown in Figure 8. The predicted max lift seating velocities range from 0.19 m/s to 0.53 m/s. These are slightly lower than the target values of 0.3 m/s to 0.6 m/s, but are acceptable. The predicted valve seating velocities for the HVA-D system range from 0.15 m/s to 0.37 m/s and are within the targeted values.

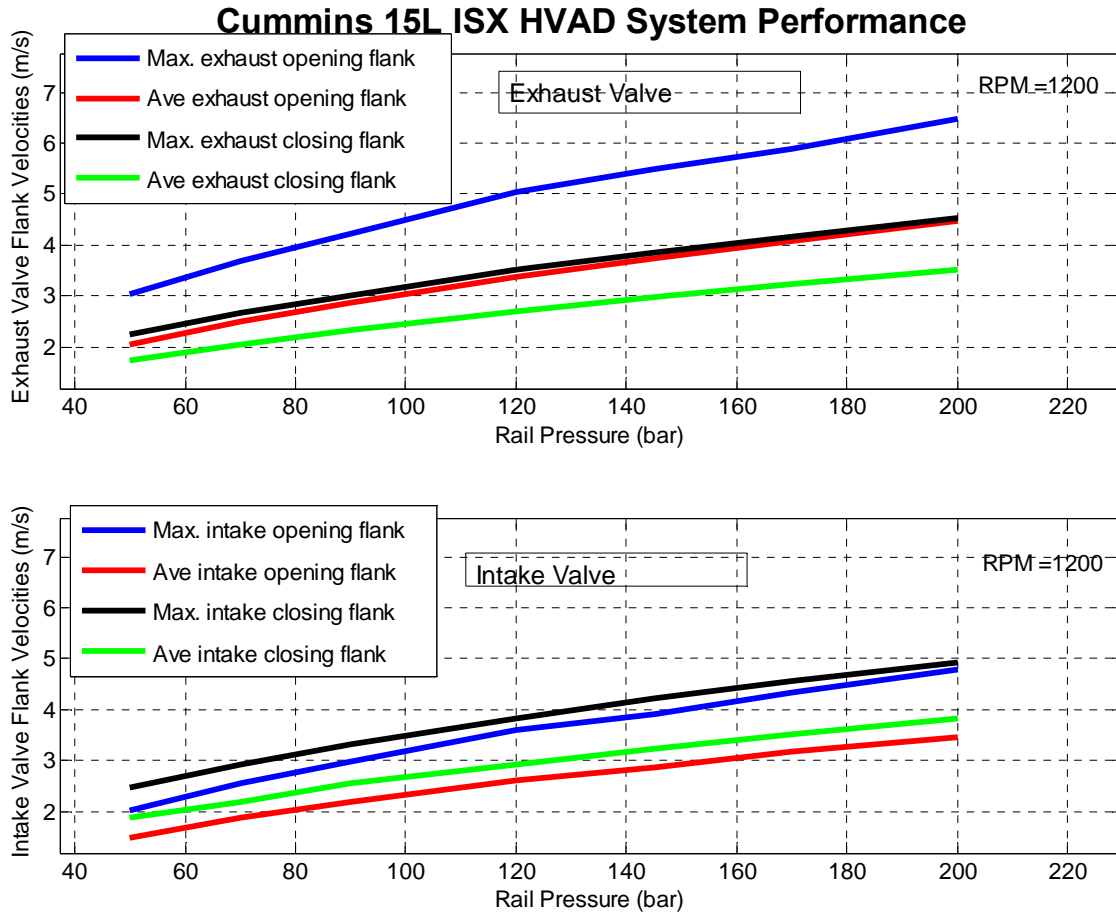
**Figure 8: Predicted Max Lift Seating Velocity and Valve Seating Velocity for Both Exhaust and Intake Valves**



Source: Sturman Industries

The predicted maximum and average open and close flank velocities for both the exhaust and intake valve as a function of the supply (rail) pressure are shown in Figure 9. The camshaft valve profile flank velocities are only a function of the engine speed and are shown in Table 1 for both the intake and exhaust valves. These velocities were calculated from the measured camshaft valve profiles shown in Table 1.

Figure 9: Predicted Flank Velocities for Both Exhaust and Intake Valves



Source: Sturman Industries

Table 1: Calculated Flank Velocities for Camshaft Valve Profiles for Cummins ISX15 Engine

Engine Speed (RPM)	INTAKE		EXHAUST	
	Avg. Open Flank (m/s)	Avg Close Flank (m/s)	Avg. Open Flank (m/s)	Avg Close Flank (m/s)
600	0.747	-0.597	0.704	-0.449
900	1.120	-0.896	1.055	-0.673
1200	1.494	-1.195	1.407	-0.897
1500	1.867	-1.493	1.759	-1.121
1800	2.240	-1.792	2.111	-1.346
2100	2.614	-2.091	2.463	-1.570

Source: Sturman Industries

The average HVA-D open flank velocity for the exhaust valve goes from 2.06 m/s to 4.46 m/s. The camshaft had average open flank velocities from 0.75 m/s to 2.61 m/s on the exhaust valve. The average HVA-D close flank velocity for the exhaust goes from 1.73 m/s to 3.52 m/s compared to 0.60 m/s to 2.09 m/s for the camshaft. Similar comparisons for the intake valve show the average open flank for the HVA-D system to be 1.49 m/s to

3.45 m/s compared to 0.70 m/s to 2.46 m/s for the camshaft and; the average close flank for the HVA-D to be 1.88 m/s to 3.82 m/s compared to 0.45 m/s to 1.57 m/s for the camshaft. In all instances, the average flank rate for the HVA-D system exceeds the camshaft, thus insuring the HVA-D valve will open and close faster than the camshaft. It should be mentioned that the HVA-D exhaust valve open flank rate is noticeably faster than the other three HVA-D flank rates. That is due to the fact that the exhaust valve actuator is designed to open against as high as 20 bar (290 psi) in-cylinder pressure and these simulations were run with less than 2 bar (29 psi) in-cylinder pressure. In actual practice, when in-cylinder pressure is present, the exhaust valve open flank velocity will be very close to the other three HVA-D flank rates.

### 2.3.3 HVA-D System Performance at Specified Operating Conditions

The performance of the HVA-D system at specified engine operating conditions was predicted to ensure that acceptable valve profiles under actual engine operating conditions were achievable with the design. Six specified points that covered the speed and load range of the Cummins ISX15 engine were identified and are shown in Table 2.

**Table 2: Engine Operating Conditions for HVA-D Dynamic Model Predictions**

Engine Speed	Pcyl @ 100 CA (bar)	Tcyl @ 100 CA (K)	Intake Manifold		Exhaust Manifold		Prail (bar)	Description
			Pim (bar)	Tim (K)	Pem (bar)	Tem (K)		
600	1.81	439	1	320	1	408	50	Idle
900	10.5	840	2	323	2.3	740	90	Low Speed, 50% Load
1200	18.7	925	3.5	328	4	830	160	Peak Torque
1500	17.9	925	3.5	328	4	830	160	High Speed, Full load
1800	17.1	925	3.5	328	4	830	160	Rated Power
2100	15.5	925	3.5	328	4	830	140	Max Speed

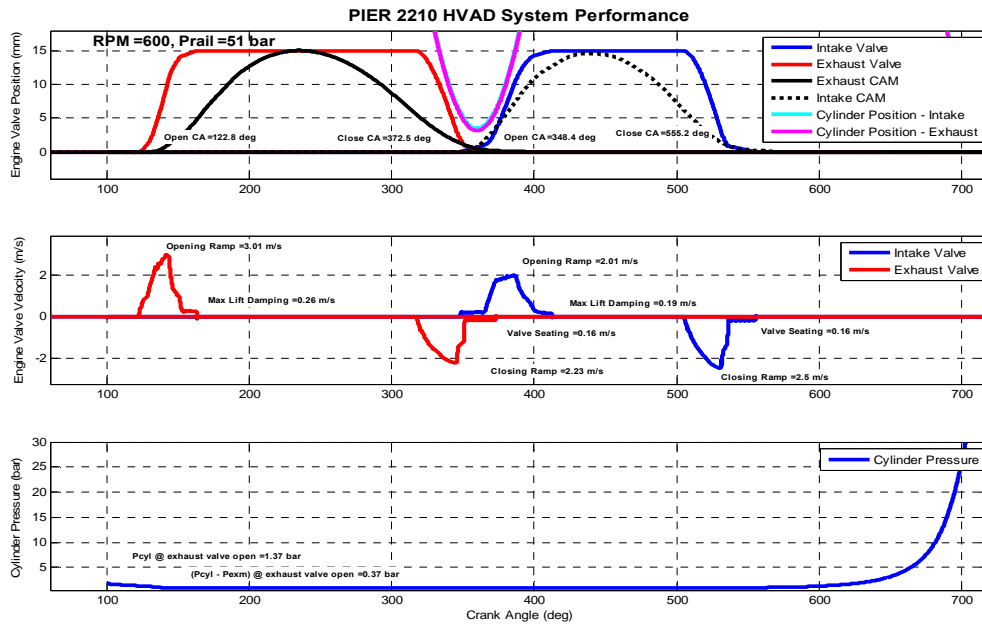
Source: Sturman Industries

The open and close engine valve timings for the HVA-D system were chosen to match the camshaft valve exhaust valve opening and intake valve closing. The exhaust valve closing and intake valve opening timings were chosen to provide a minimum clearance between the valve and the piston of 5 CA degrees. The value of 5 CA degrees clearance was chosen because it is currently the most common clearance used in the safety code of our HVA-D controller.

Figure 15 show the results of the model for the six engine operating conditions. The figures each have three plots, the top graph shows the predicted HVA-D valve profiles, the camshaft valve profiles and piston location. The open and close timing of both valves are also shown on the graph. The open timings and close timings are measured at 0.1 mm of lift. The second graph shows the predicted HVA-D valve velocities. The maximum open and close flank rates, the max lift seating velocity and the valve seating velocity for each valve are also shown on the graph. The third graph shows the cylinder pressure. The cylinder pressure at exhaust valve opening (EVO) and the pressure differential between the cylinder and exhaust manifold at EVO are also shown on the graph. In all cases the HVA valve profile lies outside the camshaft trace which provides

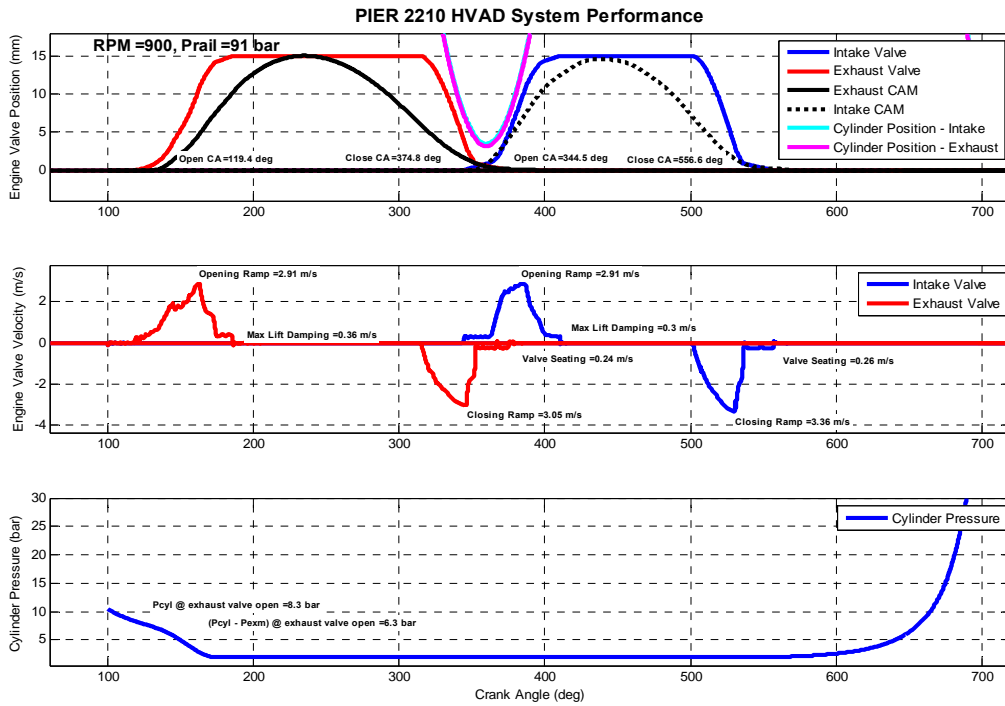
a mechanism for improving the engine airflow. The highest engine speed case shows flank rates comparable to the camshaft. These could be faster with slightly higher rail pressure, if so desired. It should also be noted that valve overlap between the exhaust and intake valves under the piston at TDC is evident for all cases. The opening velocity of the intake valve for the first 1 mm was restricted by an orifice in order to achieve valve overlap at all engine speeds.

**Figure 10: Predicted HVA-D Valve Profiles at Engine Idle Operating Conditions**



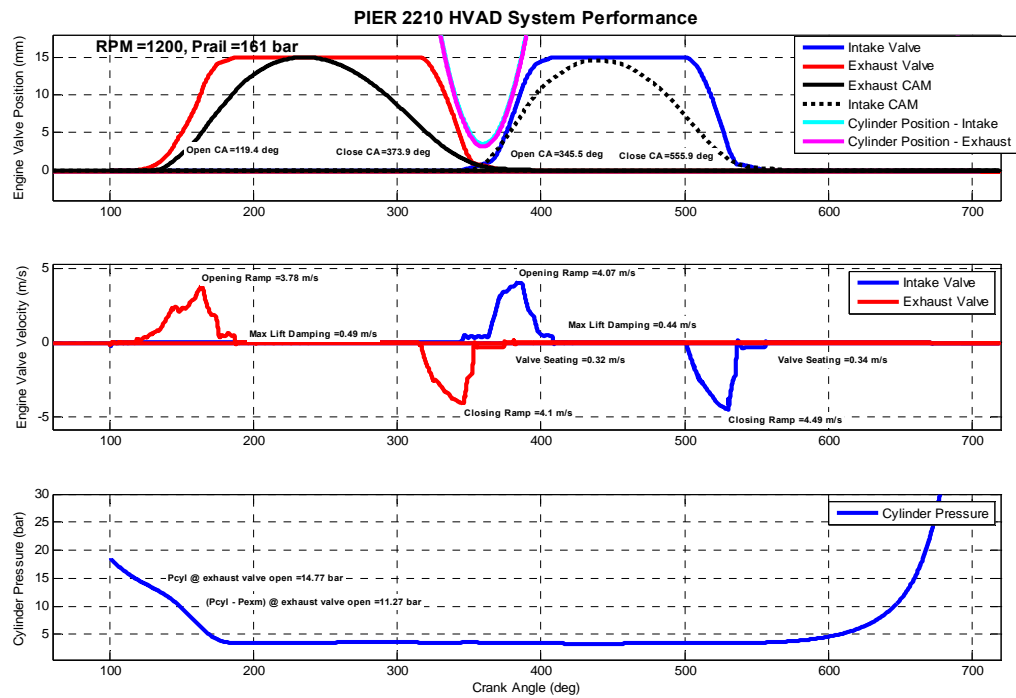
Source: Sturman Industries

Figure 11: Predicted HVA-D Valve Profiles at Low speed, 50% Load Operating Conditions



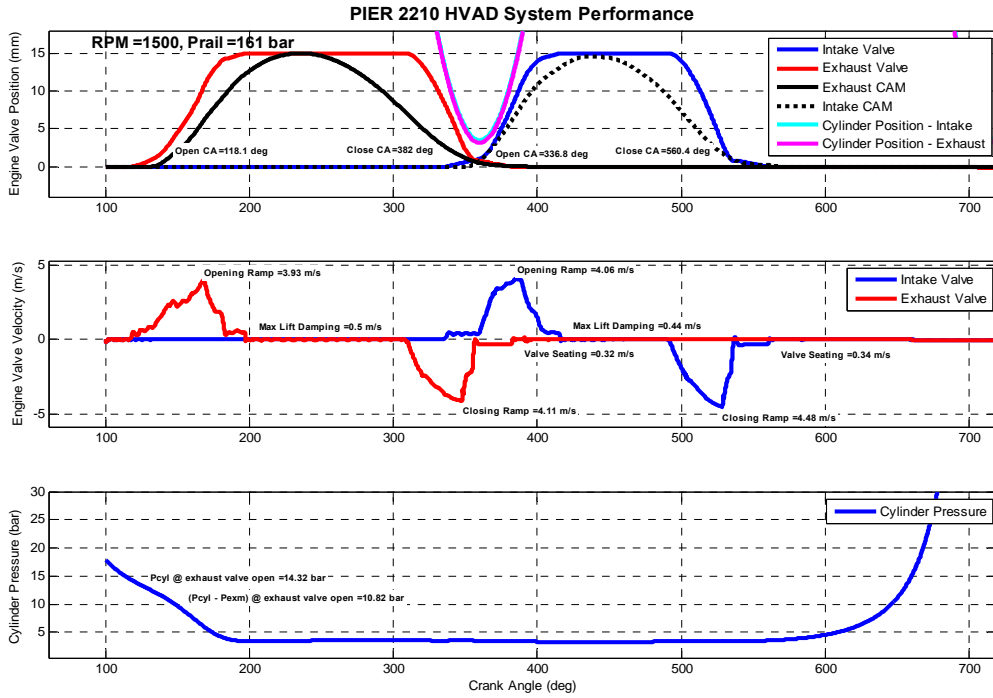
Source: Sturman Industries

Figure 12: Predicted HVA-D Valve Profiles at Peak Torque Operating Conditions



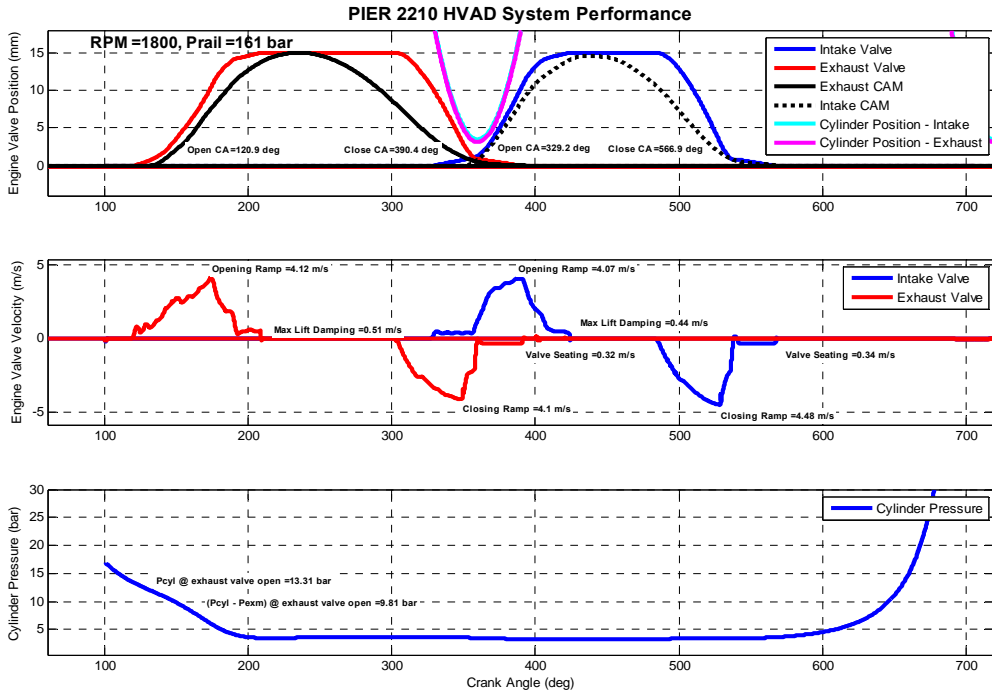
Source: Sturman Industries

Figure 13: Predicted HVA-D Valve Profiles at High Speed, Full Load Operating Conditions



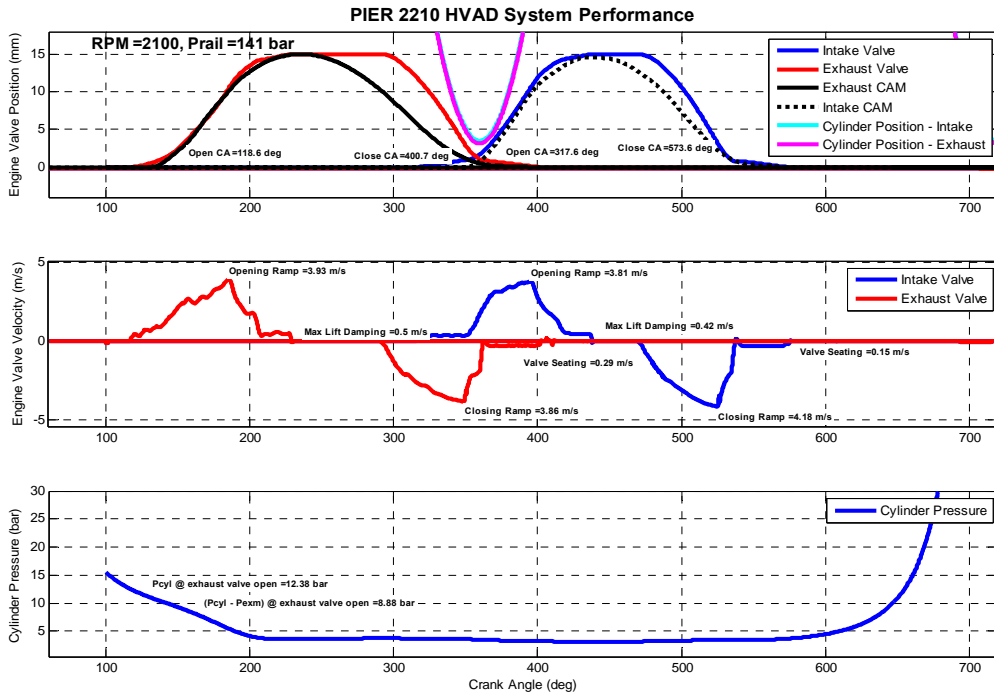
Source: Sturman Industries

Figure 14: Predicted HVA-D Valve Profiles at Rated Power Operating Conditions



Source: Sturman Industries

**Figure 15: Predicted HVA-D Valve Profiles at Max Speed Operating Conditions**



Source: Sturman Industries

### 2.3.4 HVA-D System Power Consumption

The HVA-D system uses high pressure oil or hydraulic fluid to operate the engine valves. High pressure oil from the oil rail flows to the main actuator to open an engine valve. That oil is then vented to a back pressure 5 bar (72 psi) rail during closing of the engine valve. The supply of the high pressure oil to the system via an oil pump represents a parasitic loss to the engine. Keeping the parasitic loss as low as possible, without compromising system performance is an important part of the design process for an HVA-D system. Use of hydraulic returns instead of valve springs, optimizing the size of the actuators, reducing flow losses, reducing high pressure oil leakage and recovering some of the valve kinetic energy as hydraulic energy are just some of the methods for reducing system power consumption.

The composite power consumption for this system was calculated from a standard 13-mode operating point matrix for a 298 kW (400 HP) engine, since that is the peak HP that will be realized in this project. The lowest rating for this engine was selected due to dynamometer facility limitations. The operating conditions for the 13-mode points and their weighting for the composite power consumption calculation are shown in Table 3.

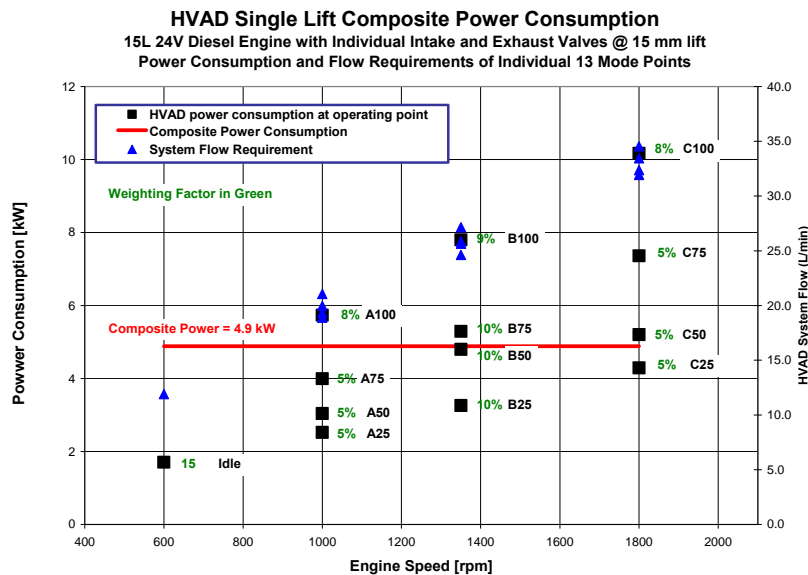
**Table 3: Engine Operating Conditions for 13-Mode Points**

Mode Point	Engine speed [rpm]	Hydraulic Pressure [bar]	% Weighting	In-Cylinder Pressure @ EVO [bar]	Exhaust Manifold Pressure [bar]	Intake Manifold Pressure [bar]	Notes
1	600	50	15%	1.5	1.0	1.0	idle, normal operation
7	1000	60	5%	6.0	1.3	1.2	A25
5	1000	70	5%	9.0	2.6	2.3	A50
6	1000	85	5%	12.0	4.0	3.5	A75
2	1000	110	8%	15.0	4.0	3.5	A100
9	1350	60	10%	6.0	1.7	1.7	B25
3	1350	85	10%	9.0	2.8	2.5	B50
4	1350	90	10%	12.0	4.0	3.5	B75
8	1350	120	9%	15.0	4.0	3.5	B100
11	1800	60	5%	6.0	2.2	1.9	C25
13	1800	70	5%	9.0	3.1	2.7	C50
12	1800	95	5%	12.0	4.0	3.5	C75
10	1800	120	8%	15.0	4.0	3.5	C100

Source: Sturman Industries

The system power consumption includes the hydraulic supply pressure needed to operate the system and all the fluid used by the system. The fluid usage includes the actuator fluid volumes, the compression fluid volumes and all leakages. The power consumption calculation also includes the electrical energy necessary to operate the magnetic digital valves in the system and the hydraulic pump efficiency. The predicted power consumption and the oil flow requirements of the HVA-D system for all 13-mode points and the weighted composite power consumption are shown in Figure 16. The weighted composite power consumption of the HVA-D system is 4.9 kW (6.6 HP). At idle, the system will use only 1.7 kW (2.3 HP). At the C100 point, which is very close to the rated power point on this engine, the HVA-D system consumes 10.2 kW (13.6 HP). This is ~ 3.5 percent parasitic loss due to the valve train at rated power of 298 kW (400 HP) for this engine.

**Figure 16: Power Consumption of HVA-D System for 13 Mode Operating Points**



Source: Sturman Industries

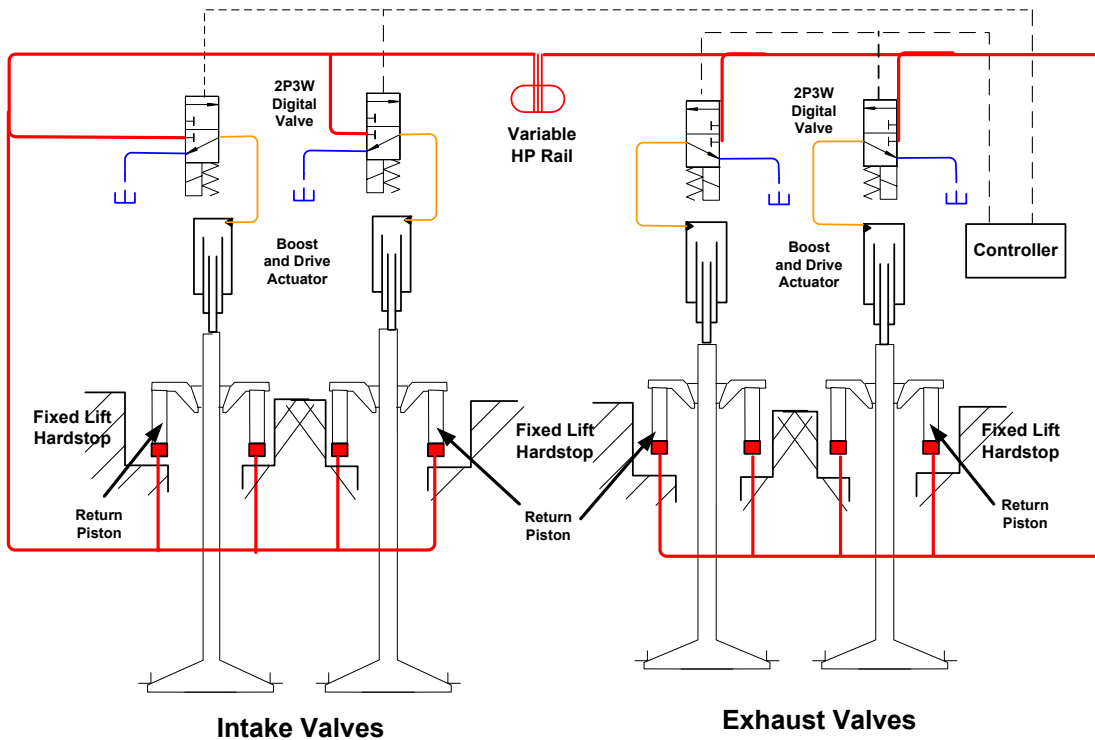
# CHAPTER 3: HVA-D Design Summary

## 3.1 System Overview

Sturman has designed an integrated HVA system for this engine. The HVA system consists of a single lift system that provides independent control of each individual air valve on a cylinder. Exhaust valves were originally planned to be bridged. However, the bridging was eliminated due to the added risk associated with that design direction. This added risk was not justified by the calculated efficiency benefit. In fact, the module symmetry allowed by the non-bridged design allowed for improved production direction.

The HVA system is a single lift design in order to provide the highest level of reliability and lowest power consumption. The hydraulic control of the actuator employs three basic components: a three-way control valve for flow control, a compound actuator for opening an engine valve and a simple actuator for returning an engine valve. The three-way control valve is used to connect the compound actuator to either the high pressure supply rail or the back pressure (BP) rail. The schematic shown in Figure 17 details the schematic of the system for both the intake and exhaust valves.

**Figure 17: Final Schematic of HVA System for Natural Gas Engine**



Source: Sturman Industries

The compound actuator is a patented Sturman design which reduces energy consumption. The boost piston has a large area exposed to pressure that provides high force at the start of opening up to 3.5 mm (0.118 in) of lift. The high opening force is used to overcome in-cylinder pressures and create high acceleration. From the boost pin stroke (typically 2 mm (0.078") to 4 mm (0.157")) to the maximum lift, the valve stroke is achieved via a drive piston which has a smaller area exposed to pressure and produces a significantly lower opening force. The smaller area reduces the overall swept volume of the actuator which, in turn, reduces the hydraulic flow of the system and thus improves power consumption.

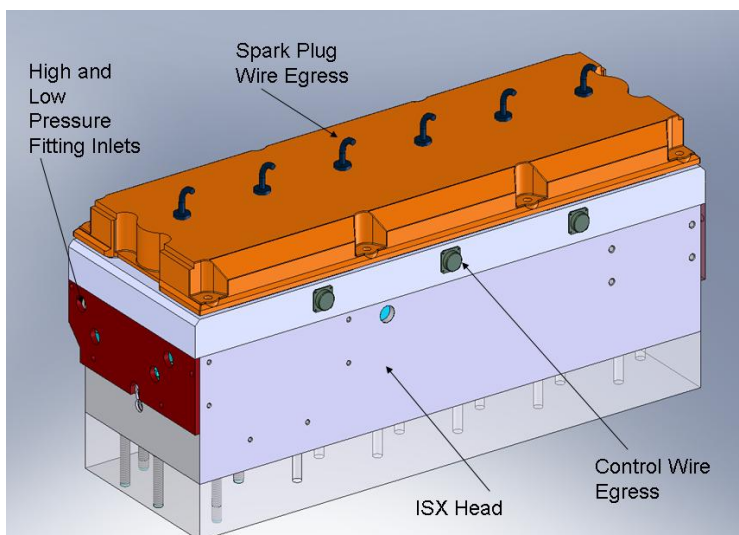
The simple return actuator is also designed to enable further reduction in power consumption. It is connected directly to the high pressure rail so that the actuation force is varied with pressure and does not change with valve stroke. This simple design requires no active control of the return force and reduces power consumption by reducing the return force necessary at lower engine speeds and loads.

The HVA system offers infinitely variable and independent valve timing for intake and exhaust valve opening and valve closing. The maximum lift point is determined by a fixed mechanical stop whereas the duration can be varied without effect on the lift. The opening and closing velocities of the valves can also be varied independently of engine speed by nature of a variable pressure rail. Therefore, valve traces with short duration and high lift can be achieved at lower speeds. In addition, the system can perform multiple valve events per engine cycle or deactivate valves or cylinders for engine braking and to reduce parasitic losses. This system requires one control valve per engine valve, for a total of four control valves per cylinder. This results in a relatively simple system that offers a great deal of functionality.

## **3.2 HVA-D System Design**

An overview of the HVA hardware design implemented on the ISX head is detailed in the following section. The HVA system was fully integrated under the stock ISX valve cover with the addition of a small spacer to allow connectors for the control wires as shown in Figure 18. Spark plug wires necessary for the connections to the spark plugs are shown routed through the valve cover. The ignition coils necessary to drive the spark plugs are attached to the side of the engine and are not shown for clarity. This figure also shows the interface to the hydraulic system that was accomplished through high pressure hoses that interface to the rails on either side of the valve actuation components.

**Figure 18: ISX15 Head with HVA Packaging**

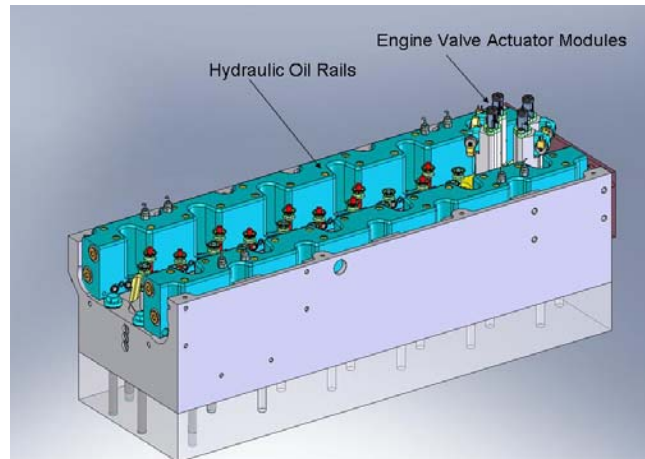


Source: Sturman Industries

Removal of the valve cover and spacer as shown in Figure 19 allows access to the HVA system. The actuator modules for only one cylinder are shown to improve clarity for this figure; whereas, actuators for each cylinder are identical to enhance the production intent of the system. The valve cover wiring for the actuators has also been removed to show the overall system installation.

The design includes two identical hydraulic rails that capture the high pressure and low pressure cavities. The rail design allows access to all of the head bolts so the head could be removed from the engine without removing the HVA system. This feature provides production intent flexibility to allow the HVA system to be validated off-line before installation on the actual engine.

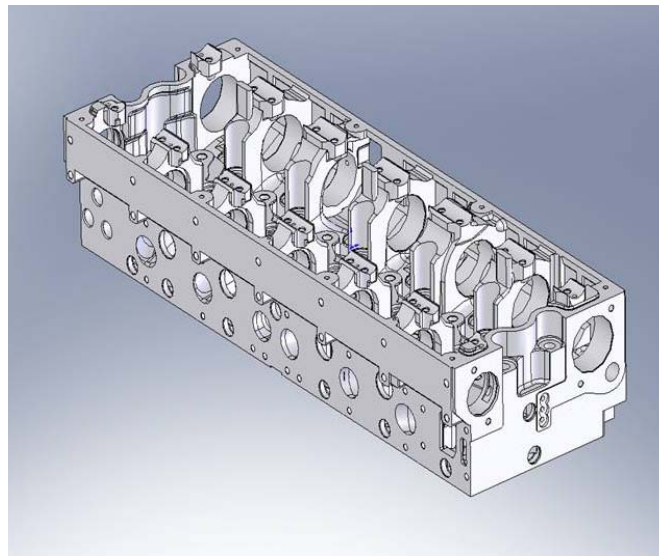
**Figure 19: HVA Packaging Overview**



Source: Sturman Industries

The ISX15 head requires modification to accept the HVA hardware. The head was reverse engineered to provide a foundation to these modifications. The baseline head is shown in Figure 20.

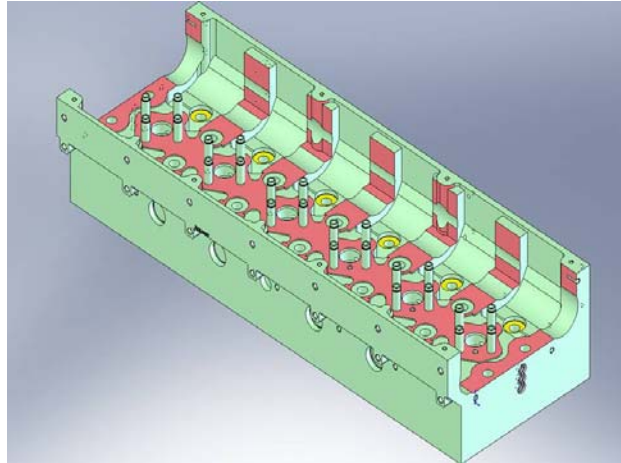
**Figure 20: Baseline ISX15 Cylinder Head**



Source: Sturman Industries

As can be seen in the baseline head model, the camshaft carriers must be removed to allow room for the hydraulic rails. The head modifications necessary to package the HVA system on the head are shown as highlighted surfaces in Figure 21. The ends of the head are also modified to allow improved module packaging.

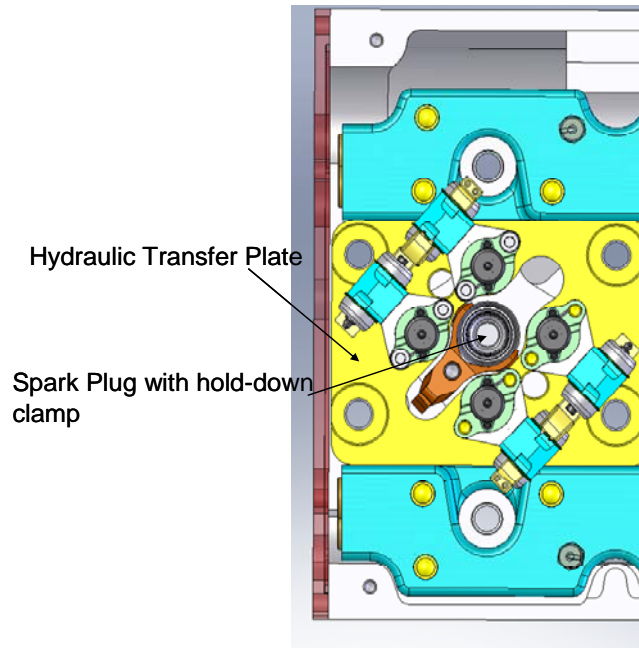
**Figure 21: ISX15 Head Modifications**



Source: Sturman Industries

The hydraulic transfer plate (yellow) shown Figure 22 provides the high and low pressure oil connections between the oil rails and actuator modules in a simple, attractive, production viable manner. This allows the oil connections to be fully contained and provides cylinder-to-cylinder symmetry. The spark plug necessary for natural gas ignition is fitted to an adapter that utilizes the geometry in the old fuel injector bore. This new adapter is held in place with the existing ISX fuel injector clamp (brown) to reduce costs.

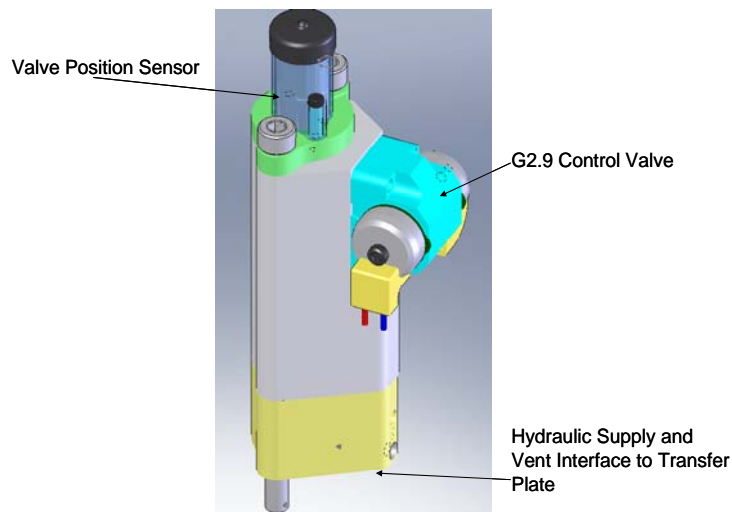
**Figure 22: Top View Single Cylinder Detail**



Source: Sturman Industries

The engine valve actuator is shown in Figure 23. The external geometry between intake and exhaust actuators is identical. There are minimal internal differences between the intake and exhaust module which simplifies manufacturing and installation. The G2.9 control valve is based on a production component currently in-use on a diesel fuel injector. The engine valve position sensors are used interchangeably on the intake and exhaust module, again for simplicity in manufacturing and installation.

**Figure 23: HVA Actuator Module Overview**

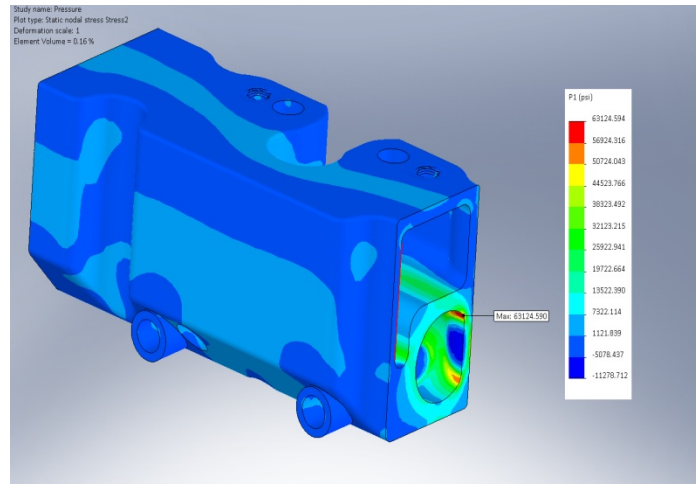


Source: Sturman Industries

### 3.3 HVA-D System Structural Analysis

Structural analysis of the hardware, known as Finite Element Analysis (FEA), was conducted on all of the new hardware. A few examples of these design efforts are shown in the following figures. The FEA was performed using Solidworks Cosmos software which allows the proper mesh and boundary conditions to be defined for each component. Figure 24 documents the FEA performed on the hydraulic rail. The rail shows acceptable stress levels for operation of the system.

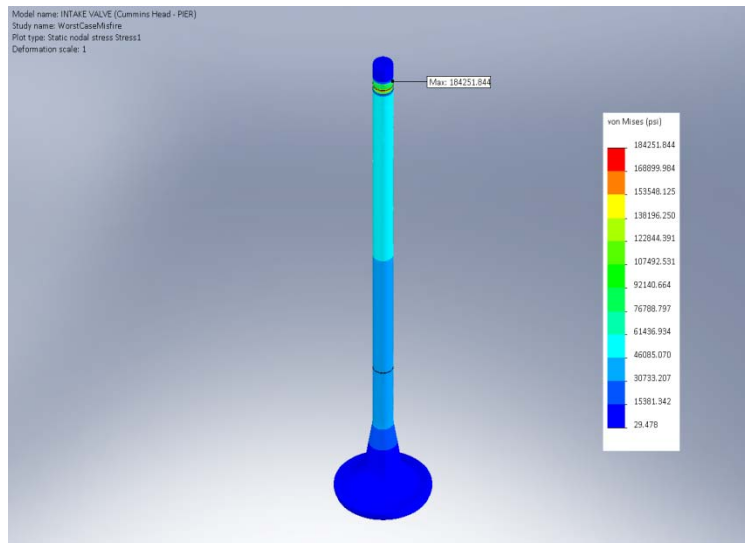
**Figure 24: Hydraulic Rail FEA Overview**



Source: Sturman Industries

Another example of the application of the FEA for the system is shown in Figure 25. The production engine valves are going to be used for this application of the HVA system. Since the valve keeper geometry had to be modified to allow the interface with the HVA system, an analysis was performed to insure that the stress on the production valves would be acceptable.

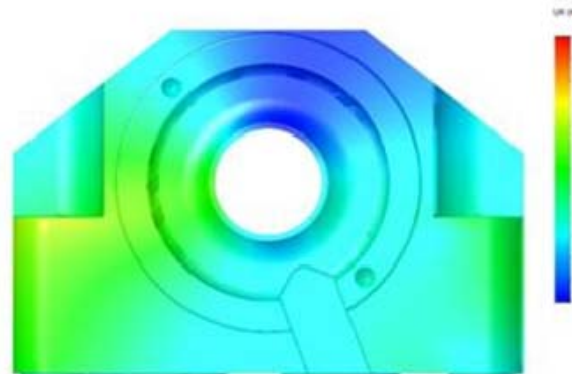
**Figure 25: ISX15 Stock Engine Valve Tip FEA Overview**



Source: Sturman Industries

Another example of the application of FEA is shown in Figure 26. Although many components of the production control valve are to be utilized, a new body was designed to properly capture the actuation fluid. This housing was reviewed for proper operation with bolt clamp load and full oil pressure as shown in the following figure.

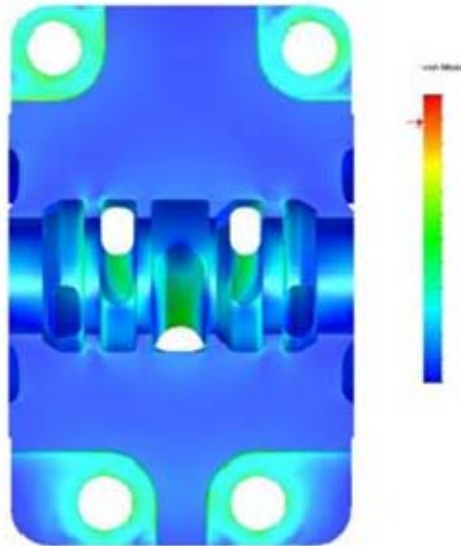
**Figure 26: HVA Control Valve Bore Distortion**



Source: Sturman Industries

The bolt clamp load and the separating pressure both tend to shorten the spool bore causing it to clamp down top to bottom. The bore distortion under full load is smaller than the minimum allowed spool to bore clearance and is therefore acceptable. The housing stress under full pressure is shown below in Figure 27. The valve housing stresses under full load are low and satisfy both static and fatigue failure criterion.

**Figure 27: HVA Valve Housing Stress Analysis Results**



Source: Sturman Industries

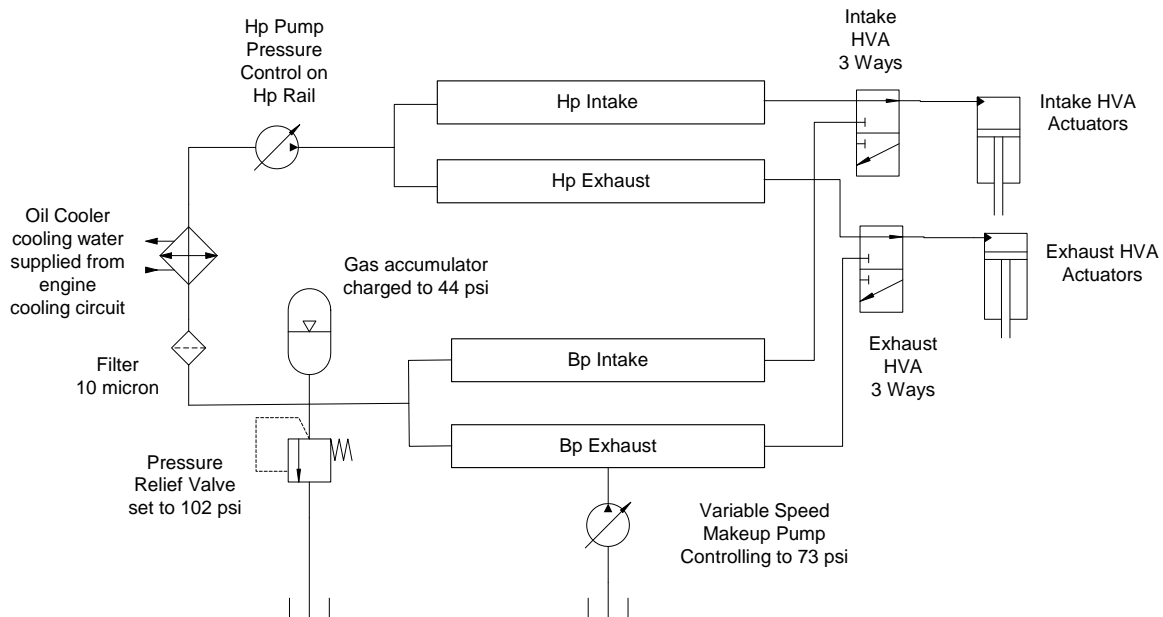
A full Computational Fluid Dynamics (CFD) analysis was performed on the control valve in both the supply to control and control to vent spool positions in order to determine the valve pressure drop characteristics and the magnitude of the flow forces on the spool. The axial and radial flow forces on the spool in both the supply to control and control to vent positions were within acceptable levels.

# CHAPTER 4: Hydraulic Supply System Design

## 4.1 System Overview

The hydraulic supply system for the HVA system is shown schematically below in Figure 28.

**Figure 28: Hydraulic Supply System Schematic**



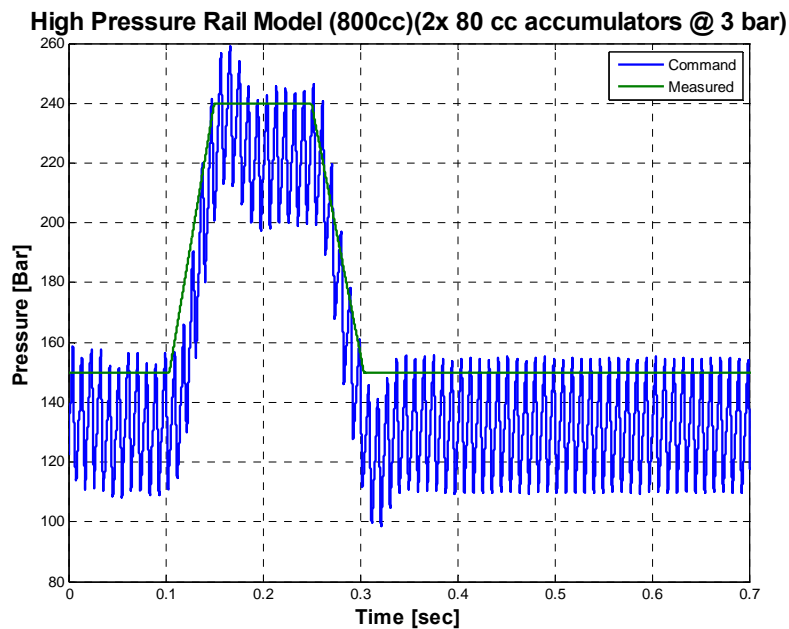
Source: Sturman Industries

The HVA system is driven using engine oil as the working fluid. Filtered and cooled engine oil enters a variable displacement pump which delivers pressurized oil to the high pressure rails at the HVA controller desired pressure. The high pressure rail commanded pressure will vary from 50 bar (725 psi) to 200 bar (2900 psi) depending on the engine operating conditions. The HVA system draws high pressure oil from the high pressure rails and exhausts the oil to the back pressure rails. The average pressure in the back pressure rails is controlled to 5 bar (73 psi) using a combination of a variable speed makeup pump to replace the oil lost due to leakage and a pressure relief valve to dump excess flow. A gas charged accumulator is added to reduce the transient pressure fluctuations in the back pressure rails. Oil from the back pressure rails runs thru a 10 micron filter and an oil to water heat exchanger before proceeding back to the high pressure pump inlet.

## 4.2 Analytical Hydraulic Supply System Predictions

The hydraulic supply system was modeled in Simulink. The analytical model includes oil compressibility effects and fluid inertia, so it is capable of predicting system resonance characteristics as well as transient pressure characteristics due to flow pulsations. The model also includes a feedback pressure controller controlling the flow from the high pressure pump to achieve the desired pressure in the high pressure rail, and a feedback controller controlling the speed of the makeup pump to maintain the desired pressure in the back pressure rail. The results for a commanded high pressure rail transient are shown below in Figure 29.

**Figure 29: High Pressure Rail Transient Prediction**

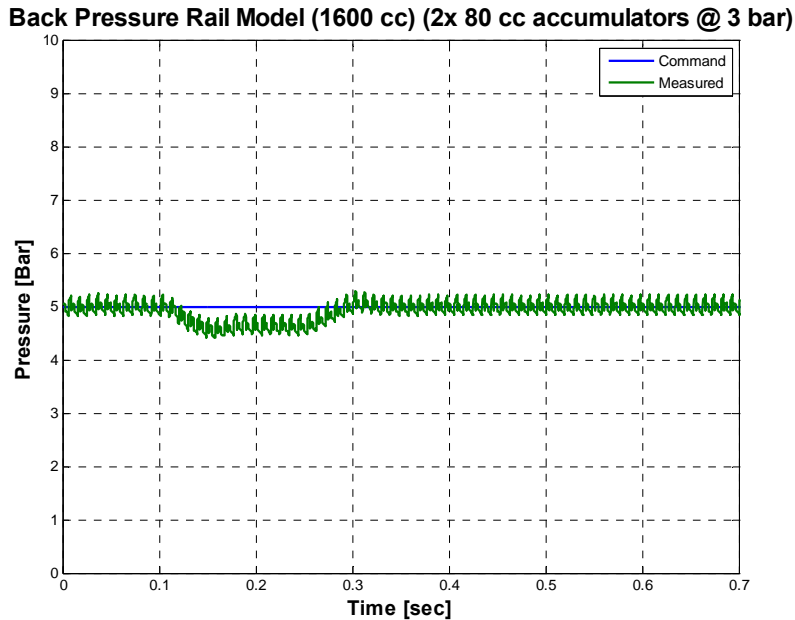


Source: Sturman Industries

The transient performance is acceptable with reasonable capacitive pressure drops and no hydraulic resonance problems in the engine operating speed range.

Since the pump flow is changing dynamically to achieve the commanded pressure change, it is necessary to look at the back pressure circuit response during this transient. The back pressure rail pressures are shown below in Figure 30.

**Figure 30: Back Pressure Rail Performance**



Source: Sturman Industries

The back pressure rails do not change average pressure during the high pressure rail transient. The intake and exhaust back pressure rails show reasonable capacitive pressure drops and high resonant frequencies well above the hydraulic excitation frequency at maximum engine speed. The gas accumulator significantly reduces the pressure fluctuations into the filter, oil cooler, and pump inlet.

### **4.3 Hydraulic Pump Overview and Mounting**

The selected pump is an 18 cc/rev (1.098 in<sup>3</sup>/rev) variable displacement piston pump capable of providing continuous pressure up to 276 bar (4,000 psi). The pump is belt driven off of the engine crank at a ratio of 1.27 times the engine speed. The pump displacement is changed to maintain the desired pressure in the intake and exhaust high pressure rails as commanded by the HVA controller. The pump control is accomplished by the HVA controller.

The pump mounting utilizes existing mounting locations on the Cummins ISX15 engine. A view of the front of the engine with a representative pump placement is shown in Figure 31. This type of mounting is consistent with other pump applications currently in production.

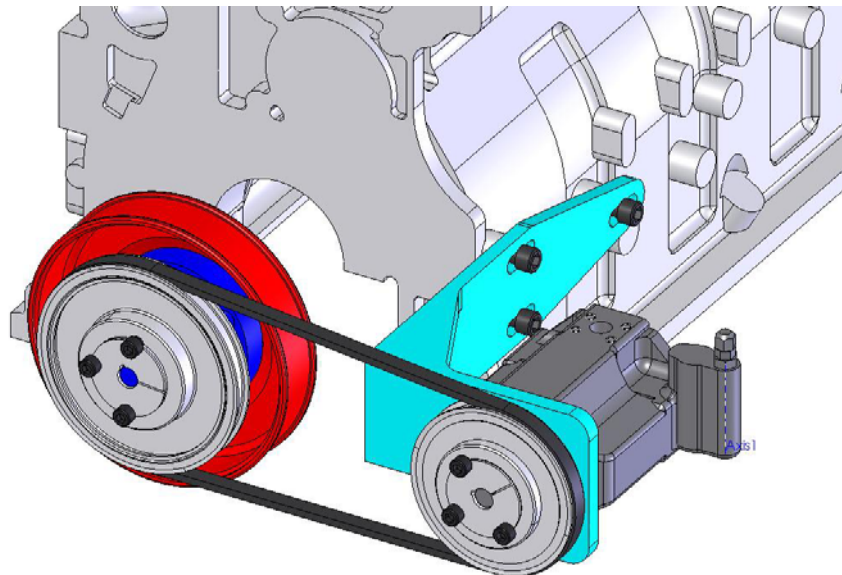
**Figure 31: Representative Hydraulic Pump Location (Front of Engine)**



Source: Sturman Industries

Figure 32 shows the layout of the hydraulic pump mounting. The pump drive consists of a “Poly Chain Carbon” cog style belt combined with pulleys to set the proper drive ratio. The mounting plate (blue) utilizes existing mounting holes on the block and interfaces to the pump with standard C-face mounting. The drive pulley is directly mounted to the crankshaft.

**Figure 32: Model of Hydraulic Pump Mounting**



Source: Sturman Industries

## **CHAPTER 5:**

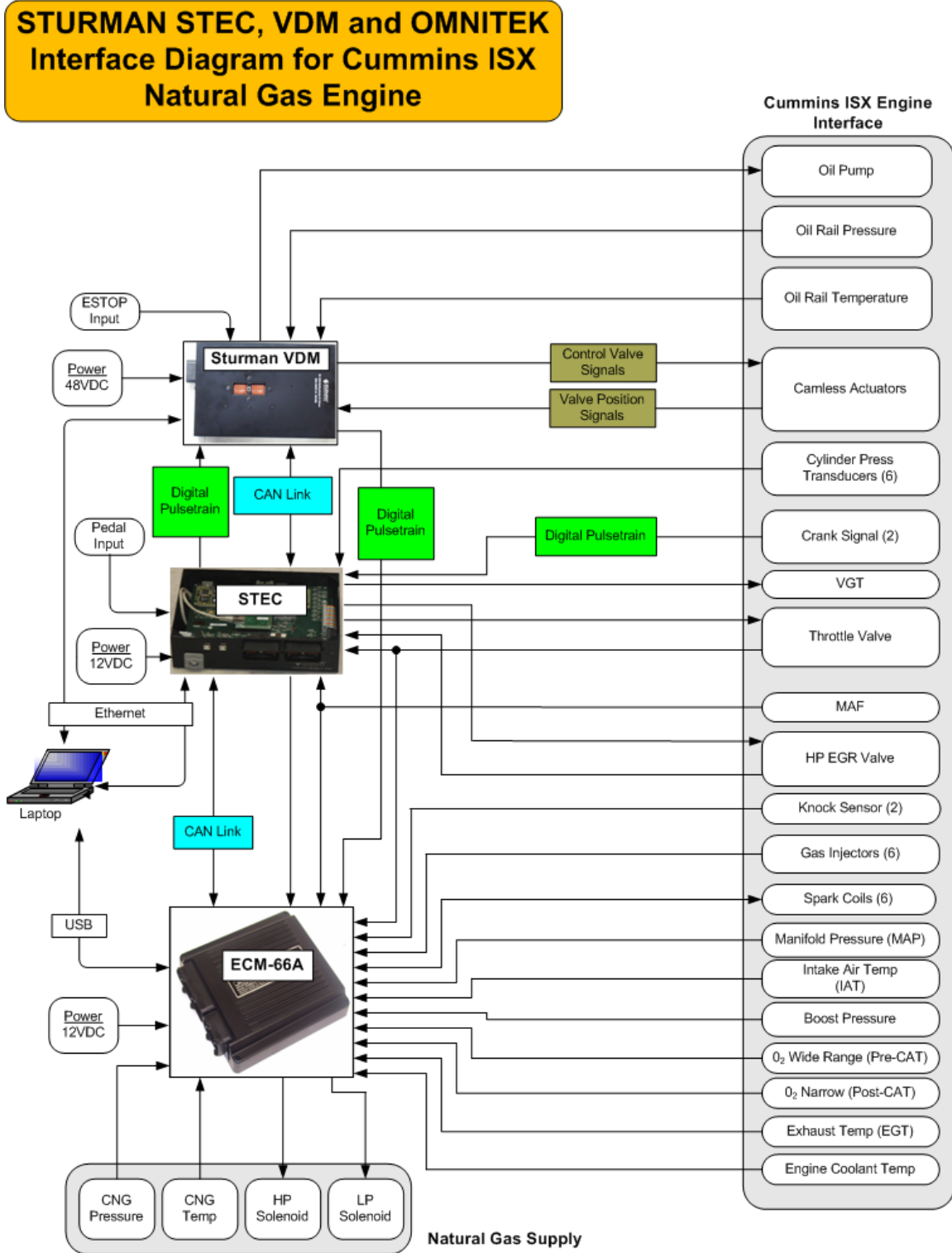
# **Controls Components Overview**

The primary controller in this system is the Sturman Total Engine Controller, or STEC. In addition to acting as the 'master' controller for all engine operation, STEC is responsible for commanding or modifying various aspects of the natural gas fuel system and the hydraulic valve actuation (HVA) system. These two subsystems have their own controller units that communicate over a Controller Area Network (CAN) to the STEC. The controllers for the fuel system and the HVA system were developed outside the scope of this program. They are briefly described in order to make this documentation self-contained. The bulk of this section describes the control code engineering for the STEC controller itself.

### **5.1 Interface Requirements**

The dynamometer test plan for PIR-08-023 requires measurement and control of many electronic components and sensors on the engine. The two subsystem controllers ("Condor" for HVA and "ECM-66A" for the Natural Gas Fuel System) each interface directly with appropriate sensors and actuators as well as communicating with the STEC over CAN. The STEC also interfaces directly to sensors and additional peripheral devices, enabling it to control all engine functions. The Condor and the STEC communicate with the Graphical User Interface (GUI) on the computer using Ethernet, while the ECM-66A uses a Universal Serial Bus (USB) connection to the computer. Figure 33 illustrates the interface requirements for this application.

Figure 33: Electronics Interface Diagram for PIR-08-023



Source: Sturman Industries

## CHAPTER 6: Fuel System Control for a Natural Gas Engine

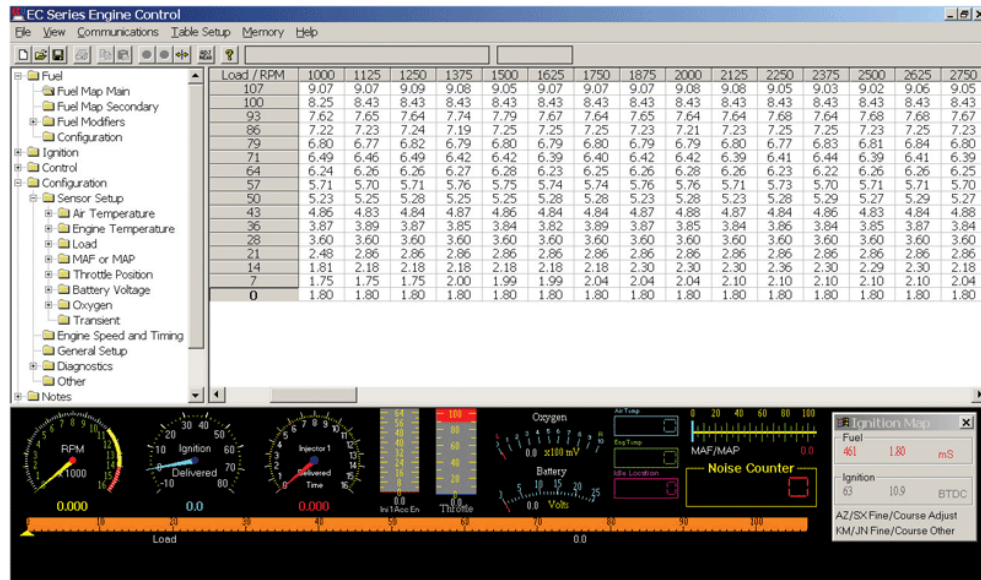
The ECM-66A is a six cylinder natural gas fuel controller provided by Omnitek, Inc. The controller used in this project has been configured to interface with the STEC over CAN, allowing STEC to modify ignition timing for the purposes of optimizing start-of-combustion timing and controlling engine knock. The ECM-66A takes in engine sensor signals and controls all aspects of the fueling. The controller unit and its user interface are shown in Figures 34 and 35 respectively.

**Figure 34: The Omnitek ECM-66A**



Source: Omnitek Engineering, Corp.

Figure 35: Example: User Interface for the Omnitek Fuel Controller

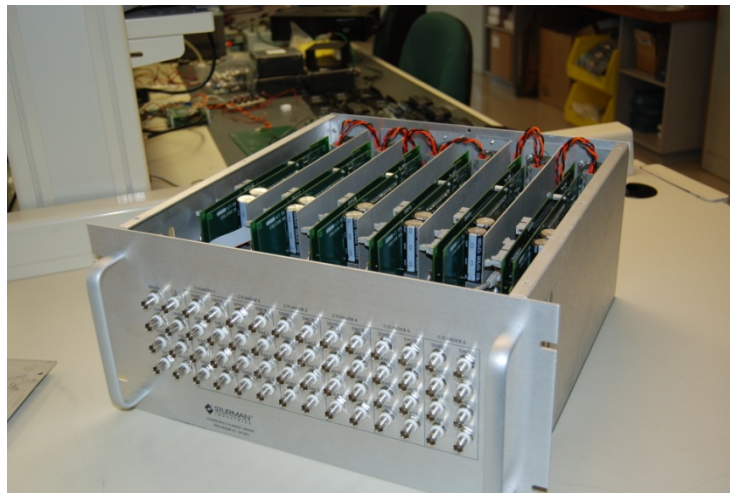


Source: Omnitek Engineering, Corp.

## CHAPTER 7: Hydraulic Valve Actuation (HVA) System Control for a Natural Gas Engine

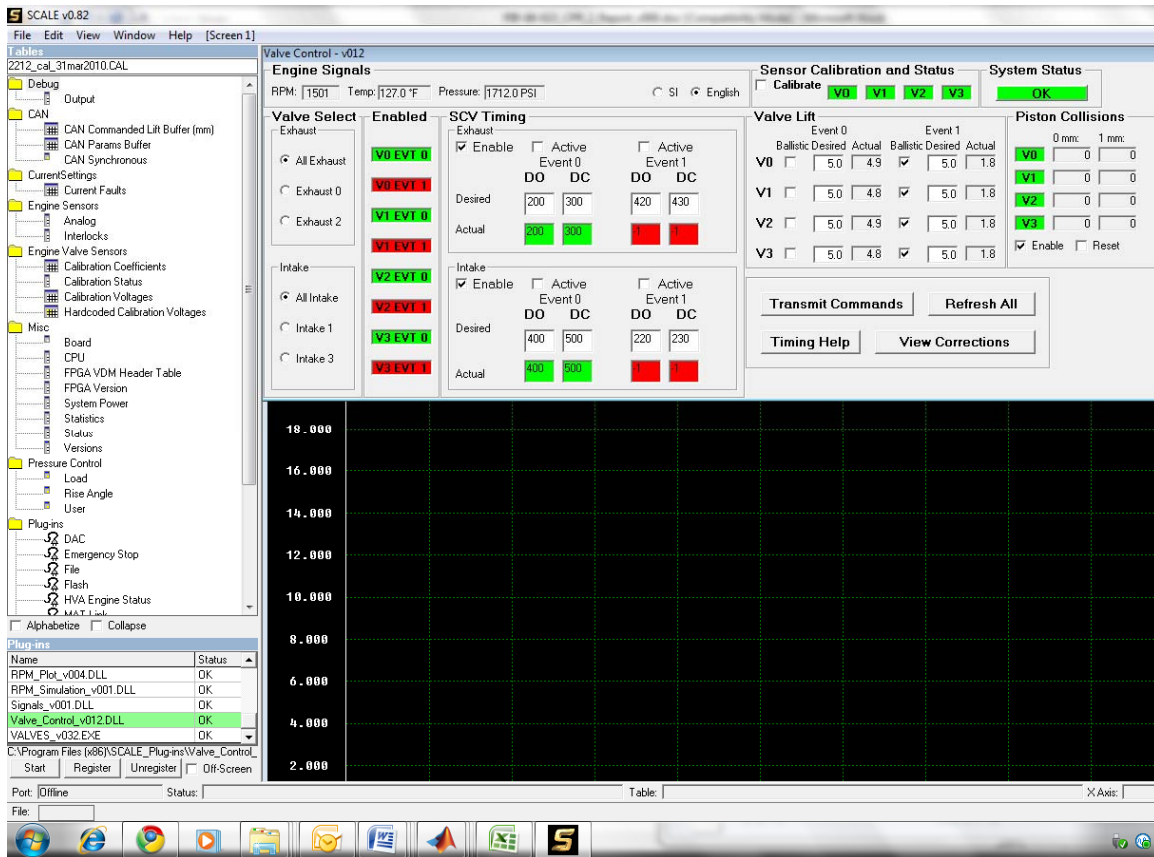
The Condor HVA controller controls all aspects of the engine valve timing subject to closed loop performance feedback and system safety algorithms. Six CAN messages are defined for communication with the Condor: two valve command messages, two valve status messages, one global command message and one global status message. The valve command messages define the requested valve profile commands on a per-valve basis, while the valve status messages relay actual valve profile measurements for use with the feedback algorithms. Global status and command messages are used to monitor and command, respectively, system-wide parameters such as oil rail pressure. On this single-lift system, the Condor controls valve opening time and valve closing time (independently for each valve) for up to two valve events per engine cycle. The Condor box is shown in Figure 36, and its user interface is shown in Figure 37.

**Figure 36: Condor Controller (Shown with Lid Removed)**



Source: Sturman Industries

Figure 37: Condor's SCALE User Interface (Typical)

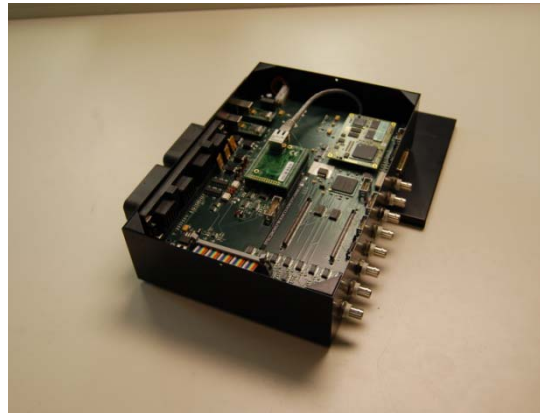


Source: Sturman Industries

## CHAPTER 8: Engine Control of a Natural Gas Engine

The STEC controller unit is shown in Figure 38. Algorithms in the firmware perform the engine control tasks. Monitoring sensor information gathered from the system, the algorithms use a combination of calibration tables and feedback control schemes to determine commands for the fuel system, the HVA system, and the engine peripherals.

**Figure 38: STEC Controller (Shown with Lid Removed)**



Source: Sturman Industries

### 8.1 Overall Structure of the STEC Control Code

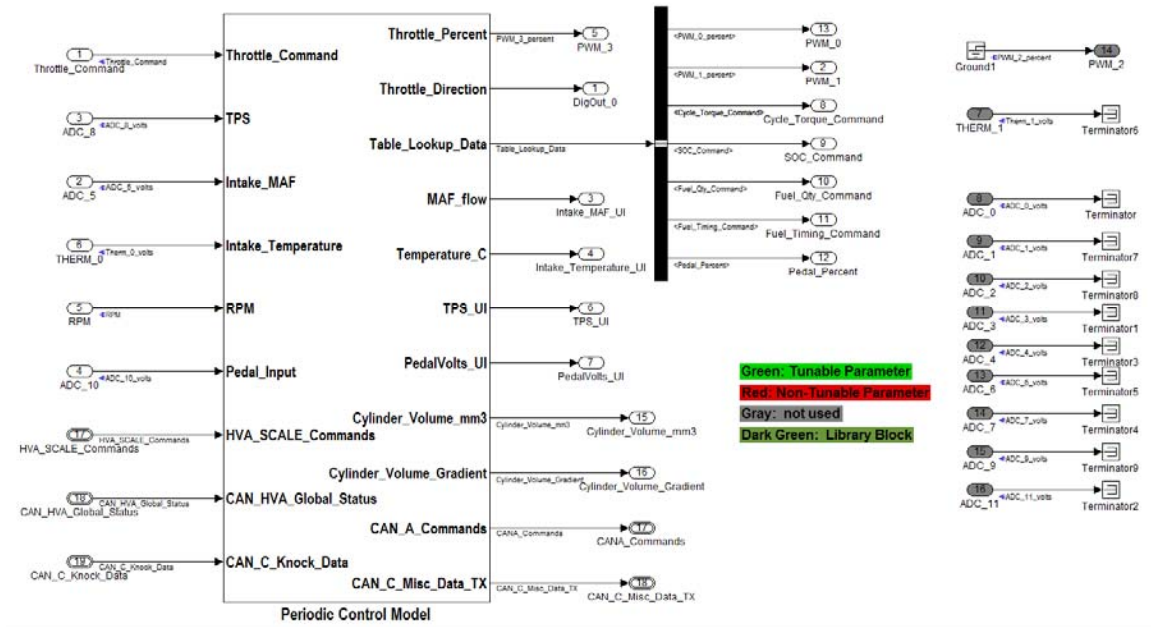
The control code for the STEC functions is implemented in C, and separated into a hand-coded hardware abstraction layer that interfaces to the electrical hardware and an auto-generated algorithm layer that is produced from models built in the Simulink environment. The algorithm level software builds upon previous applications but is unique for each project, whereas the base layer is common among projects and was developed prior to the start of PIR-08-023.

Within the algorithm layer, there are two execution units: the periodic unit and the synchronous unit. The periodic unit has been customized for the PIR-08-023 application whereas the synchronous unit was developed in its entirety prior to this project. Each of these is detailed in the following two sections.

### 8.2 Periodic Functions

The algorithms in the periodic model are updated at a constant frequency, usually 100 Hz. The top level model for the periodic execution unit is illustrated in Figure 39 primarily illustrates the sensor inputs and actuator outputs.

**Figure 39: Illustration of the Top-Level Simulink Model in the Periodic Execution Unit Showing I/O for the Unit**

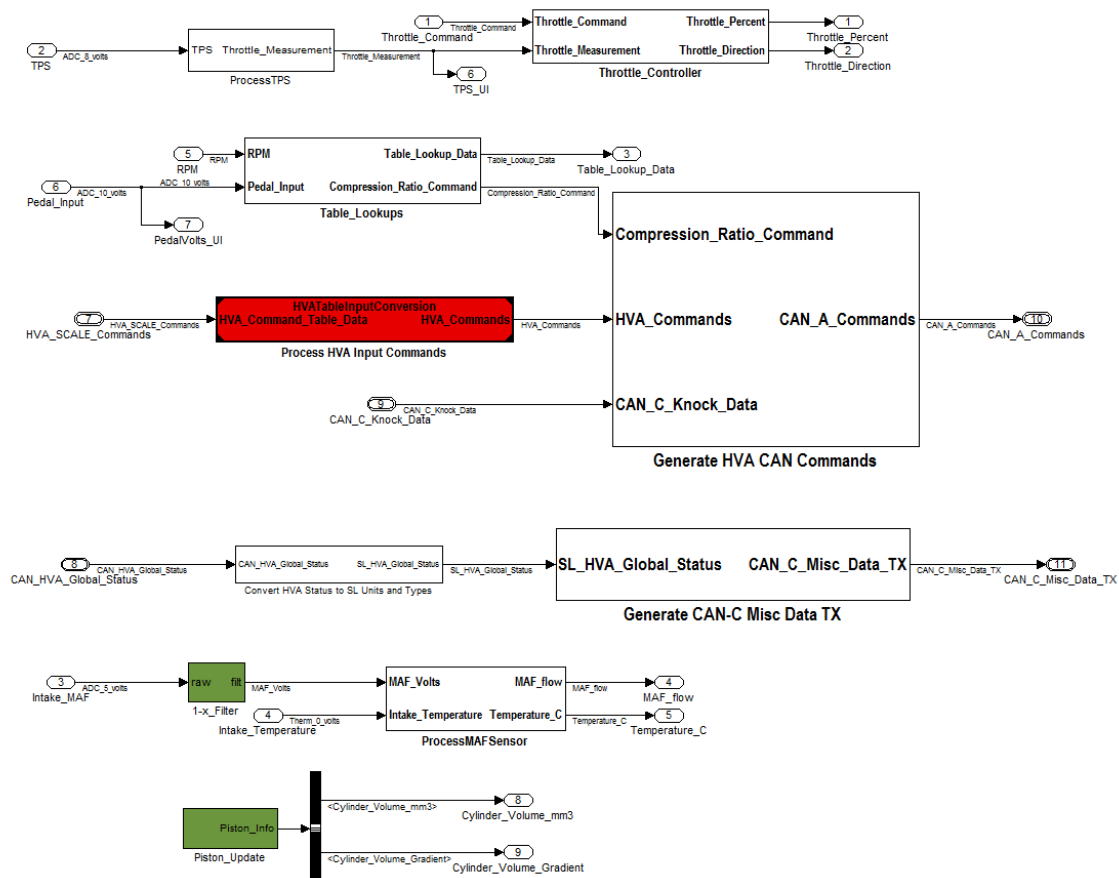


Source: Sturman Industries

Figure 40 expands the *Periodic Control Model* block and shows a breakdown of the individual algorithms at a high level. Periodic algorithms include:

- Throttle Control
- Calibration Table Look-ups
- Modifications to Intake Valve Close (IVC) Timing
- Control of Compression Ratio
- Control of Knock
- Mass Airflow (MAF) Sensor Processing
- Fuel Enable Determination
- Piston Position Update

**Figure 40: Illustration of the Functional Level Model in the Periodic Unit Showing Many of the Algorithms Contained Within the Unit**



Source: Sturman Industries

### 8.2.1 Throttle Control

The Throttle Control algorithm is contained within the *Throttle\_Controller* block shown in Figure 40 and controls the throttle percentage and direction based on user input. The algorithm is implemented using a user-defined throttle map and a proportional-integral (PI) controller.

### 8.2.2 Calibration Table Look-ups

The majority of the Calibration Lookup Tables are contained within the *Table\_Lookups* block shown in Figure 41 Using engine speed and pedal inputs, the look up tables determine values for the following parameters:

- Torque Command
- High Pressure Exhaust Gas Recirculation (EGR) Percent
- Turbo Command
- Start of Combustion Command

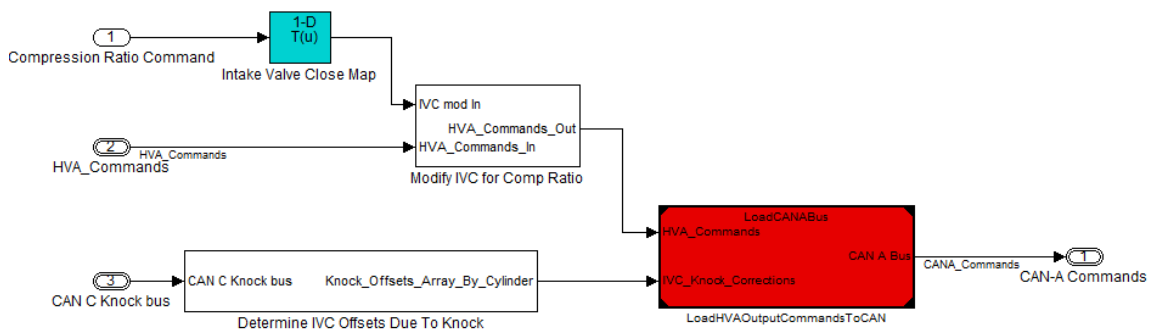
- Ignition Timing Command
- Compression Ratio Command

The table values will be mapped and populated at the start of dynamometer testing for this engine. They are housed within the software calibration file for this project and may be edited by the user at any time using the SCALE user interface program.

### 8.2.3 Modifications to Intake Valve Close (IVC) Timing

Engine valve timing for the HVA system will be commanded through the user interface for each individual valve of the system. The STEC closed-loop software provides a means to adjust the intake valve close (IVC) timing of each valve in order to monitor and control both the compression ratio and the engine knock. The algorithm for controlling the IVC timing is housed in the *Generate HVA CAN Commands* block shown in Figure 41. The expanded view is shown in Figure 42.

**Figure 41: Intake Valve Close Adjustment Algorithms**



Source: Sturman Industries

When IVC modifications for compression ratio control are enabled, the *Modify IVC for Comp Ratio* block replaces the user interface values for IVC with the values obtained from calibration maps. The *Determine IVC Offsets Due to Knock* block further adjusts the IVC timing according to calibration maps designed to eliminate knock. If the STEC is unable to eliminate knock via IVC timing alone, the Omnitek ECM-66A controller assumes this task and eliminates engine knock via spark timing.

### 8.2.4 Mass Airflow (MAF) Sensor processing

The *ProcessMAFSensor* block shown in **Error! Reference source not found.** implements calibration look-up tables that determine Mass Air Flow (MAF) and engine intake air temperature values from the voltage readings of the sensors.

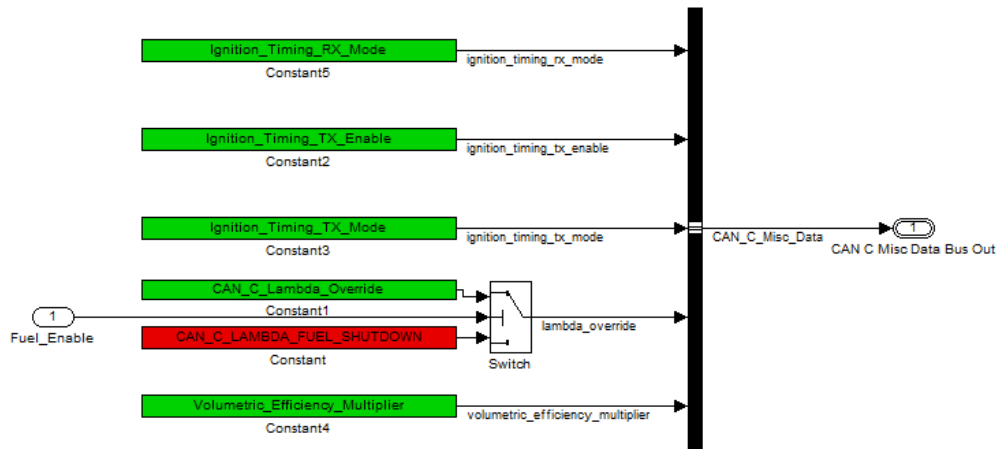
### 8.2.5 Fuel Enable determination

The *Generate CAN-C Misc Data TX* block of Figure 42 prepares the miscellaneous data bus data for the Omnitek ECM-66A controller via the CAN C communications link.

Essential to this block is the determination of Fueling Disable through the *lambda\_override* parameter. The overall control system allows the STEC to command a fuel shutdown through this parameter if any of the HVA system parameters issue a warning.

An excerpt from the *Generate CAN-C Misc Data TX* block is shown in Figure 42. An “AND” block polls the Fueling Disable parameters from each of the engine cylinders to determine overall engine fueling relevance. This parameter comes into the block as a *Fuel\_Enable* input.

**Figure 42: Preparation of CAN C Miscellaneous Data**



Source: Sturman Industries

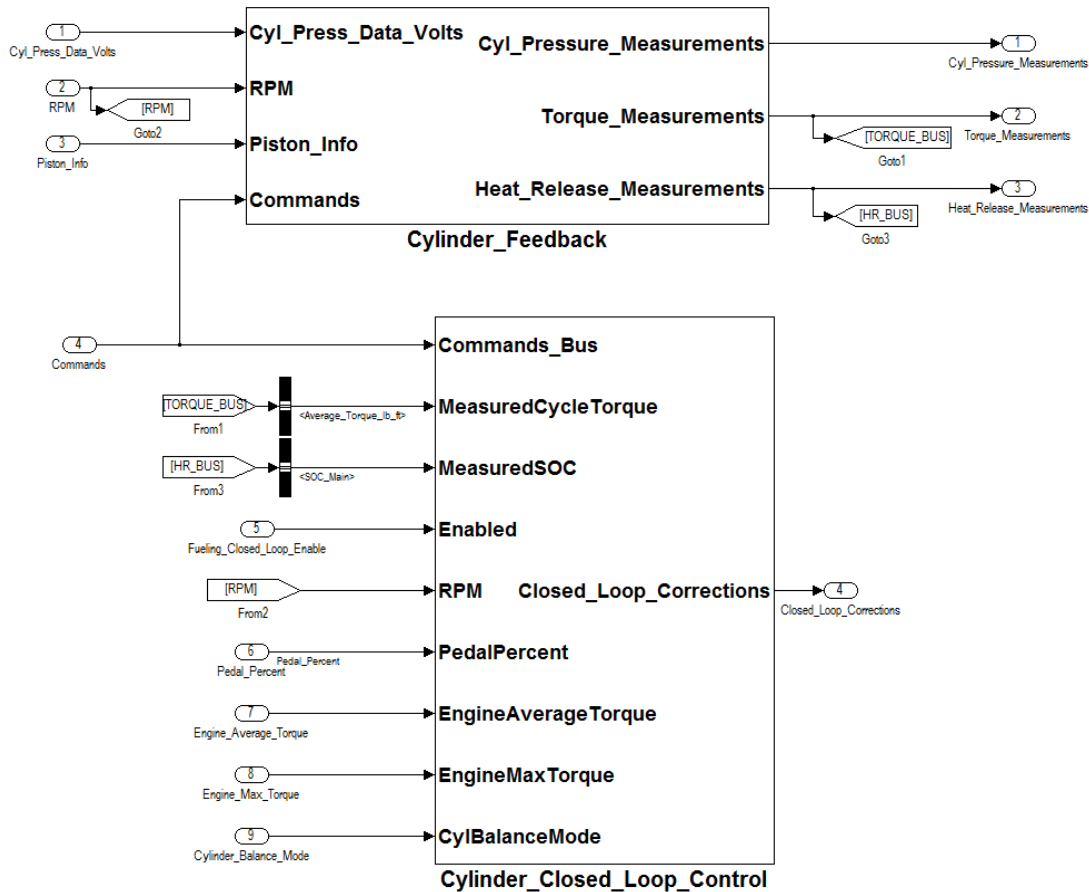
### 8.2.6 Piston Position Update

The *Piston\_Update* block of Figure 42 contains a utility function that keeps track of the engine crank angle for use by angle-based algorithms in the STEC.

## 8.3 Synchronous Functions

The algorithms in the synchronous unit are updated at every engine cycle regardless of engine speed. The top-level model for the synchronous unit is illustrated Figure 43. This portion of the model-based control code was developed prior to the PIR-08-023 program start, but it interfaces with the specific code developed for this project.

**Figure 43: Top Level Synchronous Control Model (Developed Outside of PIR-08-023)**



Source: Sturman Industries

The two main functional blocks of the synchronous model are the *Cylinder\_Feedback* block and the *Cylinder\_Closed\_Loop\_Control* block. The *Cylinder\_Feedback* block generates cylinder pressure measurements, torque measurements and heat release measurements from engine sensor signals and system commands. The *Cylinder\_Closed\_Loop\_Control* block determines the fuel timing necessary to balance the torque output from each cylinder.

## 8.4 Instructions to Operate the Code

The SCALE user interface is used to control both the Condor and the STEC graphically from a personal computer. The primary function of the Sturman Calibration Editor (SCALE) is to provide a flexible communication link between the PC and the controller. Its generic and expandable design allows it to be used for many different applications. The SCALE software (written by Sturman Industries) is packaged with up to date electronic help files describing its use. A typical user interface display is shown in Figure 44. SCALE provides display of pertinent system parameters, an input mechanism for writable parameters, and a graphical display of the HVA valve profiles. Displays may be

customized for individual applications, and a system-specific calibration (text) file contains all parameters unique to an application.

The Table of Contents for SCALE help is shown in Figure 44.

**Figure 44: SCALE Help Table of Contents**



Version 0.82

### **Table Of Contents**

- [1. Introduction](#)
  - [1.1 Overview](#)
  - [1.2 Installation](#)
  - [1.3 Connection](#)
  - [1.4 Tables And Plug-ins](#)
  - [1.5 Calibration Files](#)
  - [1.6 Window Files](#)
- [2. User Interface](#)
  - [2.1 Setup](#)
  - [2.2 File Menu](#)
  - [2.3 Edit Menu](#)
  - [2.4 View Menu](#)
    - [2.4.1 Tables](#)
    - [2.4.2 Plug-ins](#)
    - [2.4.3 Status](#)
  - [2.5 Window Menu](#)
  - [2.6 Help Menu](#)
  - [2.7 Board Menu](#)
  - [2.8 Screen Menu](#)
- [3. Errors](#)
  - [3.1 Communication Error](#)
  - [3.2 File Error](#)
  - [3.3 Plug-in Error](#)
- [4. Miscellaneous](#)
  - [4.1 Command Line Options](#)
  - [4.2 Minimum System Requirements](#)
  - [4.3 USB Driver Installation](#)
- [5. Troubleshooting](#)
  - [5.1 Ethernet Connection](#)

Source: Sturman Industries

# CHAPTER 9:

## HVA Components Overview and Validation

The HVA system is comprised of 24 independent valve actuators (12 intake, and 12 exhaust) which can operate the engine valves up to 2200 rpm and 15.0 mm of lift. One dual coil 3-way control valve is utilized on each actuator to control the flow of hydraulic fluid to the control volume. Each actuator contains a boost piston and a drive piston. Boost lift is set to 3.0 mm, and drive lift is set to 15.0 mm. Closing of the engine valve is realized with a return piston that acts upon the push plate to close the valve. Orifices are located in specific locations of the valve lift to slow down the engine valve before it hits a hard stop.

### 9.1 HVA System Validation

Before the HVA system is installed on the engine for dynamometer testing, it is assembled, documented, calibrated, and operated at specific test points to ensure trouble free operation on the engine. Items included in the validation test plan are shown below in Table 4. Since the cylinder head had been used for previous testing, it received a valve job before assembly of the HVA system.

**Table 4: HVA System Validation Test Plan**

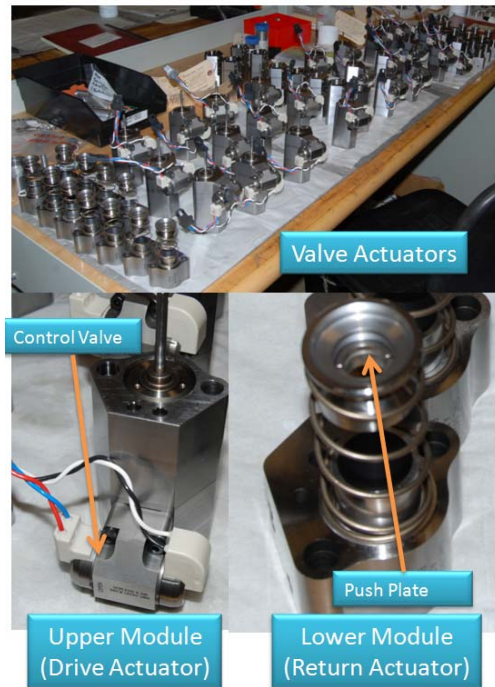
Task #	
1	Metrology (including documentation of part numbers, lapping engine valve to cylinder head valve seat)
2	Assembly (including documentation of part numbers vs. location, metrology: ensure >0.5mm clearance from boost pin to upper module when engine valve is seated, de-magnetize all parts before assembly)
3	HP Rail Pressure Sensor Calibration
4	BP Rail Pressure Sensor Calibration and Lift Pump Setup
5	Set backpressure regulator (5bar)
6	Basic functional test of HVA system to verify all control valves are operational. Check seating with 2-point calibration. Knee should occur 0.8-1.2mm above seating (1.0mm nominal, less than 0.1mm valve-to-valve is acceptable). Size orifices for landing and full lift seating
7	Run system at high speed and high pressure to fully seat valve faces and keepers, also remedy any issues with valve performance
8	Grind push plates to achieve full lift of 14.9-15.1mm (15.0mm nominal)
9	Calibrate coil sensors for lift and temperature calibration
10	Collect data for hydraulic delay tables and rpm compensation talbes
11	Generate hydraulic delay tables and rpm compensation tables (using engine geometry information provided by customer)
12	Populate hydraulic delay and rpm compensation talbes
13	Map minimum duration and minimum separation tables
14	HSU and Lift Pump tuning
15	Map pressure map
16	Run validation scripts (trial run)
17	Verify calibration file settings and correct software release, calibration review
18	Run validation scripts
19	Summarize results and send to customer

Source: Sturman Industries

## 9.2 HVA System Assembly

The assembly of the HVA system was done as sub component groups. Items such as the control valve, upper actuator, lower actuator, and sensor assemblies were put together independent of each other. Once that initial assembly process was complete, these sub-assemblies were combined to complete the assembly. Figure 45 below shows the components during the assembly steps.

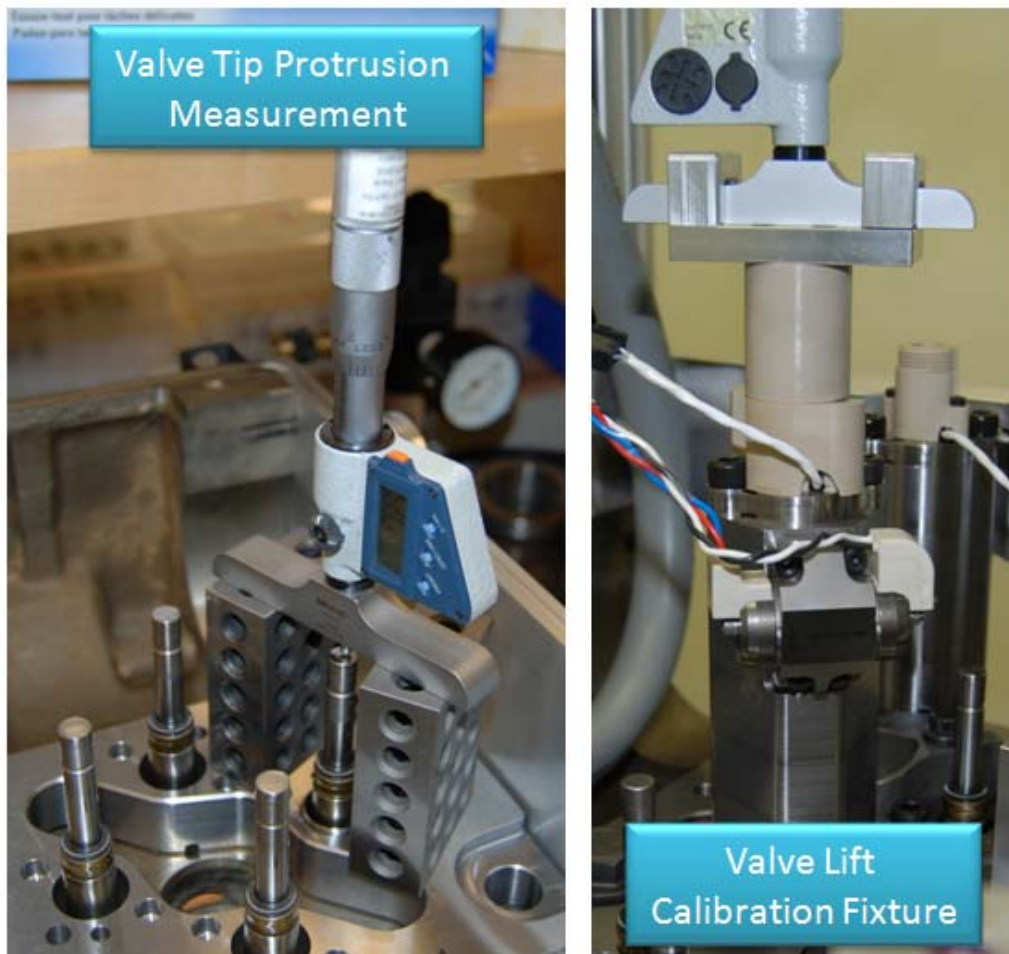
**Figure 45: HVA Actuator Modules**



Source: Sturman Industries

Setup of the HVA system consisted of taking measurements of each component to ensure correct operation. Items documented include engine valve tip protrusion, module measurements, and valve position sensor calibration. Figure 46 below shows an example of the valve tip protrusion measurement and the valve position calibration fixture.

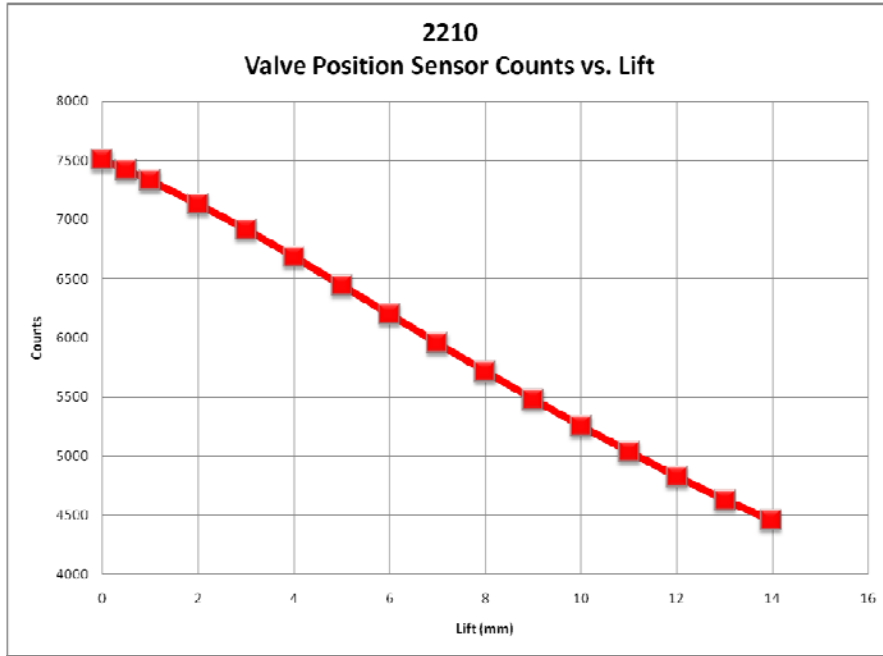
**Figure 46: Valve Tip Protrusion Measurement Setup and Assembled Exhaust Module with Calibration Fixture**



Source: Sturman Industries

The sensor for each engine valve generated a specific calibration in analog-to-digital (A/D) counts vs. lift (mm). The sensor used in this application was a custom design by Sturman Industries. It provides the accuracy, repeatability, and temperature compensation required for this HVA system. An example of the calibration curve generated is shown below in Figure 47.

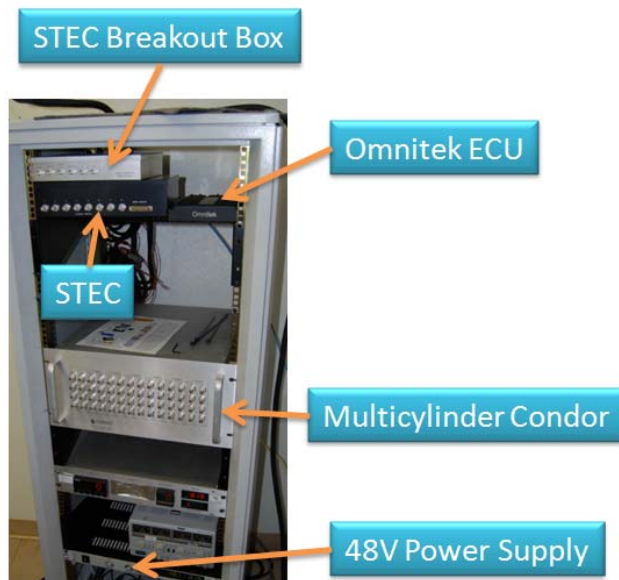
**Figure 47: HVA Valve Position Sensor Calibration Example**



Source: Sturman Industries

The test cell setup for bench testing included an electronics rack that contains all the items necessary to operate the engine. The electronics hardware as described earlier is shown below in Figure 48. This same electronics rack was moved into the dynamometer test cell for engine testing.

**Figure 48: Electronics Rack**



Source: Sturman Industries

### 9.3 Single Valve Testing

Initial single valve testing was performed to ensure the orifice sizes selected during the design phase provide the desired flank rates. A test rail was made to supply only one exhaust or one intake valve as shown below in Figure 49. Since the vent passages between two intake valves or two exhaust valves are bridged in the transfer plate, a block off plate was installed on the transfer plate opposite from the valve location being tested.

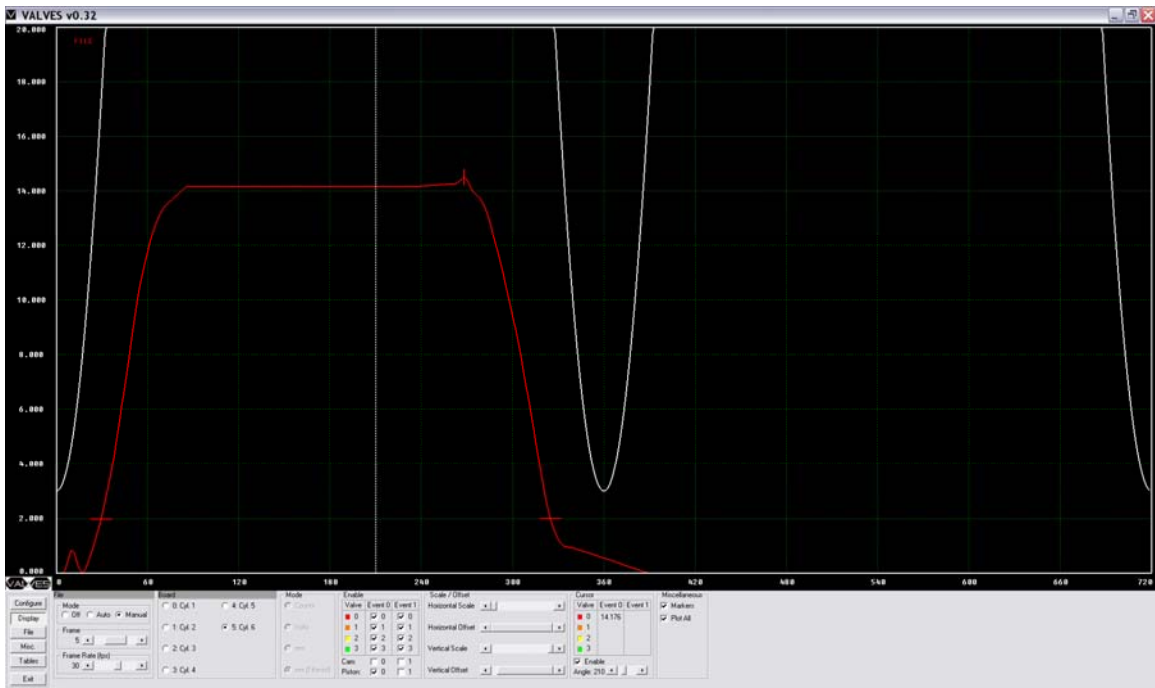
**Figure 49: Single Exhaust Valve Test Setup**



Source: Sturman Industries

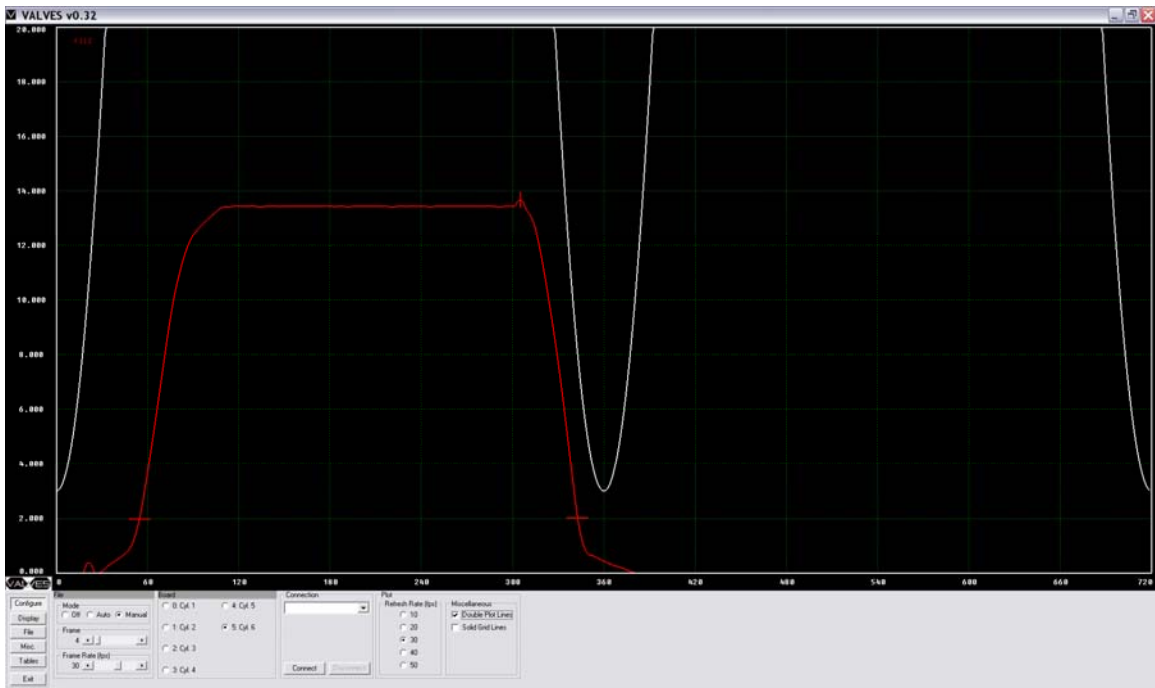
Control of the single valve testing was performed with the multi-cylinder electronics that will be utilized during the engine testing. The exhaust valve shows a fast takeoff and close flank with reduced velocity into full lift and into seating. This matches the model predictions. The intake valve shows a slow takeoff to allow for valve overlap during exhaust Top Dead Center (TDC), fast open and close flank, as well as reduced velocity into full lift and seating. Once again, this performance is consistent with the analytical predictions performed during the design phase of this program (see Figure 50 and Figure 51). The small spikes seen right before valve takeoff and just before the valve begins to close were later addressed and eliminated by shielding the sensor housings.

Figure 50: Valve Motion of Single Exhaust Valve



Source: Sturman Industries

Figure 51: Valve Motion of Single Intake Valve



Source: Sturman Industries

Test points were recorded for single valve testing at 80°C oil temperature and supply pressures from 50 to 200 bar in 50 bar increments. The data was post processed using

MATLAB and the valve velocities were compared to what was simulated. Table 5 and Table 6 below list the simulated and the measured flank velocities. The percent difference between simulation and measured is as high as 138 percent as the orifice which controls valve seating was manufactured at a reduced size to be able to increase the orifice area if necessary. Since the valve trace does not exhibit any 'bounce out' when the valve engages the seating orifice, SI has decided to leave the orifice sizes at their current size to minimize risk in hardware modification. The reduced seating velocity will also provide increased durability of the engine valve seats. In addition, the target for open and close flanks was to keep the area under the curve greater than what the stock camshaft provides. Even with the flank velocities slightly slower than simulated this target was still achieved.

**Table 5: Simulated vs. Measured Exhaust Valve Flank Velocity**

Pressure -----> Velocity	Exhaust Valve							
	Simulation				Measured			
	50 (bar)	100 (bar)	150 (bar)	200 (bar)	50 (bar)	100 (bar)	150 (bar)	200 (bar)
Avg Open Ramp (m/s)	N/A	N/A	N/A	N/A	N/A	N/A	N/A	N/A
Avg Open Flank (m/s)	2.06	3.04	3.80	4.46	1.54	2.31	3.02	3.57
Max Open Flank (m/s)	3.04	4.50	5.60	6.50	1.97	2.99	3.79	4.41
Max Lift Landing Velocity (m/s)	0.27	0.41	0.52	0.47	0.25	0.40	0.55	0.60
Avg Close Flank (m/s)	1.73	2.45	3.00	3.51	1.15	1.72	2.16	2.53
Max Close Flank (m/s)	2.24	3.18	3.91	4.55	1.46	2.21	2.83	3.45
Seating Velocity (m/s)	0.16	0.24	0.30	0.35	0.07	0.12	0.15	0.17
	% Difference Simulation from Measured							
Avg Open Flank (m/s)	34.03	31.60	25.95	24.83				
Max Open Flank (m/s)	54.08	50.50	47.76	47.39				
Max Lift Landing Velocity (m/s)	6.00	2.50	-5.45	-22.19				
Avg Close Flank (m/s)	50.04	42.44	39.21	38.74				
Max Close Flank (m/s)	53.85	43.89	38.16	31.81				
Seating Velocity (m/s)	138.46	108.70	100.00	107.83				

Source: Sturman Industries

**Table 6: Simulated vs. Measured Intake Valve Flank Velocity**

Pressure -----> Velocity	Intake Valve							
	Simulation				Measured			
	50 (bar)	100 (bar)	150 (bar)	200 (bar)	50 (bar)	100 (bar)	150 (bar)	200 (bar)
Avg Open Ramp (m/s)					0.17	0.25	0.30	0.40
Avg Open Flank (m/s)	1.50	2.33	2.92	3.45	1.26	1.92	2.37	2.97
Max Open Flank (m/s)	2.00	3.20	4.00	4.79	1.55	2.35	3.03	3.55
Max Lift Landing Velocity (m/s)	0.19	0.36	0.47	0.53	0.15	0.33	0.50	0.90
Avg Close Flank (m/s)	1.90	2.68	3.30	3.80	1.65	2.37	2.83	3.50
Max Close Flank (m/s)	2.50	3.50	4.30	4.94	2.01	2.85	3.52	4.06
Seating Velocity (m/s)	0.18	0.27	0.27	0.37	0.10	0.14	0.17	0.19
	<b>% Difference Simulation from Measured</b>							
Avg Open Flank (m/s)	18.76	21.67	23.00	16.01				
Max Open Flank (m/s)	29.03	36.17	32.01	34.93				
Max Lift Landing Velocity (m/s)	23.33	9.23	-5.60	-41.33				
Avg Close Flank (m/s)	15.15	12.89	16.73	8.57				
Max Close Flank (m/s)	24.38	22.81	22.16	21.67				
Seating Velocity (m/s)	75.00	97.06	58.68	94.74				

Source: Sturman Industries

## 9.4 Multi Cylinder Assembly

The assembly of the multi cylinder hardware matches the process of assembling the single valve setup. A test fixture for the single valve test rail was replaced with the cast rail assemblies as shown in Figure 52, which were bolted to the transfer plate and placed in the cylinder head.

**Figure 52: Hydraulic Rail Assembly**



Source: Sturman Industries

Next, the head was populated with the HVA actuators and wire harnessing as shown in the figures below:

- Figure 53 – This figure shows the transfer plate and rail assembly ready for installation on the cylinder head
- Figure 54. – This figure shows the spark plug sleeves ready to be installed in the location of the stock diesel fuel injector.
- Figure 55 – This figure shows the transfer plate assembly installed in the cylinder head. The hydraulic valve actuators will be installed between the two hydraulic rails.

- Figure 56 – This figure shows the hydraulic valve actuation system fully assembled without the valve cover.
- Figure 57 – This figure shows the head assembled in the test cell with the hydraulic valve actuation hardware. This test cell was utilized for the system validation.
- Figure 58 – The fully assembled head with the valve cover is shown in this figure.

**Figure 53: Transfer Plate and Hydraulic Rail Assembly**



Source: Sturman Industries

**Figure 54: Spark Plug Sleeves**



**Spark Plug Sleeves (replaces diesel injector)**

Source: Sturman Industries

**Figure 55: Transfer Plate Assembly Installed**



**Transfer Plate Assembly Installed on Head with Engine Valves**

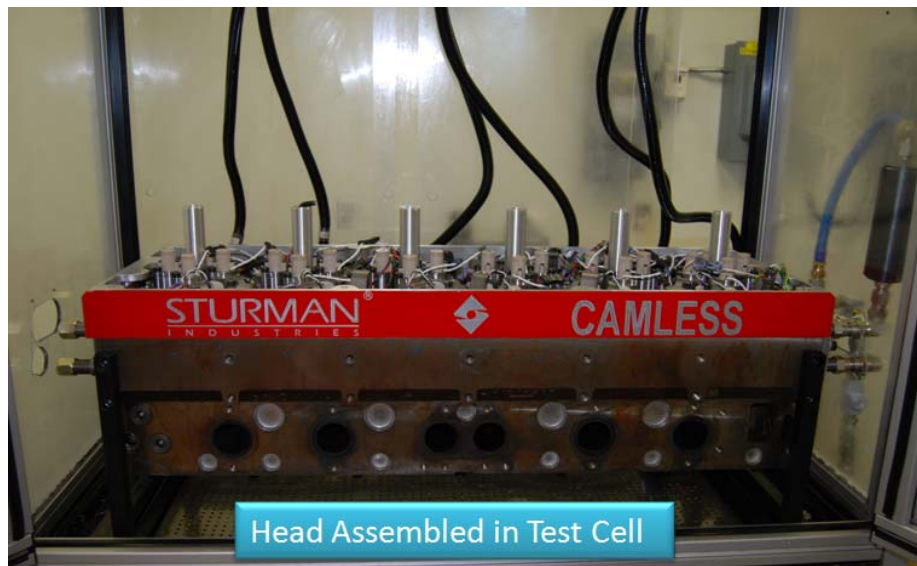
Source: Sturman Industries

**Figure 56: Head Assembly without Valve Cover**



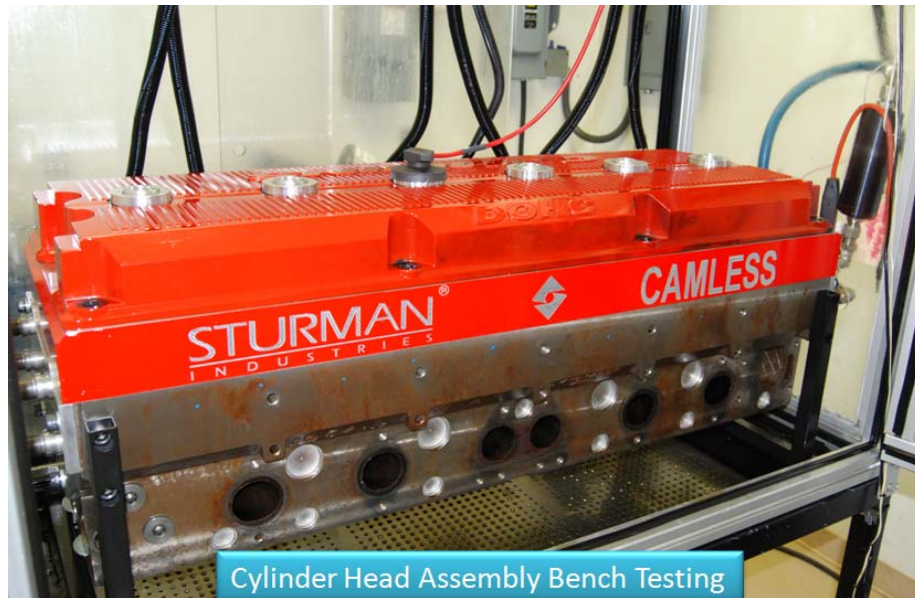
Source: Sturman Industries

**Figure 57: Head Assembled in Test Cell**



Source: Sturman Industries

**Figure 58: Cylinder Head Assembly Bench Testing**

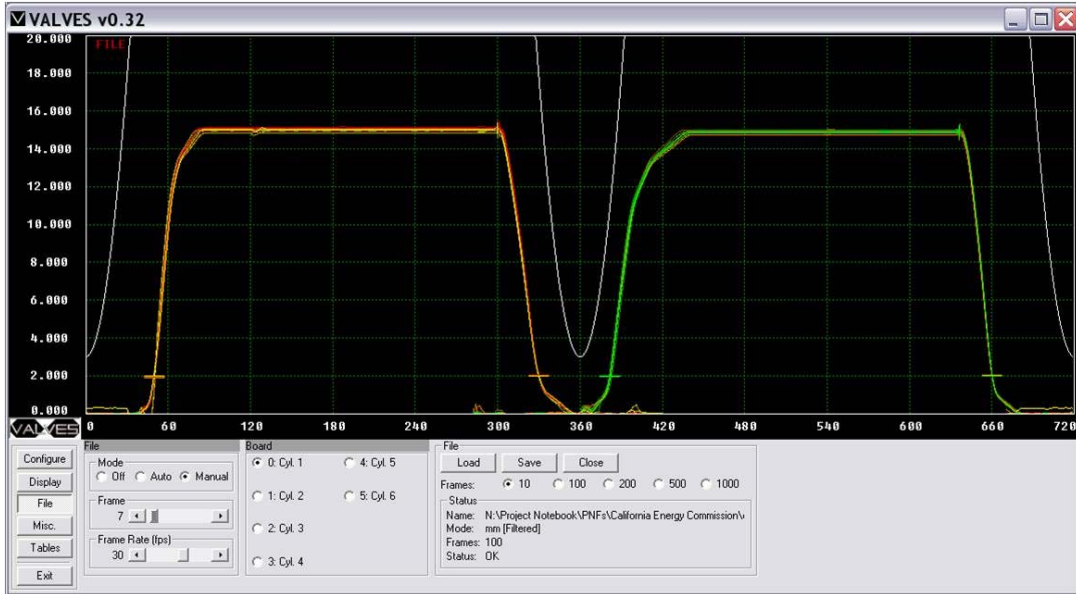


Source: Sturman Industries

## **9.5 Multi Cylinder Testing**

System tuning and calibration was performed during the multi cylinder testing phase to calibrate the valve position sensors, rail pressure sensors, and bench pump cart pressure control. This allowed for basic checks of the components with the entire multi cylinder hardware. An example of the multi cylinder valve traces is shown below in Figure 59.

Figure 59: Multi Cylinder Valve Traces Example



Source: Sturman Industries

Next, mapping was performed for the hydraulic delay tables, RPM compensation tables, and various other tables contained in the Condor control code. Once this calibration was completed, the system was ready for the validation testing.

## 9.6 Multi Cylinder Validation Testing

Bench validation testing of the HVA system consisted of acquiring performance data at various simulated engine speeds, valve timings and supply pressures. Conditions representing idle, light loads, mid loads, and full loads were tested according to Table 7 below of the validation test points matrix.

Table 7: HVA System Validation Test Points Matrix

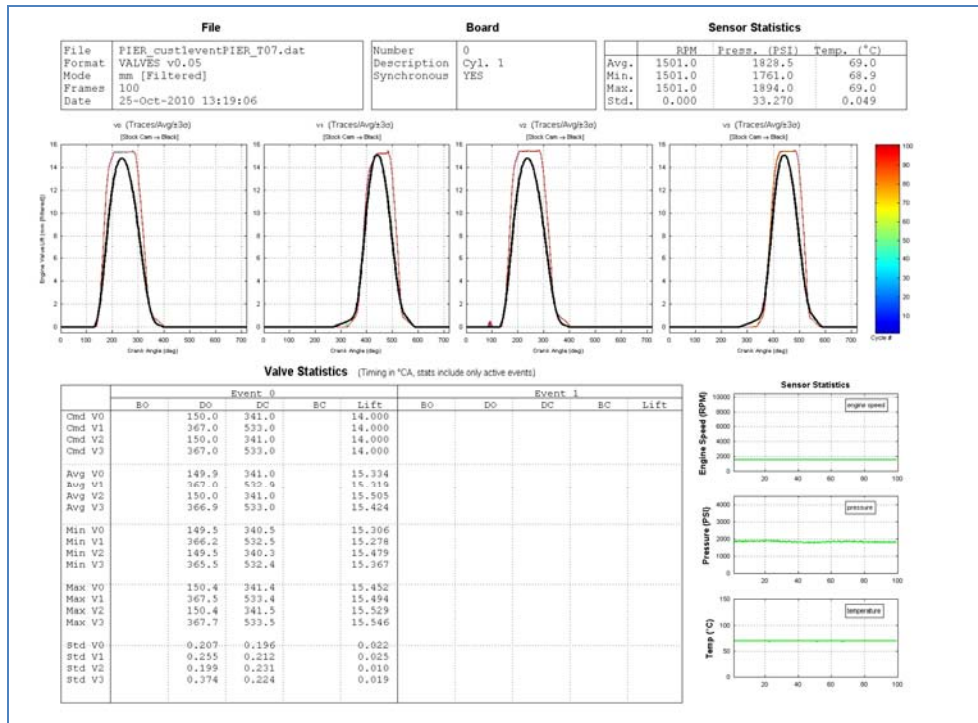
Data Pt	Temp	Speed	Lift & Timing						Pressure	Data Files
			Exhaust			Intake				
			Timing		Lift	Timing		Lift		
(#)	(deg C)	(rpm)	Open (CA)	Close (CA)	(mm)	Open (CA)	Close (CA)	(mm)	(bar)	(* .DAT)
1	100	250	146	338	15.0	384	553	15.0	50	01_Cranking_Condition
2		650	146	338	15.0	384	410	8.0	70	02_Idle
3		146	338	15.0	362	525	15.0	160	03_Max_Speed	
3A		2200	146	192	4.0	362	404		4.0	03A_Max_Speed_MinDur
4		1500	146	290	15.0	372	520	15.0	130	04_Mixed
5			160	215	8.0	390	422	4.0		05_Min_Lift
6			160	195	4.0	390	422	4.0		06_Mid_Lift
7			160	217	8.0	390	446	8.0		07_Max_Lift
8			150	341	15.0	367	533	15.0		08_Two_Event
			150	341	15.0	367	533	15.0		
			480	620	15.0	60	220	15.0		
9			150	341	15.0	367	533	15.0		09_Two_Event
	480		515	4	60	95	4			
Both Valves										
Valves 0 & 1										
Valves 2 & 3										
2nd Event (valves 0 & 1)										

Source: Sturman Industries

Target limits for the engine valve timing variability were  $\pm 2^\circ\text{CA}$  @ 600 RPM scaled linearly with engine speed to  $\pm 4^\circ\text{CA}$  @ 6000 RPM. Lift accuracy was not evaluated on this system since it was designed for fixed lift operation. Lift repeatability was evaluated during ballistic events to ensure cycle by cycle repeatability while running in this mode.

Data collection was done with Sturman’s VALVES data acquisition system. Post processing of the VALVES data was done with MATLAB to automate and calculate statistics on the valve motion. Parameters analyzed included timing variability, lift variability, and flank velocities. An example of the output files is shown below for Data Point 7. An abbreviated listing of validation test results are included in Appendix A: Multi Cylinder Validation Test Results. A review of the test points was completed by Sturman Industries and the system meets the requirements as defined for this program.

**Figure 60: Multi Cylinder Processed Data Example**



Source: Sturman Industries

Figure 61: Multi Cylinder Cycle by Cycle Review

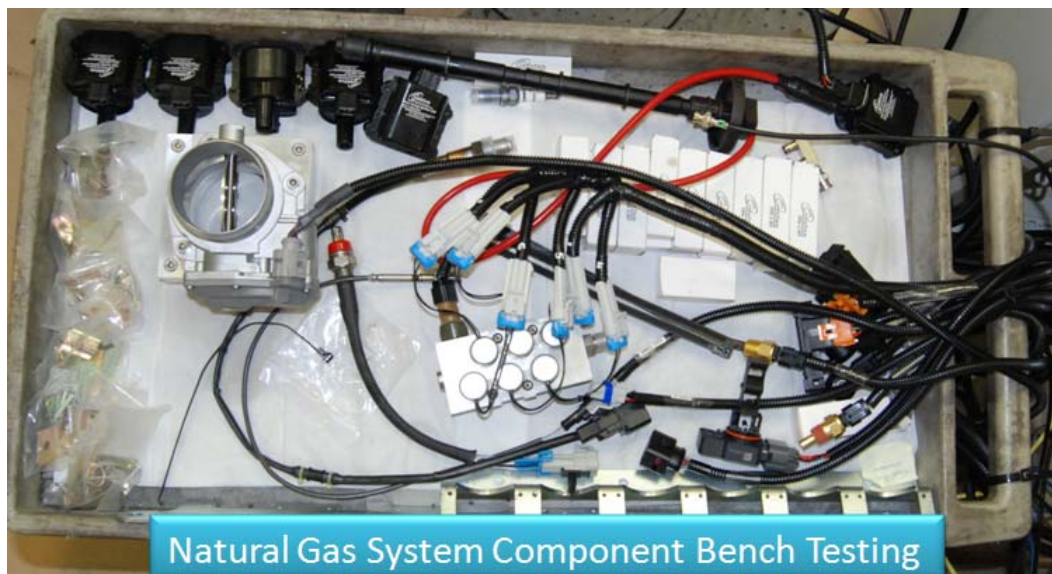


Source: Sturman Industries

## CHAPTER 10: Natural Gas System Components Bench Testing

The natural gas system as delivered by Omnitek was assembled in the test cell so that the interface with the Sturman controllers could be validated. The components of the natural gas system are shown in Figure 62. These components include the Omnitek Natural Gas System Controller (ECM-66A), spark coils and spark plugs, natural gas injectors and various sensors for proper operation. The Omnitek fuel system utilized a single-point gas injection ring supplied by 6 injectors. The system was designed to operate at 4 bar (60 psi) gas pressure. Even though the gas system was fumigated instead of port injected, cylinder deactivation was controlled by the hydraulic valve actuation system. The Controller Area Network (CAN) communication between the natural gas controller and Sturman Total Engine Controller (STEC) was validated and met the expectations for the engine testing.

**Figure 62: Natural Gas System Component Bench Testing**



Source: Sturman Industries

# CHAPTER 11:

## Dynamometer Test of Engine Platform

The following section provides an overview of the testing performed on the Cummins ISX 15L engine with the hydraulic valve actuation system. Testing was conducted to determine the engine power capability as well as the composite emissions from an industry standard 13-mode test.

### 11.1 Overview of Sturman Test Facility

The Sturman dynamometer facility consists of two dynamometer test cells and associated teardown rooms. The dynamometers input air pressure is controllable from 0 to 2000 meters (6500 feet) above sea level, or can run without control at Sturman's altitude of 2700 meters (8775 feet) above sea level. The exhaust pressure is controllable from 0 to 2700 meters (8775 feet) provided the engine airflow meets a minimum requirement. At low engine airflow conditions (for example, idle), it may not be possible to run at sea level conditions on the exhaust system. Both test cells use SuperFlow electronics for data acquisition and control. The control area for the dynamometers is shown in Figure 63.

**Figure 63: Sturman Industries' Dynamometer Facility**



Source: Sturman Industries

#### 11.1.1 Emissions Measurement Equipment

The engine emissions measurements are made using California Analytical analyzers with industry standard sampling equipment which includes heated/wet basis sampling in accordance with CFR-40 Section 86 directives.

### 11.1.2 CNG Flow Measurement Equipment

The compressed natural gas (CNG) flow rate is measured using a Micro Motion ELITE CFM025M coriolis meter. This meter is capable of measuring the natural gas rate from 2.3 g/s to 20 g/s with an accuracy of 0.35 percent of rate. At the expected idle condition of 0.4 g/s, the accuracy decreases to 1.9 percent of rate. This meter was sized for the best combination of pressure drop and accuracy for this test.

### 11.1.3 Pressure and Temperature Measurement

Pressures and temperatures are measured using industry standard equipment. The dynamometer facility uses various types of pressure transducers that are sized properly for the measurement range. The temperature measurements are performed with Type-K thermocouples.

## 11.2 Test Plan Overview

In order to satisfy the program requirements, a series of tests were conducted to validate the natural gas engine performance with the camless system. A description of the tests to be performed combined with the test objective is shown in Table 8:

**Table 8: Test Plan Overview**

Test	Test Objective
Engine start-up	Perform initial engine test to verify initial function of camless and natural gas systems
Engine break-in	Break-in engine to insure proper sealing of ring / liner interface
Initial engine shake-out	Verify all systems are functioning / controllable per system requirements; Set intake & exhaust flow restrictions
Baseline engine 13-mode and lug-line test (no catalyst)	Perform initial measurements to baseline engine without catalyst; this test will insure a proper baseline without compromising the catalyst system
Baseline engine 13-mode and lug-line test (with mid-loading catalyst)	Perform initial measurements to baseline engine with mid-loaded catalyst; Measure engine-out emissions to document baseline operation
13-mode and lug-line optimization calibration to peak brake thermal efficiency (BTE)	Perform optimization to document the peak BTE and emissions trade-off for the engine at various operating conditions

Source: Sturman Industries

Test Notes:

- Lug line: The lug line test will be conducted at 100 RPM increments from 600 RPM to 1800 RPM.
- 13-Mode Test: The 13-Mode emission test will be run in a steady-state condition with different wait times between points than defined in the CFR-40 document. The Sturman dynamometer facility requires longer wait times between points due to the constraints of operating the dynamometer facility at an altitude different than sea level. An air handling system is used to simulate sea level conditions at each test point.

## 11.3 Discussion of CNG Quality

### 11.3.1 Background

Natural gas composition and lower heating value (LHV) can vary significantly depending on the location and source of the gas. Natural gas quality is typically characterized by the methane number (MN) and the LHV of the gas. The Wobbe index is also typically used, but mainly for commercial and residential applications where the natural gas is metered by standard cubic foot. Replacing methane content with higher hydrocarbons components such as ethane, propane, butane, and so forth in the natural gas can reduce the MN of the fuel and thus lower the knock resistance of the fuel. It also affects the heating value of the fuel, the burn rate and the air/fuel (A/F) ratio needed for stoichiometric combustion. These fuel property differences can greatly affect the power level and efficiency of the engine especially if the engine control system cannot adapt to the fuel differences.

One of the major concerns with varying natural gas fuel quality is engine knock. The anti-knock property of a given natural gas is characterized by the MN. Pure methane has a MN of 100 and the higher the MN, the greater the anti-knock properties of the natural gas. The MN of a fuel is determined very similarly to the method used to determine the octane number of a gasoline and can be correlated as a function of the hydrogen to carbon (H/C) ratio of the natural gas. In general, the lower the H/C ratio, the lower the MN of the natural gas. The California Air Resource Board (CARB) uses the following correlations to calculate the motor octane number (MON) and MN of natural gas.

$$\text{MON} = -406.14 + 508.04*(\text{H/C}) - 173.55*(\text{H/C})^2 + 20.17*(\text{H/C})^3 \quad (1)$$

$$\text{MN} = 1.624*\text{MON} - 119.1 \quad (2)$$

The correlation (1) for MON is not valid for H/C < 2.5 and for inert gas concentration in fuel greater than 5 percent. The correlation shown in (2) typically predicts MNs 8.6 percent higher than the actual test values<sup>1</sup>

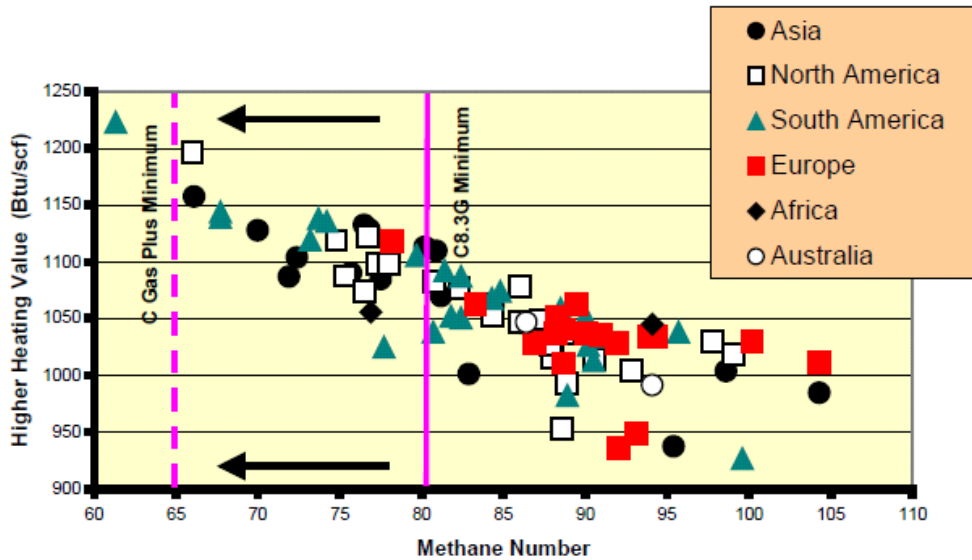
---

<sup>1</sup> "Paper Study on the Effect of Varying Fuel Composition on Fuel Supplied to Detroit Diesel Gas Engines", Report prepared for Southern California Gas Company, May 2005.

As shown in Figure 64, natural gas MNs can vary from 65 to 100 depending on the source, with the average MN being ~80. CARB specifies MNs above 80 for LNG to ensure no knock operation for reciprocating engines. Many older, open loop natural gas engines will not operate with MNs below 80. High MN natural gas is desirable because higher compression ratios and optimal spark timing can be used to improve engine efficiency without encountering engine knock.

The geometric compression ratio for the engine in this work is 14:1. This is a high compression ratio for natural gas and only high MN natural gas can be run at full load at this compression ratio. The HVA system on this engine can be used to reduce the effective compression ratio using late intake valve close timing to eliminate knock for natural gas with lower MNs.

**Figure 64: Methane Number vs. HHV for Various Natural Gas Sources around the World**



Source: NREL/SR-540-32863 Final Report

### 11.3.2 Natural Gas Properties

The natural gas composition used during the engine testing was obtained from El Paso Gas Company who was the supplier of the natural gas pipeline to the Sturman dynamometer. The test results were taken in January 2011, just prior to the start of the engine testing in the dynamometer at Sturman. The gas composition is shown in Table 9.

**Table 9: Natural Gas Composition for Engine Testing**

Gas Species	% by Volume
CH <sub>4</sub>	77.74
C <sub>2</sub> H <sub>6</sub>	6.06
C <sub>3</sub> H <sub>8</sub>	4.04
C <sub>4</sub> H <sub>10</sub>	0.99
C <sub>5</sub> H <sub>12</sub>	0.5
C <sub>6</sub> +	0.1
O <sub>2</sub>	1.5
N <sub>2</sub>	7.03
CO <sub>2</sub>	2.04

Source: El Paso Gas

This gas has a large percentage of non-methane hydrocarbons (11.1 percent) and a large proportion of inert gases (9.07 percent). The calculated MN for this natural gas is 67.7 using the CARB method shown (1) and (2). The percent of inert gases in this natural gas is higher than 5 percent, which is the limit specified for the correlation, so the MN calculated using this method may have some inaccuracy. The combustion properties for this natural gas are shown in Table 10. The low MN of this gas means its anti-knock properties are not good and the 14:1 compression ratio on the engine will need to be substantially reduced at high load to avoid engine knock. The means for reducing the effective compression ratio on this engine was to use a late intake valve close timing strategy. This strategy also reduces the volume of air/EGR that can be inducted into the engine at any given intake manifold pressure, thus reducing the maximum power output of the engine. Depending on the level of EGR used and boost pressure available, reaching the rated power at low speeds may be difficult using this natural gas.

**Table 10: Natural Gas Properties for Engine Testing**

Property	Value
Methane Number	67.7 (CARB method)
Wobbe Index based on HHV (MJ/m <sup>3</sup> )	46.78
HHV (MJ/kg)	45.40
LHV (MJ/kg)	41.87
Density at STP (kg/m <sup>3</sup> ) 14.73 psi, 60°F	0.867
Stoichiometric A/F Ratio	14.06

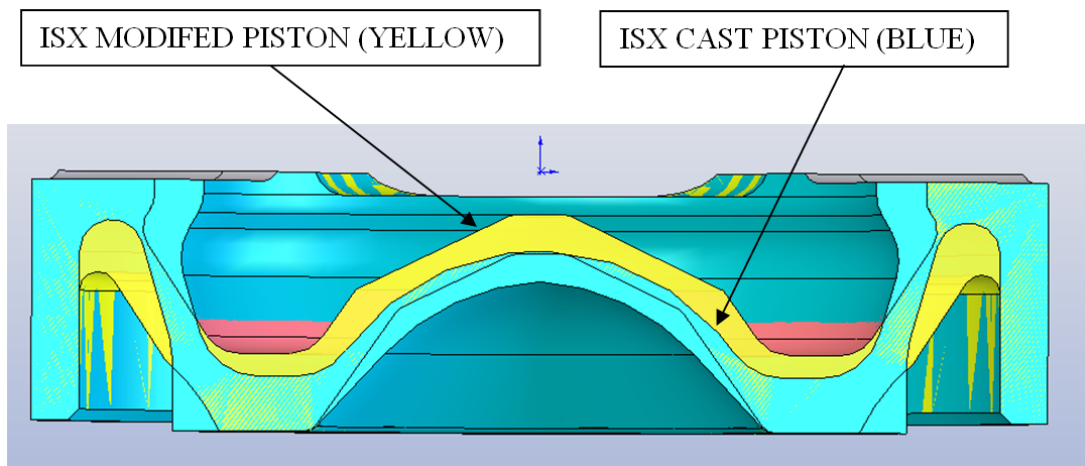
Source: Sturman Industries

## 11.4 Engine Hardware Modifications

### 11.4.1 Piston Design

The engine used for this program required the compression ratio to be reduced from 17:1 to 14:1 to operate on natural gas with better margin to knock resistance. To accomplish this, two paths were investigated. The first was to modify the existing two-piece ISX piston bowl to increase the bowl volume and the second was to source a new custom 1-piece cast piston from IPD. Review of the two designs showed only the IPD piston suitable for this application as the modified ISX piston's center 'pip' would not allow clearance for the spark plug in the center of the combustion chamber with 1.0 mm of interference. The IPD piston's raw casting allows for custom bowl geometry to give both 14:1 compression ratio as well as 3.0 mm of clearance for the spark plug. A comparison of the two piston options is shown below in Figure 65.

**Figure 65: Modified ISX vs. IPD Cast Piston**



Source: Sturman Industries

## 11.5 Engine Start-up and System Validation

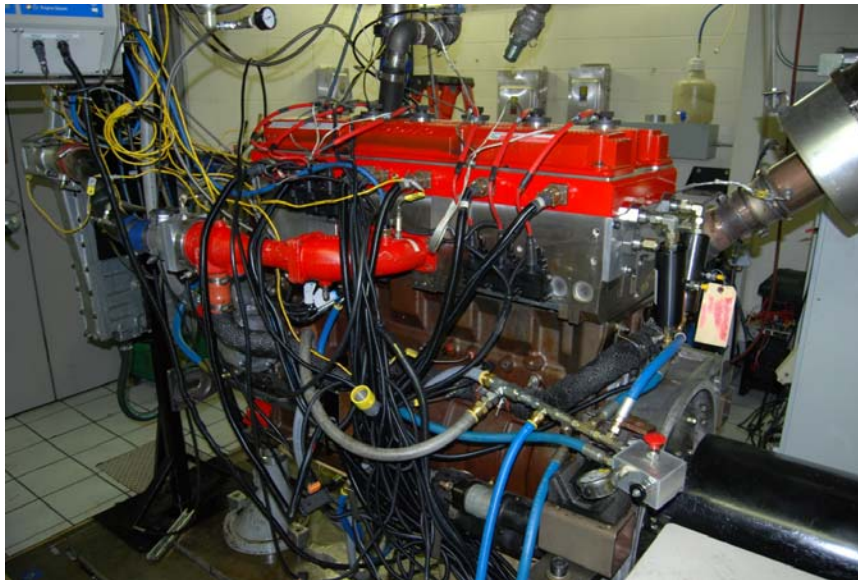
After completion of HVA bench testing, the assembly was moved to the engine dynamometer to be installed on the short block. For production intent direction, the original design intent was to be able to install the assembled cylinder head without any HVA disassembly. For this application, only one of the modules had to be removed to gain access to one of the cylinder head bolts. The removal of the module involved only removing two bolts and the head installation proceeded very smoothly. Actual piston to valve clearance was measured and verified to match values used by the Condor controller. The engine as installed in the Sturman dynamometer facility is shown in Figure 66.

During the shakeout period, the HVA pump cart was utilized instead of the engine mounted pump to minimize variables for engine startup. This allowed for all engine systems to be tested in simulation mode before fueling the engine. Several CAN communication software issues were resolved during this time to allow the Sturman

Engine Controller to control commanded lambda and ignition timing via the Omnitek ECM-66A. Various startup issues were identified and repaired. Modifications to improve the oil path from the engine to the pump cart included adding an additional low pressure lift pump and increasing the hose flow capacity. This was necessary to supply adequate feed pressure to the pump cart.

Ignition timing accuracy was verified with a timing light by setting the commanded timing to  $0^\circ$  BTDC while cranking the engine. This insured that the ignition timing matched the physical piston TDC and was important since the raw crankshaft signals were processed before being sent to the natural gas controller.

**Figure 66: Engine During De-greening Process**



Source: Sturman Industries

The first series of engine tests included performing an engine break-in to properly seat the engine rings. In place of the three-way-catalyst a 'blank' unit was inserted so as to protect the catalyst during the shakeout phase. Engine de-greening then commenced by following a schedule provided by Westport Industries shown in Table 11.

**Table 11: Break-in Cycle for Cummins ISX engine**

Sequence	Duration	Speed	Torque
	(sec)	(rpm)	(Nm)
Low Idle	90	600	min
Warm Up One	90	1600	135
Warm Up Two	90	1600	248
	90	1600	318
	90	1600	415
	90	1600	565
	90	1600	656
	90	1600	835
	90	1600	930
	90	1600	1035
	90	1600	1164
90	1600	1552	

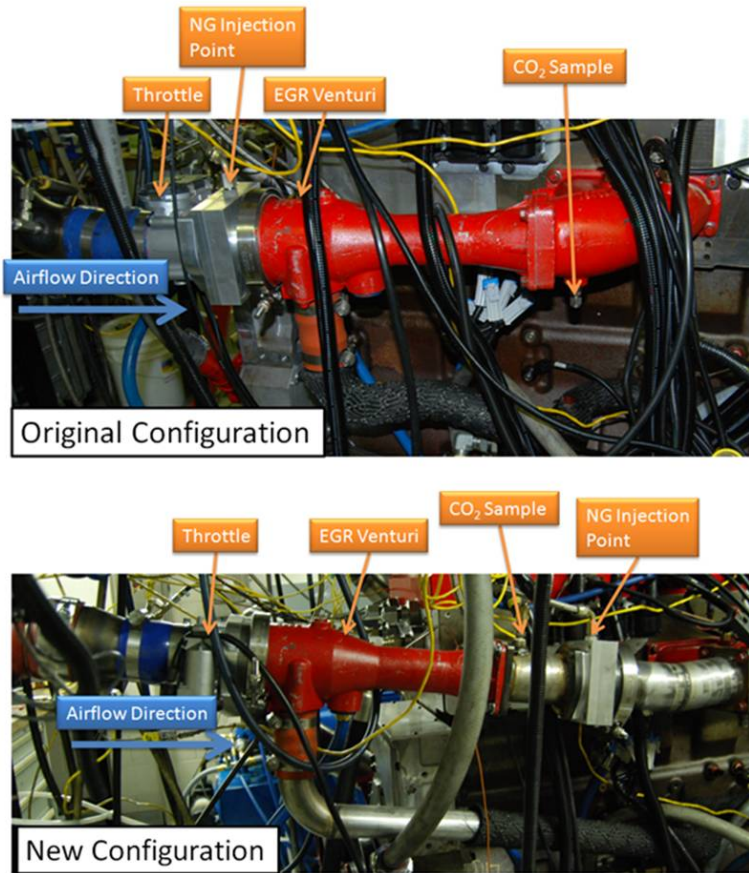
Source: Sturman Industries

Since the piston ring pack was unchanged from the diesel variant, all operation while the engine was still “green” was performed unthrottled to prevent oil blow-by from the fresh rings and cylinder liners. Since the goal was to operate the engine unthrottled for all the test points, the existing ring pack was utilized. Late intake valve close (IVC) was utilized to vary the engine load. With the stock venturi-based EGR setup in place, a very low amount of EGR could be driven with the current VGT turbo arrangement. Without any EGR, knock and turbine inlet temperature limits were observed at relatively low engine loads (~50 percent load). This prevented running the engine through the entire de-greening schedule until modifications to the EGR system were performed.

#### 11.5.1 EGR System Improvements

During the de-greening process, it was noted that the current configuration would not allow the levels of EGR for proper engine tuning. The configuration of the EGR system was revised to be able to drive sufficient EGR to keep exhaust gas temperatures within limits and mitigate engine knock. Since the EGR measurement was performed by measuring the percent CO<sub>2</sub> in the intake and comparing it to the percent CO<sub>2</sub> in the exhaust, it was necessary to modify the sample location so that natural gas was not introduced into the emissions equipment. The setup was reconfigured as shown in Figure 67.

**Figure 67: Intake Configuration Comparison**

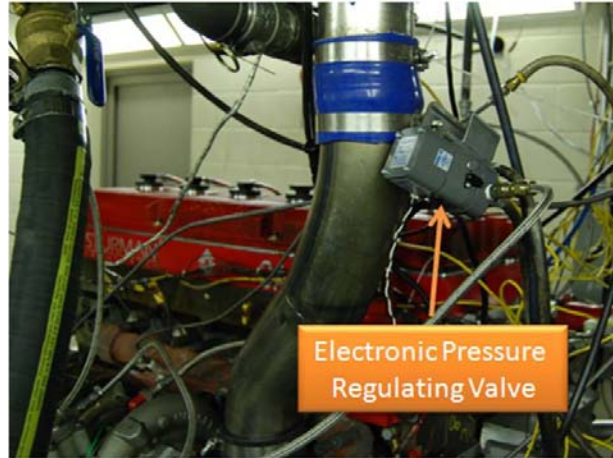


Source: Sturman Industries

After reconfiguring the intake setup, lower EGT's were realized and higher engine load was obtained without engine knock. The remaining higher load points from the de-green cycle were then completed.

During the course of this initial shake-out, instability in the turbocharger VGT control was observed with the OEM pressure regulating valve. This valve was replaced with an aftermarket pressure regulating valve as shown in Figure 68 which resulted in acceptable VGT control.

**Figure 68: Replacement Electronic Pressure Regulating Valve**



Source: Sturman Industries

Software debugging continued during this period. A glitch in the CAN communication between the STEC and Omnitek ECM-66A produced a ‘fuel cut’ issue that was causing random misfires. This was also preventing full load operation, limiting the ability to fully de-green the engine. This issue was resolved which allowed the engine to run without shutdown.

The dynamometer test configuration summary is outlined in Table 12. For all tests the code version and calibration for the STEC, Omnitek, and Condor VDM remained unchanged.

**Table 12: Dyno Test Configuration Summary**

Test #	Description	STEC		Omnitek		VDM	
		Code Version	Calibration	Code Version	Calibration	Code Version	Calibration
01	Baseline testing with no catalyst (13 mode) – Ran to 75% load on A, B, C speeds – Drove BSNOx to ≤6.5 g/hp-hr	STECM5554A v0.0 1 Rev 2239	PIER_STEC_03 -03-11.CAL	Testxdp512- 2011-01-27-2.bl_	ISX SI Firmware 2011-03-01R1.SOL	VDM555A v0.08 Rev.3046 VCM Rev. 3045	CPIER_VDM_02-23- 11.CAL
02	Testing with mid-loaded catalyst (13 mode and lug-line) – Unthrottled operation - Optimized	STECM5554A v0.0 1 Rev 2239	PIER_STEC_03 -03-11.CAL	Testxdp512- 2011-01-27-2.bl_	ISX SI Firmware 2011-03-01R1.SOL	VDM555A v0.08 Rev.3046 VCM Rev. 3045	CPIER_VDM_02-23- 11.CAL
03	Testing with mid-loaded catalyst (13 mode and lug-line) – Throttled operation - Baseline	STECM5554A v0.0 1 Rev 2239	PIER_STEC_03 -03-11.CAL	Testxdp512- 2011-01-27-2.bl_	ISX SI Firmware 2011-03-01R1.SOL	VDM555A v0.08 Rev.3046 VCM Rev. 3045	CPIER_VDM_02-23- 11.CAL
04	Testing with no- catalyst (13 mode and lug-line) – Throttled operation - Baseline	STECM5554A v0.0 1 Rev 2239	PIER_STEC_03 -03-11.CAL	Testxdp512- 2011-01-27-2.bl_	ISX SI Firmware 2011-03-01R1.SOL	VDM555A v0.08 Rev.3046 VCM Rev. 3045	CPIER_VDM_02-23- 11.CAL

Source: Sturman Industries

During engine shakeout, it was found that the laminar flow element (LFE) used to measure airflow to the engine had a non-linear offset compared to airflow values

measured by the Delphi mass air sensor installed on the engine. Using the Coriolis fuel flow meter and the Bosch LSU4.2 wideband oxygen sensor to calculate airflow confirmed that the LFE airflow values were incorrect and that the airflow from the Delphi mass air sensor was accurate. For all the data presented in this report, the airflow values are based on 'AirDelphi', or mass air flow measured by the Delphi mass airflow sensor. Due to the program's timeline, it was not possible to re-calibrate the LFE without significantly impacting the testing progress.

Another correction applied to the numbers presented in the engine testing section is for the HVA pump cart power consumption. The engine mounted pump experienced an infant failure during early shakeout testing that took several weeks to repair. Thus, data for this engine was not taken with the engine mounted pump as of this report writing. Raw data taken from the dynamometer was corrected for an assumed pump efficiency of 90 percent which is consistent with the bench test results from the engine mounted pump. The pump power was subtracted from the raw power and torque measurements according to the following equation (3):

$$HVA Power [kW] = \frac{HVA Pressure [PSI] \cdot 100000 \cdot HVA Flow \left[ \frac{in^3}{min} \right] \cdot (1 + (1 - Pump Eff))}{1000} \quad (3)$$

This also has an effect on the targeted loads for the 13-mode tests. While operating the engine, the raw torque value was used without the HVA power applied. Therefore, the torque numbers presented are slightly lower than the target torque since they have the HVA power subtracted. The pump power numbers measured during the tests were validated with the simulation as shown in Table 13.

**Table 13: Predicted and Measured HVA Pump Power**

Test Condition	Predicted Pump Power [kW]	Measured HVA Pump Power [kW] (Baseline Test)	Measured HVA Pump Power [kW] (Optimized Test)
13-Mode Composite	4.9	6.0	5.9
Idle Test Point	1.7	1.6	0.9
C100 Test Point	10.2	11.3	11.3

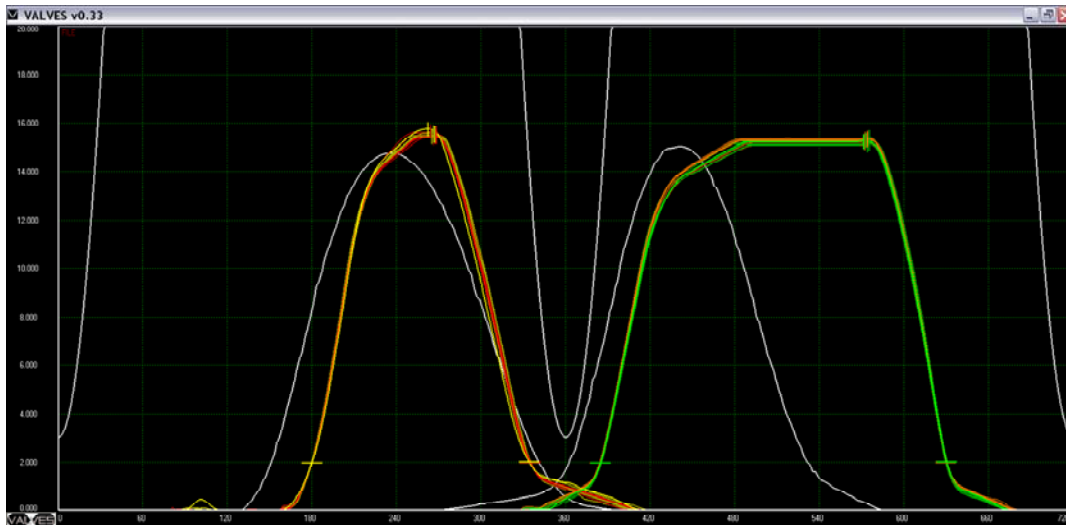
Source: Sturman Industries

## 11.6 Baseline Results (No Catalyst)

Baseline testing was conducted to determine the engine lug line and baseline 13-mode results without the catalyst. An example of the valve traces for the test points is shown

in Source: Sturman Industries. The valve traces were modified to allow unthrottled operation. The open timing was left 10° retarded to ensure margin between the piston and engine valves. Earlier intake valve opening timings were tested that closely matched the stock trace; however, no difference in engine torque or BSFC was observed.

**Figure 69: Baseline Valve Trace Example (unthrottled)**

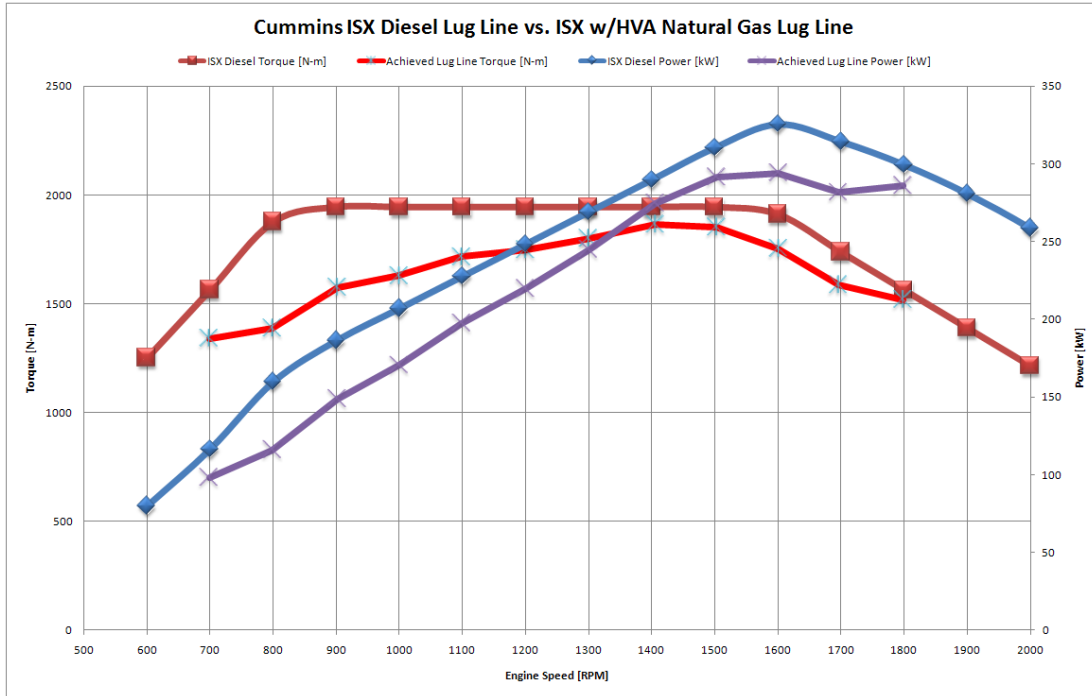


Source: Sturman Industries

A lug line was performed to determine if the engine would meet the baseline diesel torque curve. At lower engine speeds, the peak torque was limited to a value lower than the diesel baseline due to knock and turbine inlet temperature limitations as shown in Figure 70. This figure shows the comparison of the ISX diesel lug line for a 298kW (400 HP) rating and the achieved values for the spark ignited natural gas ISX with HVA. Once the torque curve was developed, it was utilized to calculate the A, B and C speeds necessary for the 13-mode emissions test. These speeds were defined as the following for the 13-mode test:

- A Speed = 1130 RPM
- B Speed = 1480 RPM
- C Speed = 1830 RPM

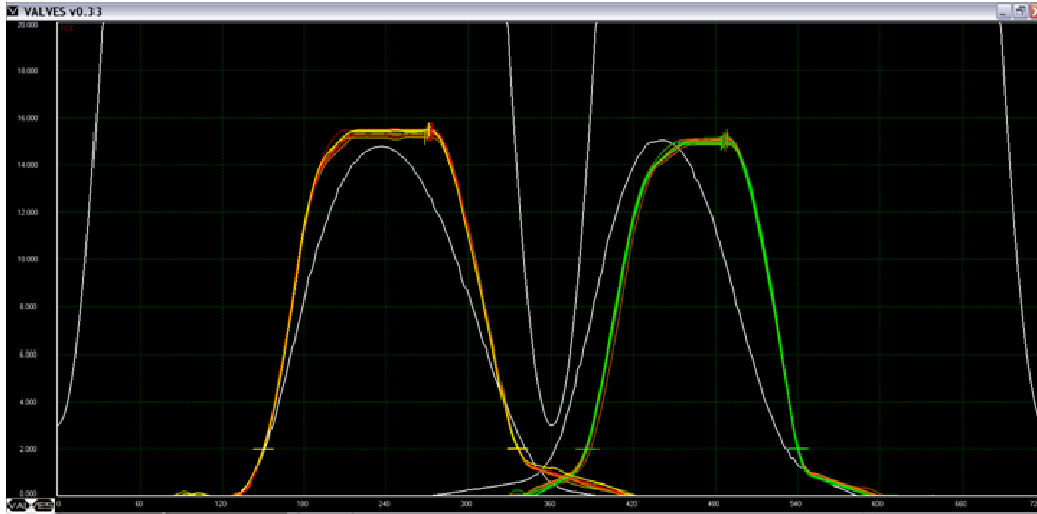
**Figure 70: Lug Line Comparison**



Source: Sturman Industries

Once the lug line was completed, the valve traces were modified to match the stock cam traces as shown in Figure 71. The valve timings similarly match the stock cam traces shown in white with the exception of the intake valve open timing. The open timing was left 10° retarded to ensure margin between the piston and engine valves. Earlier intake valve opening timings were tested that closely matched the stock trace; however, no difference in engine torque or BSFC was observed.

**Figure 71: Baseline Valve Trace Example**



Source: Sturman Industries

A full 13-mode and lug-line test was attempted with these standard valve timings, commanded lambda = 1, and throttled operation. A reasonable amount of EGR was used to mitigate engine knock and keep the turbine inlet temperature within the 750°C (1382°F) limit. Table 15 shows BSNO<sub>x</sub>, BSCO, and BSNMHC emissions were high as expected and the composite values are well outside the emissions targets. The targeting emissions results are based on the ARB's 2007 emissions regulations using CHP credits calculated from 1.5x the engine output.

**Table 14: Emissions Limits for Exhaust Components**

Target Emissions Component	2007 ARB Limit g/kWhr (no CHP credits)	2007 ARB Limit g/kWhr (with CHP credits)
BSNO <sub>x</sub>	0.0318	0.0794
BSCO	0.0454	0.1134
BSNMHC	0.0091	0.0227

Source: Sturman Industries

During the course of this testing, the dynamometer facility experienced a controller failure that resulted in only a partial 13-mode without the catalyst as shown in Table 15. As such, the lug-line during throttled operation was utilized as the baseline.

**Table 15: Baseline 13-Mode Results (No Catalyst)**

<b>298 kW HP, Cummins ISX, Omnitek Natural Gas System, Sturman HVA,                      Pump Cart, Baseline, No Catalyst</b> *numbers corrected for HVA Power and AirDelphi								
		TQ	Weighted Power	BSNOx	BSFC	BSNMHC	BSCO	BTE
Mode	RPM	N-m	kW	g/kW-hr	g/kW-hr	g/kW-hr	g/kW-hr	%
Idle	0	0	0.00	0.000	0.0	0.000	0.000	0.0
A25	1128	388	2.29	1.897	298.1	1.072	5.782	28.8
A50	1129	788	4.66	5.778	235.7	0.546	5.267	36.5
A75	1129	1204	7.12	8.360	218.2	0.267	3.520	39.4
A100	1129	1633	15.44	11.012	215.6	0.025	9.335	39.9
B25	1480	439	6.81	6.199	300.3	0.720	7.934	28.6
B50	1474	934	14.41	2.713	233.8	0.530	2.627	36.8
B75	1480	1443	22.36	5.332	220.8	0.415	5.578	38.9
B100	0	0	0.00	0.000	0.0	0.000	0.000	0.0
C25	0	0	0.00	0.000	0.0	0.000	0.000	0.0
C50	0	0	0.00	0.000	0.0	0.000	0.000	0.0
C75	0	0	0.00	0.000	0.0	0.000	0.000	0.0
C100	0	0	0.00	0.000	0.0	0.000	0.000	0.0
<b>13-Mode Composite</b>				<b>6.312</b>	<b>232.8</b>	<b>0.398</b>	<b>5.795</b>	<b>37.32</b>

Source: Sturman Industries

## 11.7 Baseline Results (With Catalyst)

Since the engine operates at a stoichiometric A/F ratio, two different 3-way catalysts were procured to meet the emissions requirements for this program. The catalysts were sized to insure proper gas velocity and conversion efficiencies with each catalyst having a volume of 30L. The catalyst substrates utilized two different loading arrangements, mid-loading and high-loading, in order to investigate conversion efficiency requirements.

Testing was conducted with the mid-loaded three-way catalyst using stock valve timing and throttled operation for load control. This testing included both lug line and 13-mode test points. The lug-line results matched the baseline results very well without the catalyst in place. The commanded lambda was adjusted slightly rich of stoichiometric operation to achieve high catalyst conversion efficiency. It was found that the catalyst was highly sensitive to air-fuel ratio to balance the conversion of NOx and CO.

Table 16 shows that the 13-mode composite BSNOx is well within the target of  $\leq 0.064$  g/kw-hr, but BSNMHC and BSCO are slightly above the targets of 0.0169 g/kw-hr and 0.084 g/kw-hr respectively. The idle test point was taken at altitude conditions due to dynamometer facility limitations to hold sea-level backpressure at low engine flow rates. At each test point, the cylinder pressure was measured in order to calculate the heat release and indicated heat release. The results of those measurements are summarized in Appendix B.

Due to time constraints, these test points were not repeated to achieve emissions compliance since that was to be performed during the optimization process. Based on later testing, it was found that emissions targets could have been achieved with additional optimization of the air-fuel ratio.

**Table 16: Baseline 13-Mode Results (With Catalyst)**

298 kW HP, Cummins ISX, Omnitek Natural Gas System, Sturman HVA, Pump Cart, Baseline, Mid-Loaded 3-Way Catalyst								
*numbers corrected for HVA Power and AirDelphi								
		TQ	Weighted Power	BSNOx	BSFC	BSNMHC	BSCO	BTE
Mode	RPM	N-m	kW	g/kW-hr	g/kW-hr	g/kW-hr	g/kW-hr	%
Idle	688	0	0.00	-72.681	-1891.9	-43.743	-1194.696	-4.5
A25	1148	391	2.35	0.083	294.9	0.000	0.241	29.2
A50	1128	808	4.77	0.000	249.7	0.004	0.146	34.4
A75	1127	1215	7.17	0.000	223.7	0.003	0.383	38.4
A100	1129	1657	15.67	0.000	216.7	0.003	0.171	39.7
B25	1479	451	6.98	0.000	302.6	0.006	-0.035	28.4
B50	1474	933	14.40	0.000	241.2	0.003	0.218	35.6
B75	1478	1440	22.29	0.005	225.8	0.013	-0.003	38.1
B100	1484	1912	26.74	0.005	219.6	0.015	0.154	39.1
C25	1827	303	2.90	0.131	384.6	0.175	0.200	22.4
C50	1824	692	6.61	0.006	271.3	0.150	0.087	31.7
C75	1826	1062	10.15	0.006	240.6	0.045	0.017	35.7
C100	1830	1447	22.18	0.000	233.3	0.258	0.110	36.9
<b>13-Mode Composite</b>				<b>0.007</b>	<b>238.4</b>	<b>0.060</b>	<b>0.122</b>	<b>36.51</b>

Source: Sturman Industries

## 11.8 Optimized Results (With Catalyst)

The next series of tests involved optimizing the engine using the HVA system to perform load control in an unthrottled condition. This was accomplished by adjusting the intake valve close (IVC) timing with the throttle at 100 percent open for all test points. The same catalyst system (mid-loaded) was utilized as the baseline for emissions reduction. Exhaust backpressure, ignition timing, engine load, and EGR percent were targeted the same as the baseline condition.

Table 17 shows all composite emissions targets were achieved except for BSCO being 0.004 g/kW-hr too high. The most notable difference between the optimized and baseline tests is the decrease in BSFC of 3.8 percent and increase in BTE of 1.27 points over the composite 13-mode test. This shows that running the engine unthrottled decreases pumping losses and increases performance compared to running throttled. Also, note that both the A100 and B100 points show a BTE greater than 40 percent. At each test point, the cylinder pressure was measured in order to calculate the heat release and indicated heat release. The results of those measurements are summarized in Appendix C.

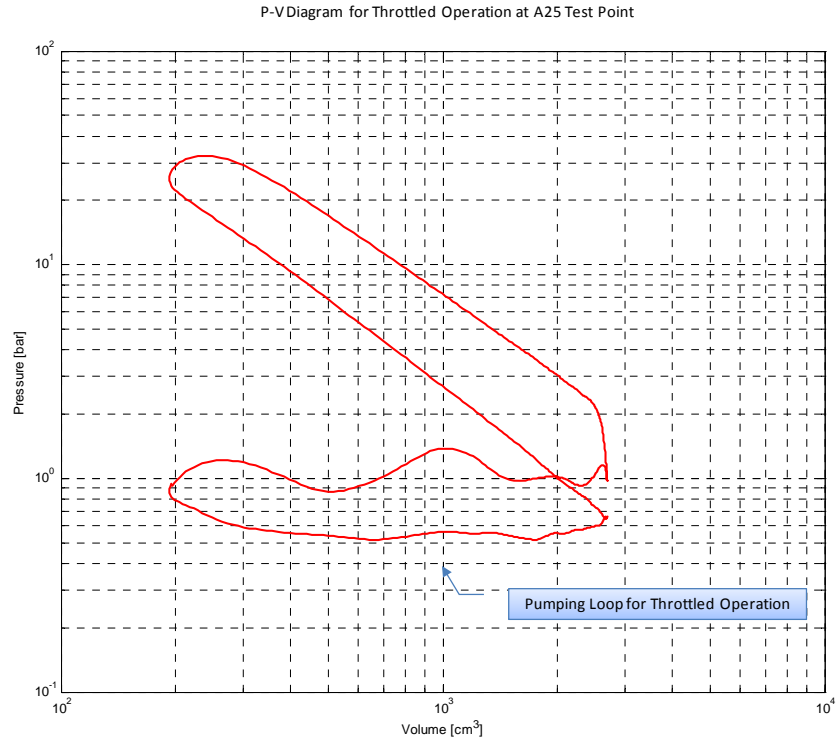
**Table 17: Optimized 13-Mode Results (6 Cylinder Operation)**

<b>298 kW HP, Cummins ISX, Omnitek Natural Gas System, Sturman HVA,                      Pump Cart, Optimized, Mid-Loaded 3-Way Catalyst</b> *numbers corrected for HVA Power and AirDelphi								
		TQ	Weighted Power	BSNOx	BSFC	BSNMHC	BSCO	BTE
Mode	RPM	N-m	kW	g/kW-hr	g/kW-hr	g/kW-hr	g/kW-hr	%
Idle	700	0	0.00	-0.107	-2958.3	-0.048	-0.131	-2.9
A25	1127	394	2.32	0.249	292.7	0.032	0.734	29.4
A50	1118	823	4.82	0.011	234.9	0.000	0.043	36.6
A75	1129	1251	7.40	0.015	219.2	0.003	0.052	39.2
A100	1130	1682	15.92	0.005	207.9	0.035	0.043	41.4
B25	1481	448	6.95	0.013	281.9	0.016	0.168	30.5
B50	1478	945	14.62	0.000	232.4	0.000	0.253	37.0
B75	1479	1450	22.47	0.005	218.1	0.024	0.074	39.4
B100	1482	1928	26.93	0.005	213.6	0.000	0.084	40.3
C25	1824	321	3.06	0.058	349.0	0.172	0.141	24.6
C50	1830	675	6.46	0.006	256.2	0.013	0.437	33.6
C75	1829	1065	10.20	0.011	227.2	0.008	0.020	37.8
C100	1828	1420	21.75	0.005	228.7	0.003	0.068	37.6
<b>13-Mode Composite</b>				<b>0.011</b>	<b>229.3</b>	<b>0.014</b>	<b>0.117</b>	<b>37.87</b>

Source: Sturman Industries

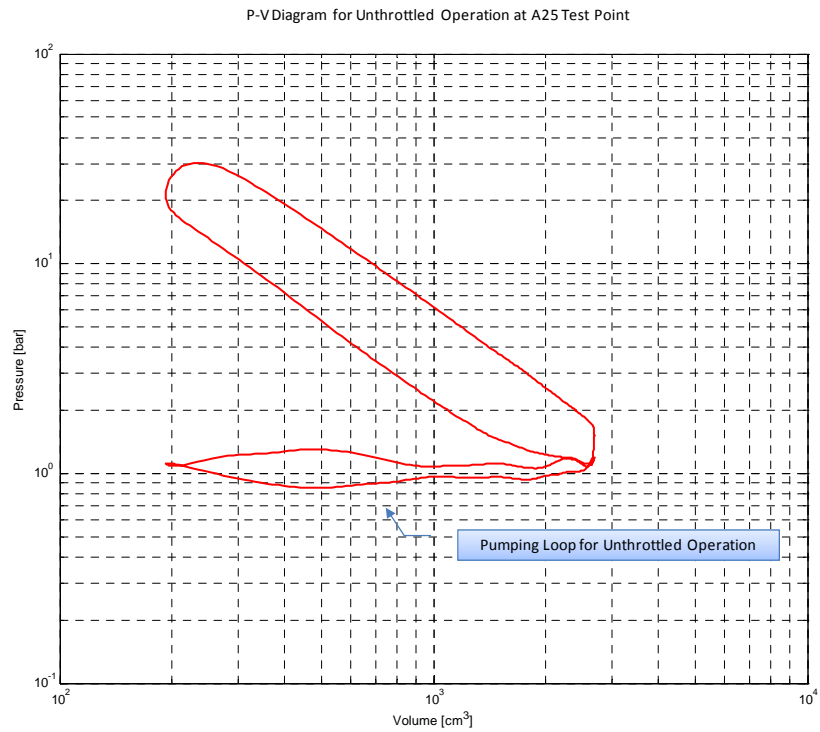
Improvements in the pumping loop due to unthrottled operation for the A25 test point are shown in Figure 71 and Figure 72. The equivalent torque due to the pumping losses was measured as 59.8 N-m for the throttled test point and 22.3 N-m for the unthrottled test condition.

**Figure 71: P-V Diagram for Throttled Operation at A25**



Source: Sturman Industries

**Figure 72: P-V Diagram for Unthrottled Operation at A25**



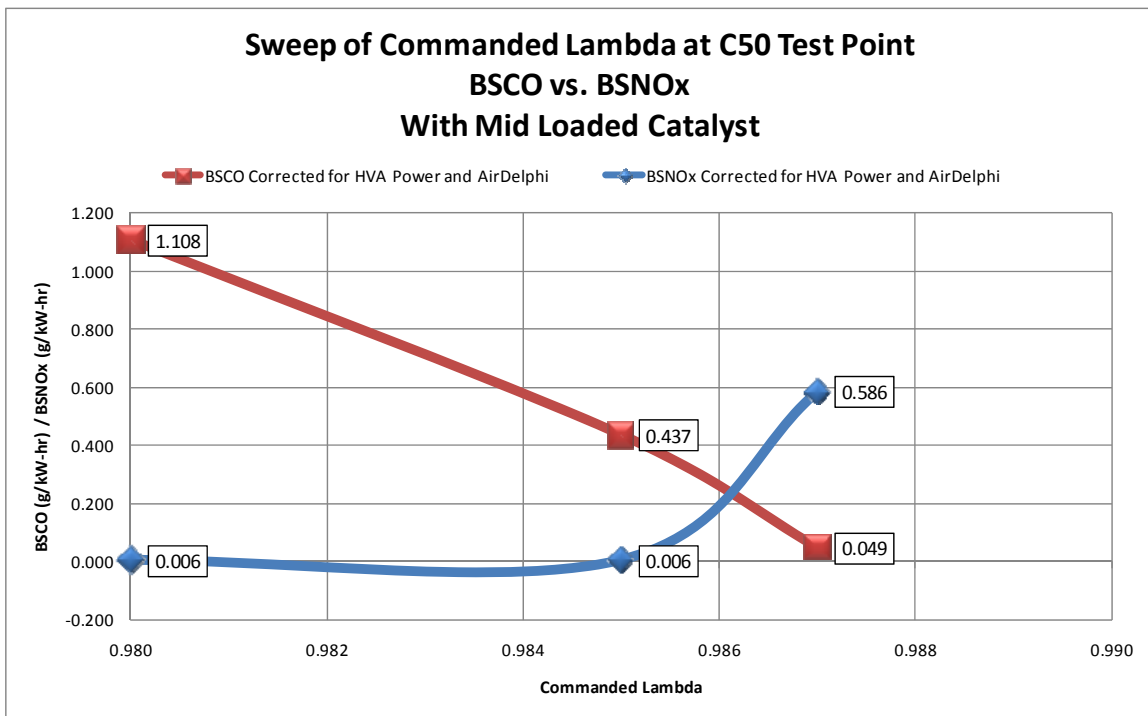
Source: Sturman Industries

### 11.8.1 Catalyst Sensitivity to Air/Fuel Ratio

During optimization sweeps it was found that the mid-loaded catalyst was highly sensitive to air/fuel ratio to balance the tradeoff of BSCO and BSNO<sub>x</sub>. With all variables held constant, a change in commanded lambda from 0.985 to 0.987 increased the BSNO<sub>x</sub> from 0.006 g/kW-hr to 0.586 g/kW-hr, and reduced the BSCO from 0.437 g/kW-hr to 0.049 g/kW-hr shown in Figure 73. As such, to create the optimized results required careful attention to the adjustment of the commanded lambda value.

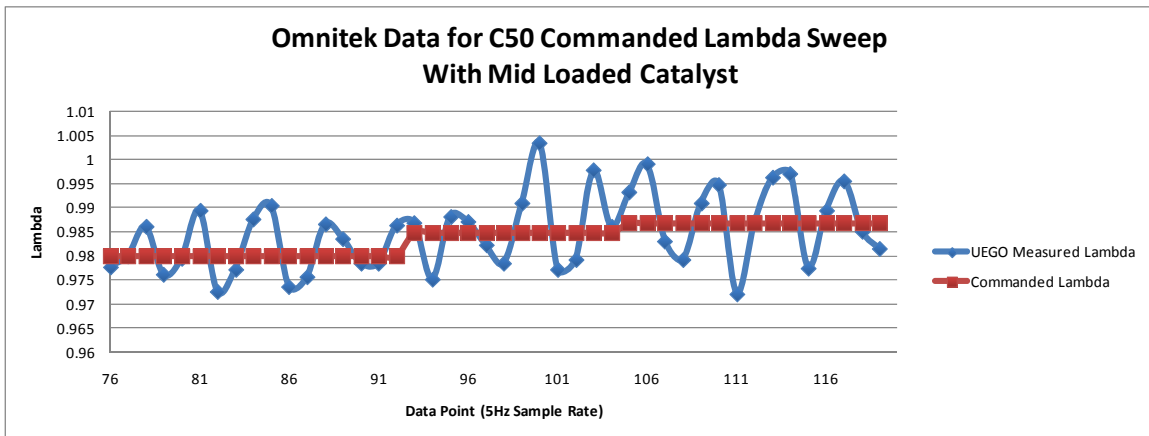
Figure 74 shows UEGO measured lambda from the Bosch LSU4.2 wideband O<sub>2</sub> sensor and the commanded lambda values taken with Omnitek's Omniwatch data logging interface. The sample rate of the program is limited to 5 Hz with 61 variables being recorded. Approximately 3 seconds of data was taken for each lambda step. It can be seen that the UEGO measured lambda cycles up to 3 percent while operating steady state. The mean lambda value entering the catalyst should ultimately determine emissions post catalyst. This inherent dither in lambda entering the catalyst improves the catalyst conversion efficiency. A feature not explored during this program was to monitor the narrow band O<sub>2</sub> sensor post catalyst.

**Figure 73: Sweep of Commanded Lambda at C50 Test Point**



Source: Sturman Industries

**Figure 74: Omnitek Data for C50 Commanded Lambda Sweep**

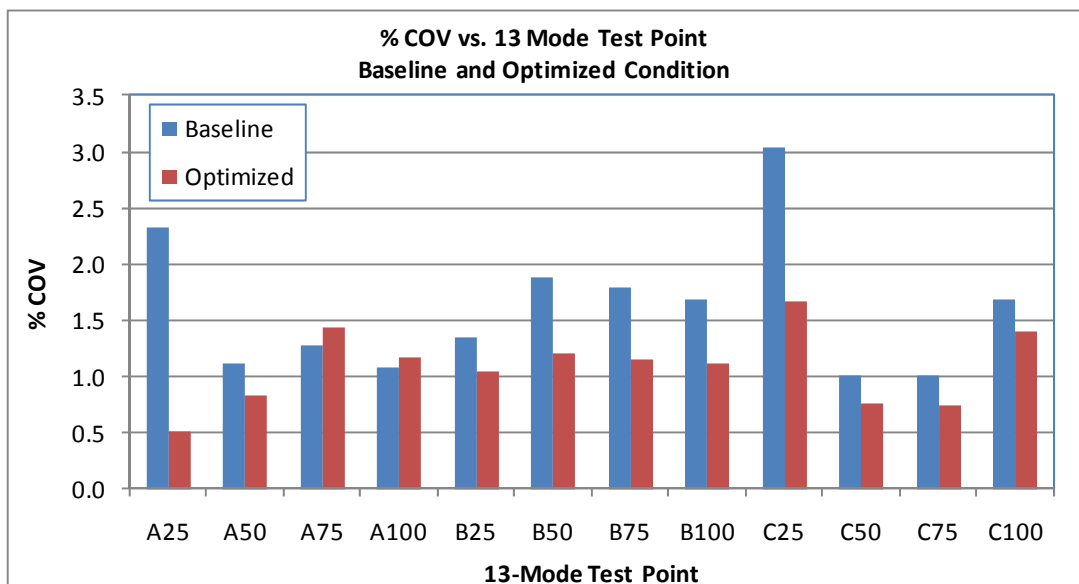


Source: Sturman Industries

### 11.8.2 Optimized Cylinder Pressure Coefficient of Variation

Investigation of the coefficient of variation (COV) shows differences between the baseline and optimized tests. In general the COV improves while running the engine in the unthrottled condition during optimized testing as shown in Figure 75. This can be attributed to better charge mixing, adding turbulence and residence time by re-breathing the air/fuel mixture back into the intake manifold.

**Figure 75: %COV vs. 13 Mode Test Point**



Source: Sturman Industries

### 11.8.3 Effects of Late Intake Valve Closing

Late intake valve closing had an effect on both the volumetric compression ratio of the engine as well as the amount of air mass trapped in the cylinder. Table 18 below

illustrates the optimized 13-mode test data. The *IVC Timing* is the commanded value for the HVA controller at 2.0 mm valve lift. The *IVC Seating Angle* is the angle at which the valve is at 1.0 mm lift, and will change based on HVA rail pressure and engine speed. The valve seating time from 2.0 mm to 1.0 mm is a fixed value in the time domain at a constant HVA rail pressure regardless of engine speed. Thus the difference between the *IVC Timing* and the *IVC Seating Angle* changes with engine speed.

Since effective compression ratio can be based on different methods, two different values are presented. The volumetric compression ratio is defined as the ratio of cylinder volume at *IVC Seating Angle* to the TDC volume. However, during the data processing, it became apparent that this method of definition did not account for the actual in-cylinder compression process. It was noted that the calculated motoring pressure from the expected pressure at BDC and *IVC Seating Angle* was much lower than the actual cylinder pressure especially at very late *IVC Seating Angles*. This led to a modification of the *IVC Seating Angle* to account for the compression process that was occurring in the cylinder. From this modified value, an effective compression ratio (pressure based) was calculated. In addition to these calculations, a 50 percent heat release angle was calculated.

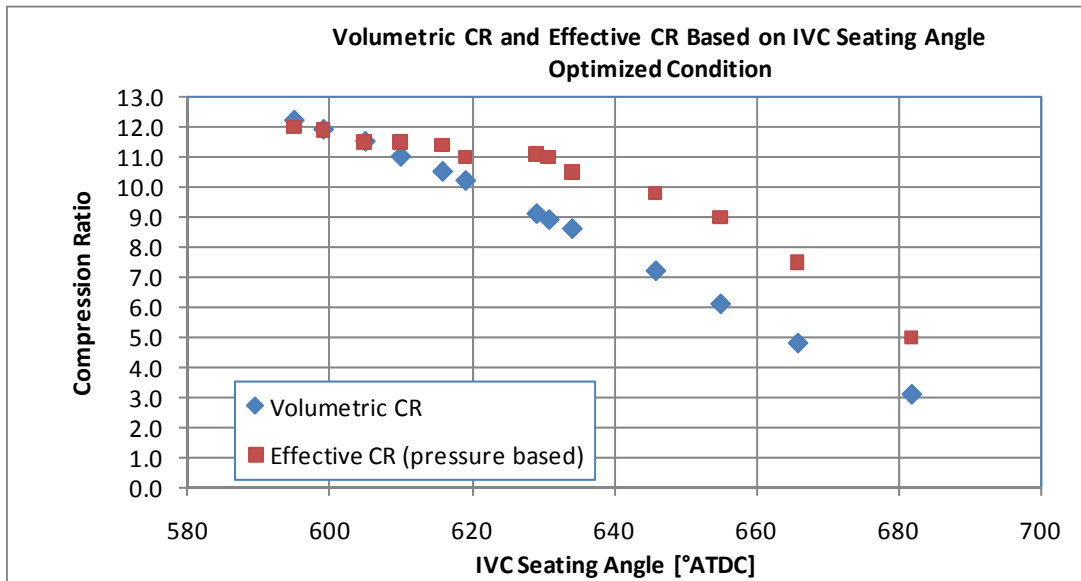
**Table 18: Effective Compression Ratio and Heat Release Results**

Test Point	Engine Speed [RPM]	IVC Timing [°ATDC]	IVC Seating Angle [°ATDC]	Volumetric CR	Effective CR (pressure based)	COV %	50% Heat Release Angle [°ATDC]
Idle	700	670	682	3.1	5.0	34.7	29.7
A25	1130	610	629	9.1	11.1	0.5	6.0
A50	1130	615	634	8.6	10.5	0.8	5.5
A75	1130	600	619	10.2	11.0	1.4	6.0
A100	1130	580	599	11.9	11.9	1.2	10.3
B25	1480	630	655	6.1	9.0	1.1	5.7
B50	1480	585	610	11.0	11.5	1.2	11.7
B75	1480	580	605	11.5	11.5	1.2	12.3
B100	1480	570	595	12.2	12.0	1.1	13.5
C25	1830	635	666	4.8	7.5	1.7	10.2
C50	1830	615	646	7.2	9.8	0.8	8.2
C75	1830	600	631	8.9	11.0	0.8	5.8
C100	1830	585	616	10.5	11.4	1.4	13.2

Source: Sturman Industries

Figure 76 shows the different values for the volumetric and effective compression ratios as defined for the different conditions during the 13-mode test. It is believed that some additional throttle effects (intake manifold, later intake valve opening) are also contributing to the lower effective compression ratio.

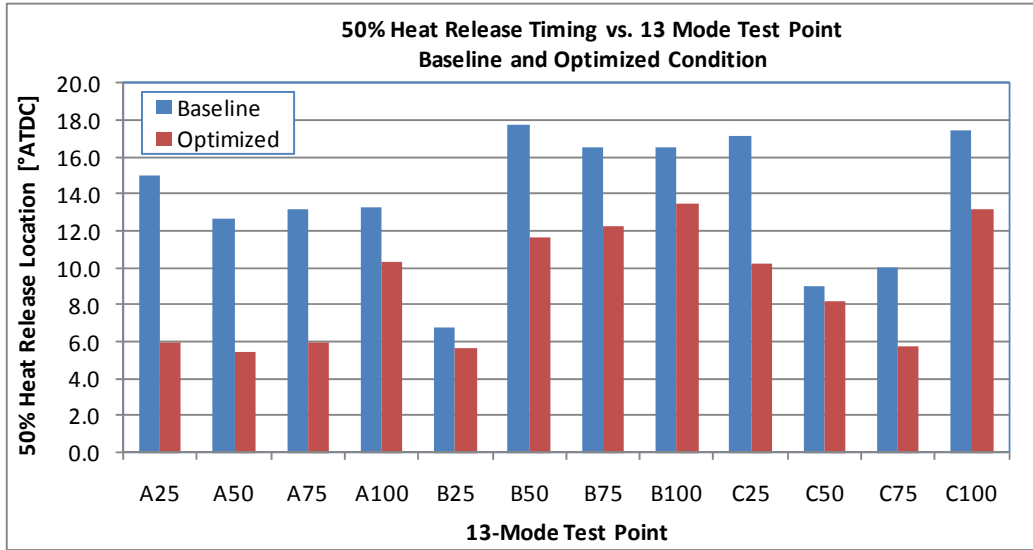
Figure 76: Optimized Volumetric CR and Effective CR Based on IVC Seating Angle



Source: Sturman Industries

A comparison was performed for the 50 percent heat release location between the baseline and optimized tests for the 13-mode. It can be seen in Figure 77 that the 50 percent heat release location is more advanced for the optimized condition. The cause of this difference could be attributed to the different effective compression ratio, in-cylinder charge motion due to the different IVC timings or differences in actual EGR percent. This phenomenon should be investigated with further testing.

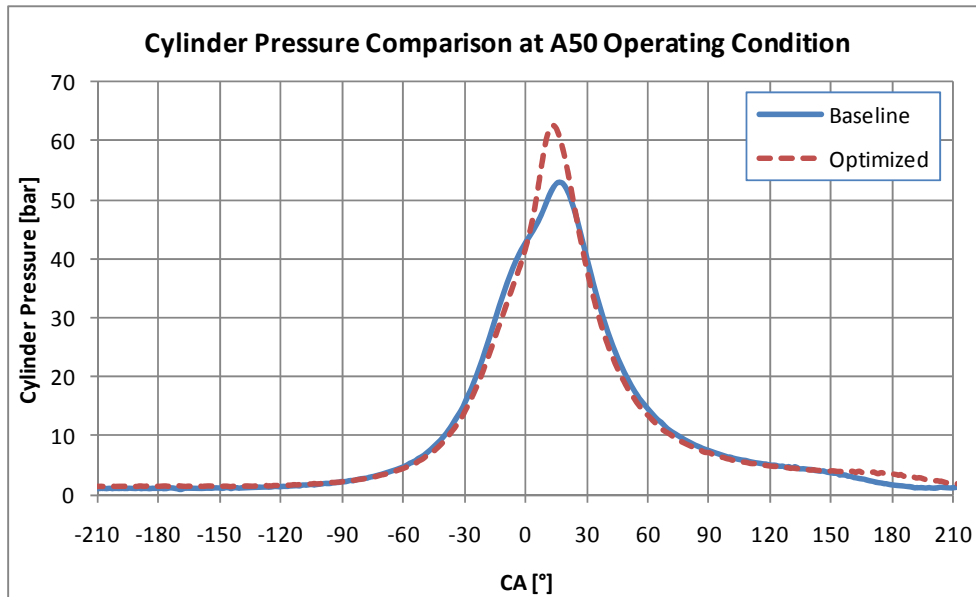
**Figure 77: 50% Heat Release Timing vs. 13 Mode Test Point**



Source: Sturman Industries

Figure 78 shows the cylinder pressure condition for the baseline and optimized tests at the A50 operating condition. The baseline compression shows a higher value due to the increased effective CR; however, the combustion shows a lower peak than the optimized for the same engine load.

**Figure 78: Cylinder Pressure Comparison at A50 Operating Condition**

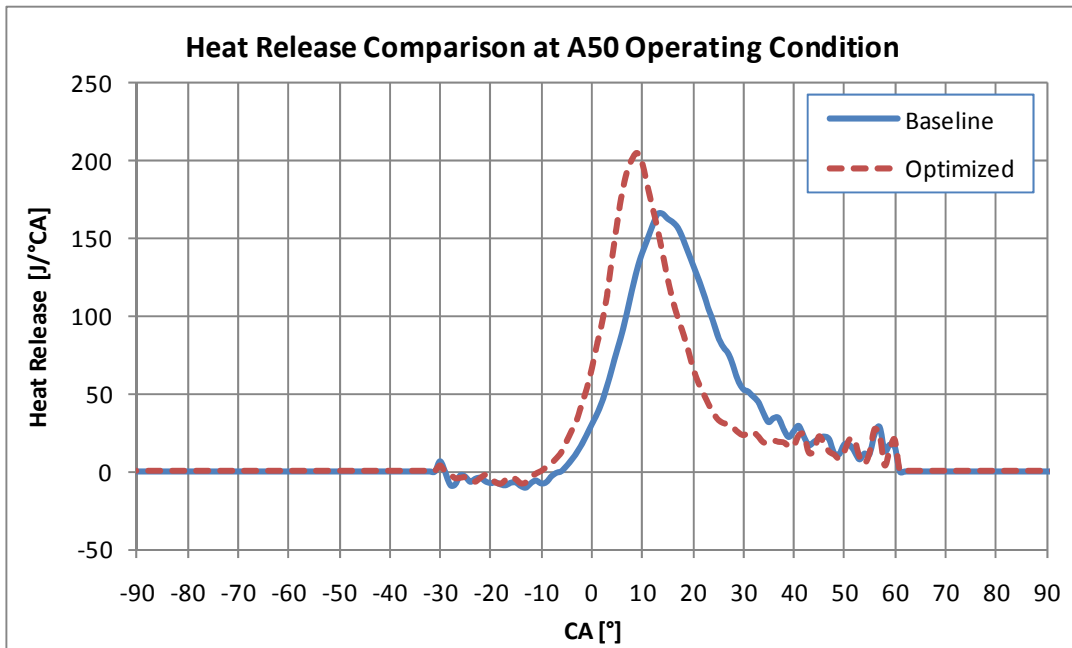


Source: Sturman Industries

Figure 79 shows the heat release comparison for A50 operating condition. The heat release for the optimized point shows a slightly more advanced ignition delay, shorter

combustion duration and higher peak rate. This is an indication of a lower amount of EGR than measured and will be the focus of further development.

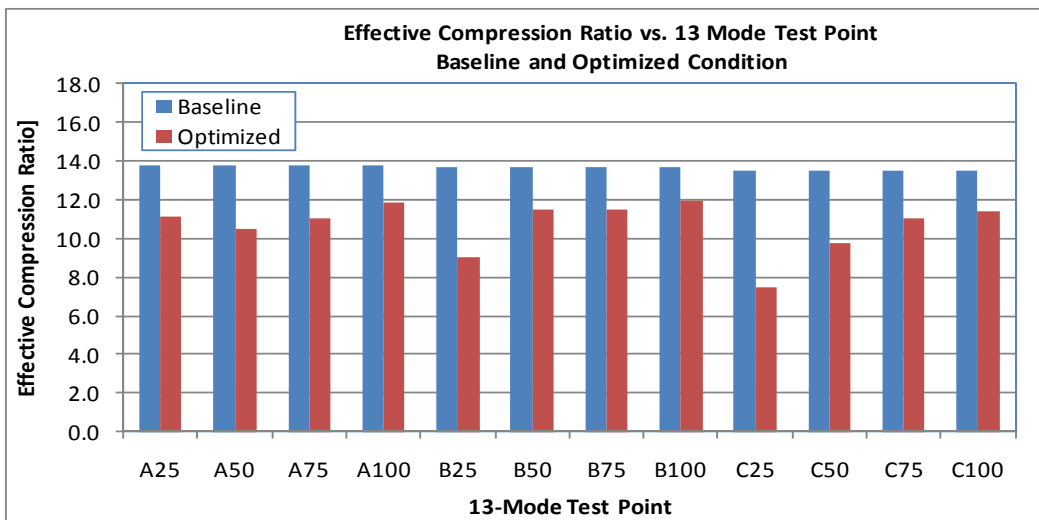
**Figure 79: Heat Release Comparison at A50 Operating Condition**



Source: Sturman Industries

Figure 80 shows the difference between the effective compression ratio between the baseline and optimized conditions for the entire 13-mode test. It can be seen that the intake valve close timing for the optimized test results in an effective compression ratio that can be modified for each test point.

**Figure 80: Effective Compression Ratio vs. 13 Mode Test Point Baseline and Optimized**



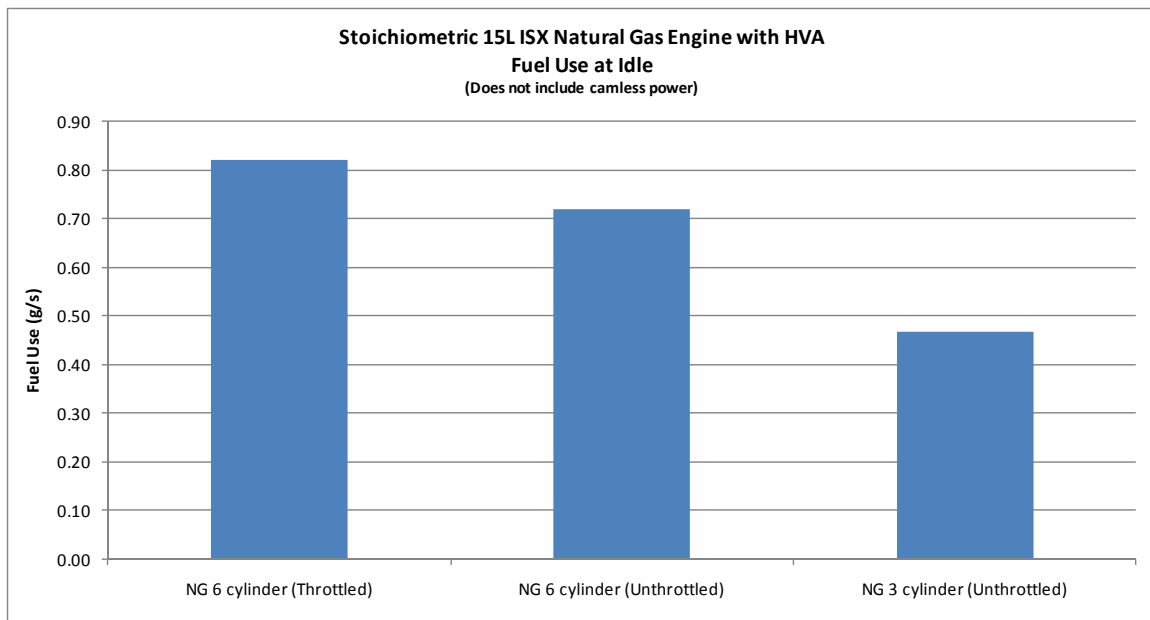
Source: Sturman Industries

### 11.8.4 Optimized Idle Condition

The idle test point was achieved with extremely late IVC (670°BTDC for cylinders 1-3, and 671°BTDC for cylinders 4-6) and only one intake valve active. This allows for lower power consumption of the HVA system, as well as cylinder specific control for idle speed control. With all intake valves closing at 670 °BTDC the idle speed was 750 RPM, and with all intake valves closing at 671°BTDC idle speed was 650 RPM. Compared to the baseline idle condition, the HVA power was reduced from 1.56 kW to 0.89 kW for the optimized condition. Fuel flow also dropped from 0.82 to 0.72 g/s to maintain the same 700 RPM idle speed.

Additional idle testing was performed by running the idle condition on 3 cylinders using the late IVC operating condition. During this test, only one intake and one exhaust valve were utilized for the active cylinders. This resulted in a reduction of fuel flow to 0.47 g/s to maintain 700 RPM idle speed as shown in Figure 81.

**Figure 81: Fuel Use Optimization at Idle**

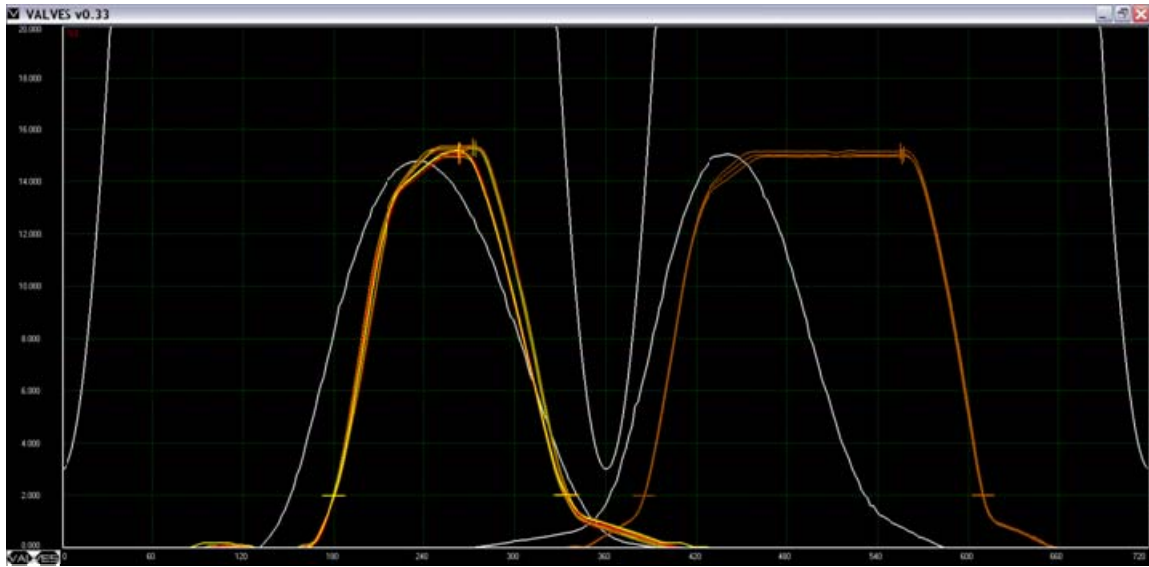


Source: Sturman Industries

### 11.8.5 Three Cylinder Operation at A25, B25, C25

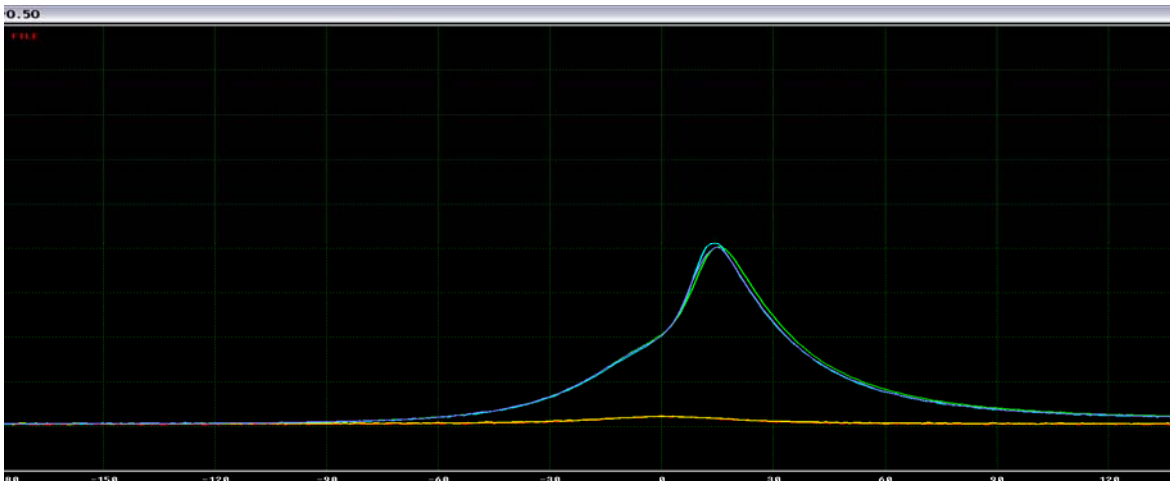
Another operating mode explored with HVA was to run on 3 cylinders at the 25 percent load points. To keep the firing order even, either the front or rear 3 cylinders were switched off to reduce the required flow from the hydraulic system, as well as reduce pumping losses for the engine. The A25, B25, and C25 operating points were explored to investigate any performance improvement. Cylinders 1-3 were deactivated by closing all engine valves for those cylinders. In addition, only 1 intake valve was utilized for cylinders 4-6. The representative HVA valve traces are shown in Figure 82 with the cylinder pressure trace shown in Figure 83 for the A25 operating condition.

**Figure 82: A25\_3Cyl Valve Trace Example**



Source: Sturman Industries

**Figure 83: A25\_3Cyl Cylinder Pressure Example**



Source: Sturman Industries

Resulting performance at this A25 point showed a decrease in BSFC of 11.0 percent and an increase of 3.6 points in BTE as compared to the baseline condition. At the B25 operating point, a decrease in BSFC of 13.9 percent and an increase of 4.6 points in BTE was measured. Finally, the C25 operation with three cylinders resulted in a decrease in BSFC of 18.3 percent and an increase of 5.0 points in BTE as compared to the throttled baseline with 6 cylinders. In addition, replacing these points or the optimized 13-mode composite emissions test allowed all of the values to fall within the emissions targets as shown in Table 19.

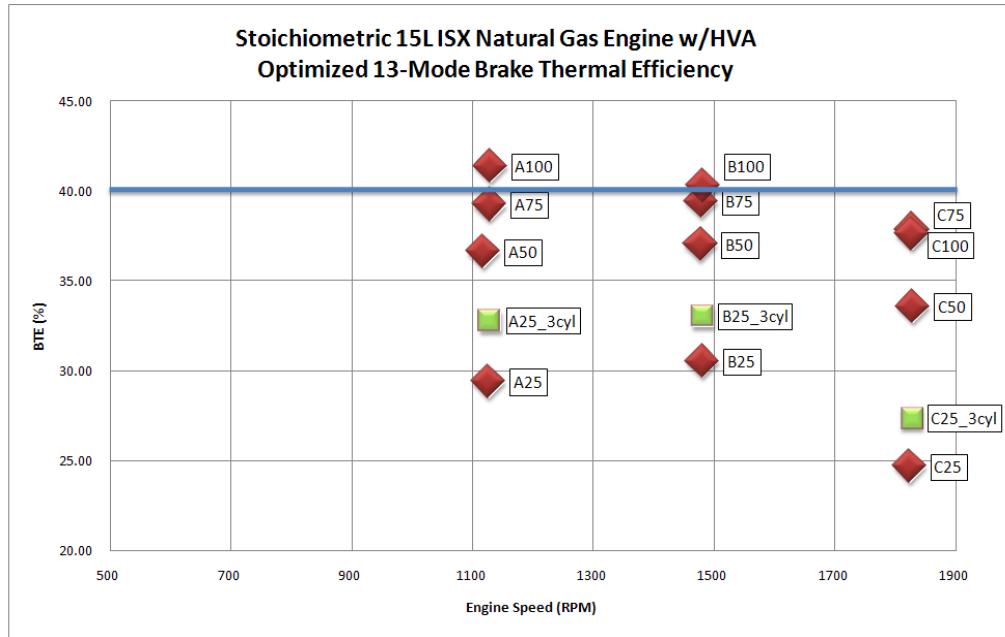
**Table 19: Optimized 13-Mode Results (3 Cylinder Operation at A25, B25, and C25)**

<b>298 kW HP, Cummins ISX, Omnitek Natural Gas System, Sturman HVA, Pump Cart, Optimized (A25, B25, C25 3-Cyl), Mid-Loaded 3-Way Catalyst</b> <i>*numbers corrected for HVA Power and AirDelphi</i>								
		TQ	Weighted Power	BSNOx	BSFC	BSNMHC	BSCO	BTE
Mode	RPM	N-m	kW	g/kW-hr	g/kW-hr	g/kW-hr	g/kW-hr	%
Idle	713	0	0.00	0.000	0.0	0.000	0.000	0.0
A25	1130	406	2.40	0.000	262.4	0.004	0.089	32.8
A50	1118	823	4.82	0.011	234.9	0.000	0.043	36.6
A75	1129	1251	7.40	0.015	219.2	0.003	0.052	39.2
A100	1130	1682	15.92	0.005	207.9	0.035	0.043	41.4
B25	1482	434	6.74	0.000	260.5	0.004	0.207	33.0
B50	1478	945	14.62	0.000	232.4	0.000	0.253	37.0
B75	1479	1450	22.47	0.005	218.1	0.024	0.074	39.4
B100	1482	1928	26.93	0.005	213.6	0.000	0.084	40.3
C25	1828	292	2.79	0.015	314.3	0.000	-0.009	27.4
C50	1830	675	6.46	0.006	256.2	0.013	0.437	33.6
C75	1829	1065	10.20	0.011	227.2	0.008	0.020	37.8
C100	1828	1420	21.75	0.005	228.7	0.003	0.068	37.6
<b>13-Mode Composite</b>				<b>0.006</b>	<b>226.8</b>	<b>0.010</b>	<b>0.105</b>	<b>38.13</b>

Source: Sturman Industries

A graphical representation of the optimized BTE is shown in Figure 84. Two of the test points, A100 and B100, are above the targeted single point efficiency of 40 percent at 41.37 percent and 40.26 percent respectively. Additional points shown are A25\_3cyl, B25\_3cyl and C25\_3cyl which represent the BTE achieved while operating the engine on 3 cylinders and only 3 valves per cylinder (x1 intake and x2 exhaust valves).

**Figure 84: Optimized BTE Summary**

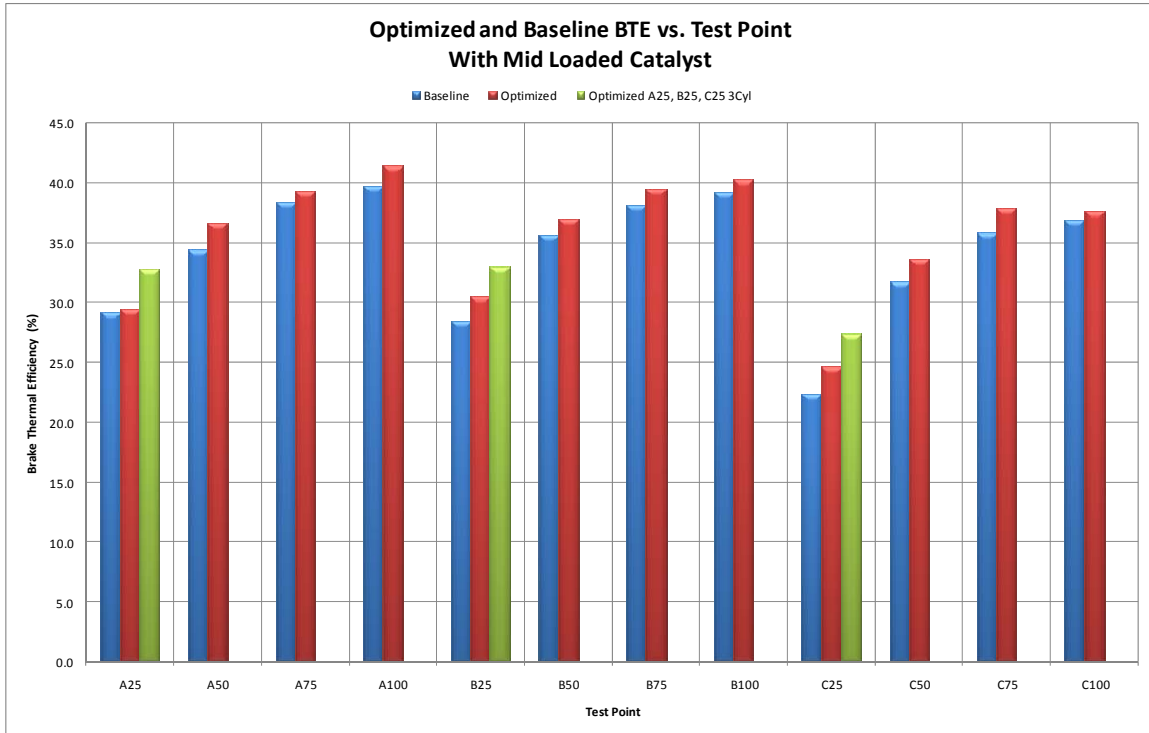


Source: Sturman Industries

### 11.8.6 Optimized Comparison to Baseline

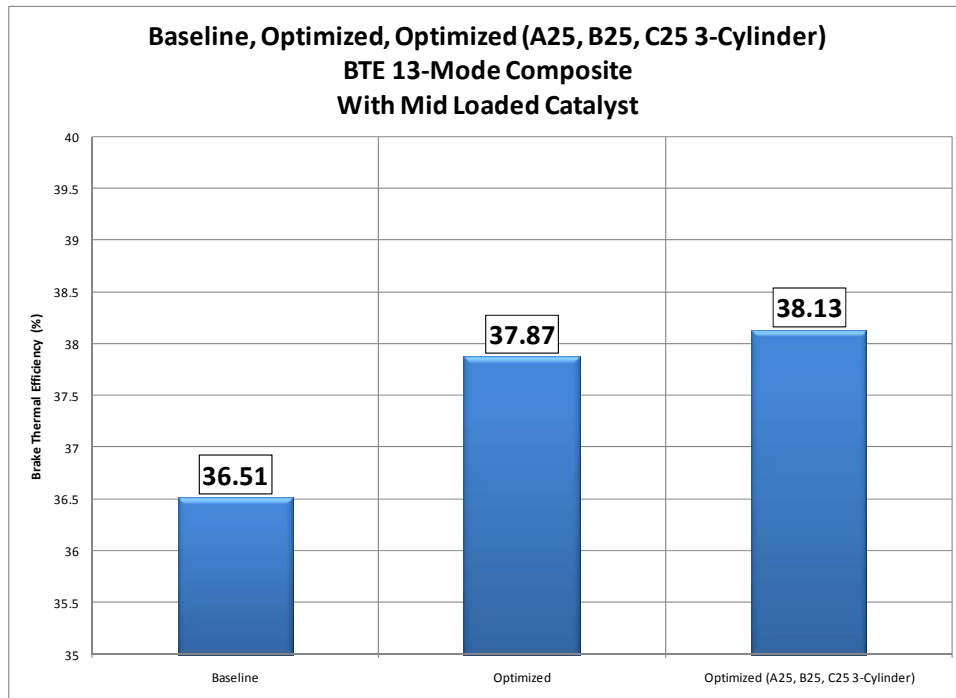
Comparing BTE per 13-mode operating point between Optimized and Baseline shows a positive trend towards unthrottled operation, increasing BTE by a minimum of 0.21 to a maximum of 3.57 points shown in Figure 85. Composite BTE values are shown below in Figure 85 comparing Baseline, Optimized, and Optimized 3-Cylinder points. By operating the engine unthrottled the composite 13-mode BTE increases by 1.41 points.

**Figure 85: Optimized and Baseline 13-Mode BTE Comparison**



Source: Sturman Industries

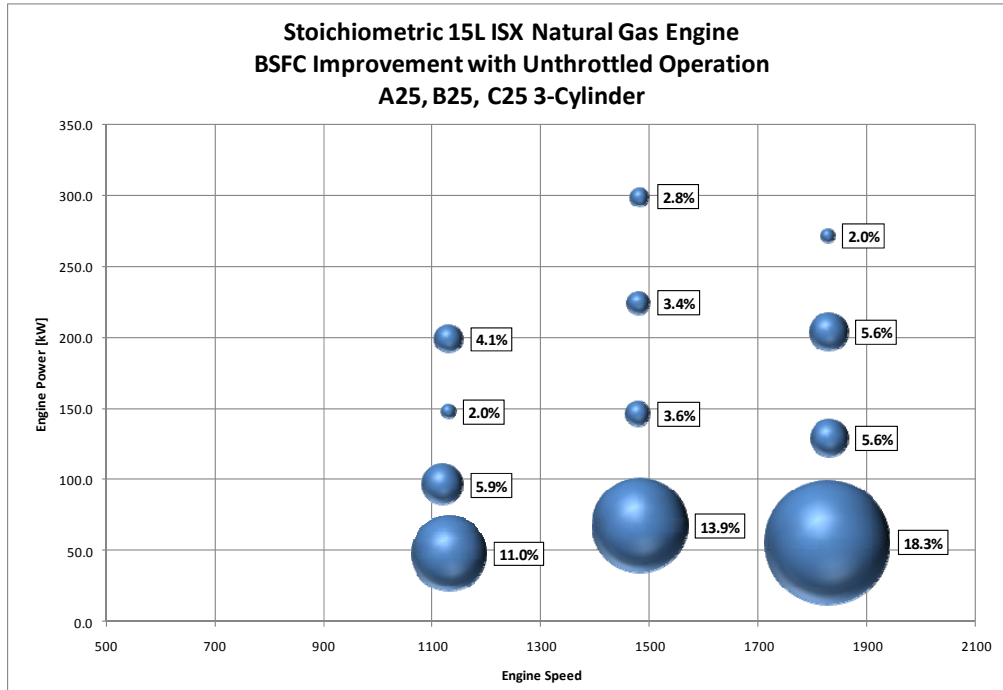
**Figure 86: 13-Mode Composite BTE Comparison**



Source: Sturman Industries

Figure 87 below shows the BSFC improvement over the 13-mode test for the condition in which test points A25, B25 and C25 were run in 3-cylinder mode. The general trend is that as engine load increases, the benefits of running the engine unthrottled is reduced as the pumping losses decrease with increasing throttle opening.

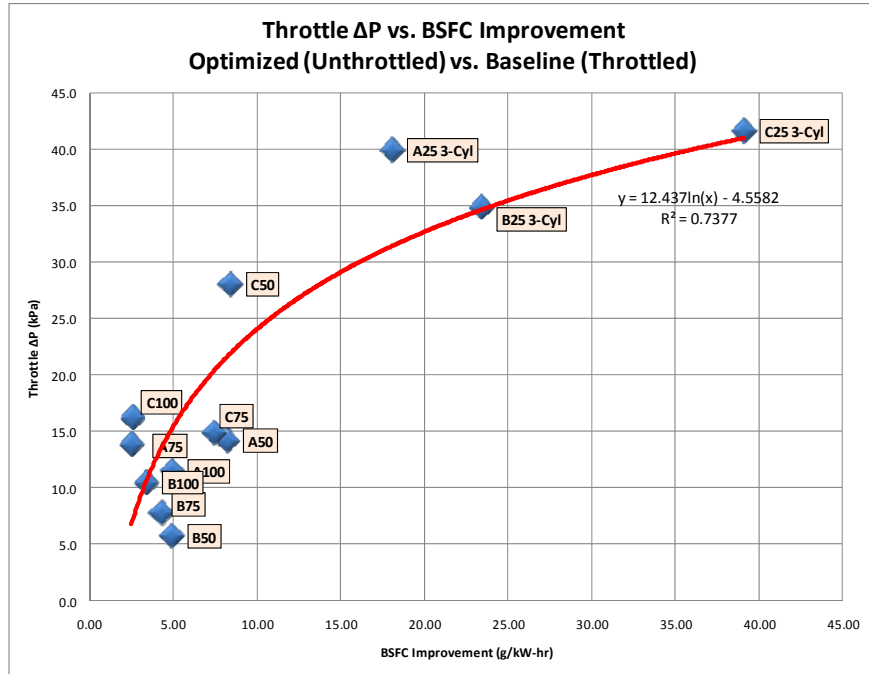
**Figure 87: Optimized vs. Baseline BSFC Improvement**



Source: Sturman Industries

Figure 88 below displays a non-linear trend of BSFC improvement in g/kW-hr as the pressure differential across the throttle plate increases. Again, significant improvements in fuel economy are noted at the light load points with cylinder deactivation.

**Figure 88: Throttle ΔP vs. BSFC Improvement**



Source: Sturman Industries

Table 20 displays the composite 13-mode results of the three test cases performed. Results in red fall outside the emissions targets, and results in green fall within the emissions targets. The higher CO values shown in Table 20 are the result of the A/F ratio control at low load and the narrow window of A/F ratios where the catalyst can reduce both NOx and CO and not necessarily combustion stability. During testing, effort to reduce the NOx emissions caused the CO emissions to be higher than the target. Optimized A25, B25, C25 3-Cyl composite results achieve two test points with BTE ≥40 percent and have emissions values that are within target values. This highlighted that additional combustion temperature from the higher loaded cylinders improved the overall emissions results. Additional data for Optimized and Baseline operation is contained in Appendix D and Appendix E.

**Table 20: 13-Mode Composite Comparison**

13-Mode Composite Values Per Test			
	Baseline	Optimized	Optimized (A25, B25, C25 3-Cyl)
<b>BTE</b>	36.51	37.87	38.13
<b>BSFC (g/kW-hr)</b>	238.4	229.3	226.8
<b>BSNO<sub>x</sub> (g/kW-hr)</b> Target ≤ 0.0794	0.007	0.011	0.006
<b>BSCO (g/kW-hr)</b> Target ≤ 0.1134	0.122	0.117	0.105
<b>BSNMHC (g/kW-hr)</b> Target ≤ 0.0227	0.060	0.014	0.010

Source: Sturman Industries

# CHAPTER 12: Conclusions and Recommendations

## 12.1 Conclusions

This report documents the design of an HVA system for the Cummins ISX15 for use with natural gas. Analysis and simulation show that the system met the technical requirements for use on this program. The HVA system consists of a single-lift actuator for each engine valve combined with a transfer plate and rail assembly. The modular HVA design allows the system to be installed on the head and tested before installation on the engine. The hydraulic simulation showed acceptable system response with an engine mounted pump.

The HVA system allowed unthrottled operation with load control done with IVC timing. Improvements in efficiency have been realized by way of unthrottled operation, valve deactivation, and complete cylinder deactivation afforded by the flexibility of the HVA system.

The low MN natural gas used at the dynamometer facility limited full load operation without engine knock. This utility-supplied natural gas illustrated the potential of the HVA to operate the engine in a highly efficient manner. The test results show optimized composite 13-mode results as follows:

- BTE : 38.13%
- BSFC : 226.8 g/kW-hr
- BSNO<sub>x</sub>: 0.006 g/kW-hr
- BSCO: 0.105 g/kW-hr
- BSNMHC: 0.010 g/kW-hr

Both the optimized A100 and B100 points illustrate greater than 40 percent BTE. This achieves the program's targets of ARB 2007 emissions compliance with CHP credit and at least one operating point above 40 percent BTE. In addition, it is believed that a higher MN gas would have contributed to both higher efficiency and increased engine load capability.

## 12.2 Commercialization Potential

### 12.2.1 Regulatory and Institutional Factors

Regulation of criteria pollutants has been the single greatest driver of advanced emission controls and engine development in general. This trend is especially true in the mobility market, while in the power generation market, fuel prices have also been technology drivers for improved efficiency.

US EPA emission regulations for distributed resources set for 2014 will be the single greatest driver for retrofit of existing power generation and gas compression engines

with advanced emission controls. The effect of this regulation is already being felt as sales of lean burn engine engines, which will require Lean NO<sub>x</sub> after treatment, have practically ceased in the United States, with the less efficient Stoichiometric engines dominating the market. For California, where emission limits are even lower, there are no engines currently offered for sale that will meet California's standard. Sturman is focused on incorporating the technology demonstrated under this project into emission control kits for 300kW – 1MW genset engines in the 2014 timeframe.

Natural Gas prices are also expected to remain historically low, ~\$4/MCF, into the foreseeable future. While these prices may discourage investment into engine efficiency for power generation, they will invariably be major drivers for efficiency in the gas compression industry where profits will be squeezed and efficiency will play an increasingly important role.

Finally, while the future of CO<sub>2</sub> regulation is uncertain, global climate change remains a monumental challenge of historic proportion and some level of regulation is inevitable. CO<sub>2</sub> reduction is expected to be a major driver for reduced fuel consumption in the near future.

Turning our attention to institutional factors, distributed power generation presents a major paradigm shift in the way electricity is generated. Decentralized generation will require significant advances in supply side management and smart grid technologies. The utility companies who today control the US utility grids must be willing to adopt a new way of thinking and doing business which presents new control and safety challenges. However, the opportunity to double overall engine efficiency through distributed CHP systems cannot be ignored in the face of rising energy prices and global climate change. Sturman looks forward to and is committed to developing energy solutions that not only meet these challenges, but present real economic benefit and opportunities to suppliers and consumers alike.

### 12.2.2 Required Business and Commercial Relationships

A shift to distributed power generation employing CHP systems will require a multi-disciplinary collaboration between industry, government, and investment capital. To this end Sturman has developed strategic relationships to commercialize HVA and closed-loop control technologies.

- Rotating Energy Services of Commerce City, CO is a strategic partner involved in deployment and servicing of NG power generation and gas compression equipment. RES currently services NG producers in North and Central America and will serve as a technology implementation partner and commercial product distributor.
- The State of California and more specifically the Energy Commission have been an excellent partner assisting with the demonstration of Sturman's advanced engine technology. Sturman looks forward to a continued relationship focused on commercializing energy solution that reduce criteria pollutants and GHG emission, reduce energy costs, and secure our energy future.

- Investment Capital. Sturman is in active negotiations with private investors to commercialize the technology demonstrated under this project by 2014.
- Mechanical and Electronic system suppliers. Sturman is developing strategic relationships with component and system suppliers including volume manufacturers, electronic suppliers with experience in the gas compression and power generation markets, and industrial test labs. Current activities include early stage cost analysis, manufacturing process development, and project planning.

### 12.2.3 Economic Market Potential

Sturman is in the process of completing a detailed market analysis with our commercial partners. Preliminary results suggest Sturman's technology presents a strong value proposition that aligns with regulatory, institutional, and commercial needs. Key economic criteria being studied include the following and can be shared with the Energy Commission upon request:

- Commercial Product Costs (estimated as a function of sales per year)
- Classes of Customers
  - Requirements, needs, and benefits induce them to buy your product
- Projected selling prices for your product consistent with the projected sales volume and market position
- Projected rate of penetration of sales of your product/technology in California and elsewhere, including expected sales in each year

## 12.3 Recommendations

Further development work recommended for this engine includes the following:

1. Continued controls work to add load based torque control and reduce engine starting time. Additional closed loop knock control should be added to improve catalyst monitoring via an onboard NOx sensor.
2. Optimize HVA opening and damping rates
3. Add a low pressure EGR system to improve efficiency
4. Replace turbocharger with better matched unit to provide higher pressure ratios at lower engine speeds that can also handle higher inlet temperatures for NG operation (waste-gated turbine vs. VGT)
5. Test engine for IVC vs. Boost Pressure to optimize efficiency
6. Test engine with higher MN natural gas to achieve higher load without knock
7. Test engine with lower MN natural gas to develop cylinder based IVC knock control
8. Test engine with engine mounted hydraulic pump

9. Package and test DI NG injection system
10. CFD analysis of natural gas injection point and combustion chamber design
11. Investigation of multiple valve events, split intake valve events, and early intake valve close as well as cylinder-to-cylinder balancing
12. Install a venturi-based measurement system for the EGR percent measurement to improve accuracy

## **12.4 Benefits to California**

Sturman's HVA and closed-loop combustion control have broad applicability to mobile and stationary internal combustion engines, however this program specifically focuses on distributed power generation, including Combined Heat and Power (CHP) systems, which will be the subject of the discussion on benefits to the State of California. Under this program, Sturman has demonstrated NG engine efficiencies over 40 percent, while meeting California emission standards for distributed resources without the use of lean NO<sub>x</sub> after treatment. The high level accomplishments of this program include:

- Peak Brake Thermal Efficiency of 41.4 percent and composite efficiency of 38.1 percent
- It is expected that even greater improvements in efficiency are possible with higher quality gas as the gas used for this testing was of exceptionally poor quality (~65MN)
- Composite NO<sub>x</sub> emissions levels of 0.006 g/kW-hr, target was <0.064 g/kW-hr in CHP systems; Composite CO emissions levels of 0.105 g/kW-hr, target was <0.1134 g/kW-hr in CHP systems; Composite NMHC emissions levels of 0.010 g/kW-hr, target was <0.0227 g/kW-hr in CHP systems
- Elimination of lean NO<sub>x</sub> after treatment system translating in approximately \$40,000 savings per engine (assuming technology is scaled up to 1MW power rating per engine)
- Adaptation to varying fuel quality using control of effective compression ratio

### **12.4.1 Background of California's Energy Problem**

The state of California intends to install up to 4000 MW of new power generating capacity over the next decade. Thus, the implementation of Distributed Power Generation is of great interest and is the only practical way to fully utilize the potential of CHP systems (power generation at the point of use allows for the practical recovery of low quality waste heat for industrial processing, hot water, and space heating. CHP Systems offer up to 80 percent overall efficiency, effectively doubling the efficiency of today's simple power generating units without heat recovery. Distributed Power Systems can be implemented on small as well as large scale using reciprocating piston internal combustion engines; large scale installations making use of a plurality of engines. By turning engines on and off in order to match supply and demand, peak

efficiencies can be achieved nearly all of the time, avoiding the poor efficiencies associated with part load operation. Reciprocating piston engines are the most responsive power generating systems making them ideally suited to respond to fluctuating loads and wind and solar generation.

#### 12.4.2 Assumptions used in Calculations of Energy Savings

- For purposes of calculating expected benefits of this project, 30 percent of the new 4000 MW of power generating capacity is assumed to come from distributed CHP systems.
- The ideal engine size for implementing the new distributed generation will be between 500 kW and 1 MW; 1M engines are assumed for purpose of calculations.
- Distributed Power System will typically run at a duty cycle of 60 percent of rated power.
- NG costs in the future will average a conservative \$4 / MCF (1000 cu. ft.) in today's dollars.
- All cost savings calculations are in today's dollars and do not reflect inflation or rising fuel costs
- Engine efficiency increase to an average of 38 percent compared to today's 34 percent BTE

#### 12.4.3 Expected Benefits (Energy and Savings to Ratepayers)

- Efficiency gains will result in a reduction in fuel consumption of 6.8 billion MCF (1000 cu. ft.) per year or 205 billion MCF over the 30 year life of the engines. If CHP systems are enabled by the distributed power approach, the reduction in fuel consumption increases dramatically to 31 billion MCF per year and 914 billion MCF over 30 years.
- The reduction in fuel consumption triggered by the efficiency gains will also result in a fuel cost savings of \$27B per year and \$820B over 30 years (in today's dollars) for California's rate payers. Again analyzing the potential in the context of CHP systems, the savings increase dramatically to \$122B per year or \$3.7T over 30 years (in today's dollars.)
- The elimination of lean NOx after treatment is estimated to save \$40,000 per engine, translating into \$48M in the implementation of 30 percent of the 4000 MW of power.

Closed-loop combustion control will allow for the efficient use of many more NG supplies including low quality or low energy content gas.

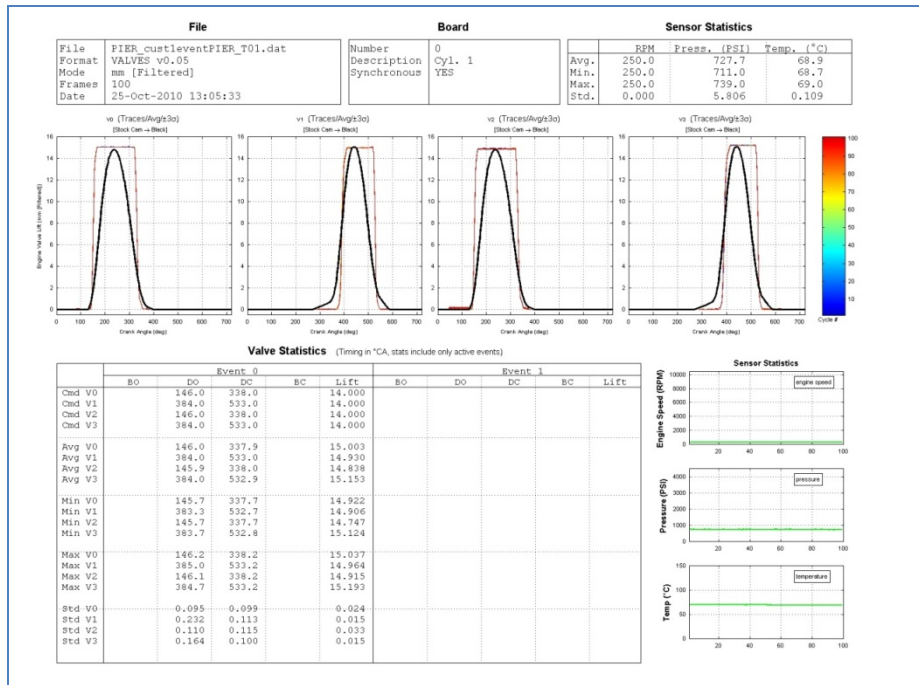
## GLOSSARY

<b>A/F</b>	Air-fuel
<b>ARB</b>	Air Resources Board
<b>ARES</b>	Advanced Reciprocating Engine Systems
<b>BMEP</b>	Brake Mean Effective Pressure
<b>BSCO</b>	Brake Specific Carbon Monoxide Emissions
<b>BSFC</b>	Brake Specific Fuel Consumption
<b>BSNMHC</b>	Brake Specific Non Methane Hydrocarbons Emissions
<b>BSNOx</b>	Brake Specific NOx Emissions
<b>BTE</b>	Brake Thermal Efficiency
<b>CAN</b>	Controller Area Network
<b>CARB</b>	California Air Resources Board
<b>CFD</b>	Computational Fluid Dynamics
<b>CHP</b>	Combined Heat and Power
<b>CNG</b>	Compressed Natural Gas
<b>Condor</b>	Designation for HVA Controller
<b>COV</b>	Coefficient of Variation
<b>ECM-66A</b>	Designation for Natural Gas Control Unit
<b>EGR</b>	Exhaust Gas Recirculation
<b>FEA</b>	Finite Element Analysis
<b>FPGA</b>	Field Programmable Gate Array
<b>GUI</b>	Graphical User Interface
<b>HC</b>	Hydrocarbon
<b>HCCI</b>	Homogeneous Charge Compression Ignition
<b>HVA</b>	Hydraulic Valve Actuation
<b>HVA-D</b>	Hydraulic Valve Actuation – Digital
<b>ISX</b>	Cummins Engine Platform Designation
<b>IVC</b>	Intake Valve Close
<b>MAF</b>	Mass Air Flow
<b>NGFS</b>	Natural Gas Fuel System
<b>PI</b>	Proportional-Integral
<b>SCALE</b>	Sturman CALibration Editor
<b>SCR</b>	Selective Catalyst Reduction
<b>SHRED</b>	Sturman Heat Release EDitor
<b>SISt</b>	Spark-Ignited Stoichiometric
<b>STEC</b>	Sturman Total Engine Controller

<b>THC</b>	Total Hydrocarbons
<b>TWC</b>	Three Way Catalyst
<b>VGT</b>	Variable Geometry Turbo

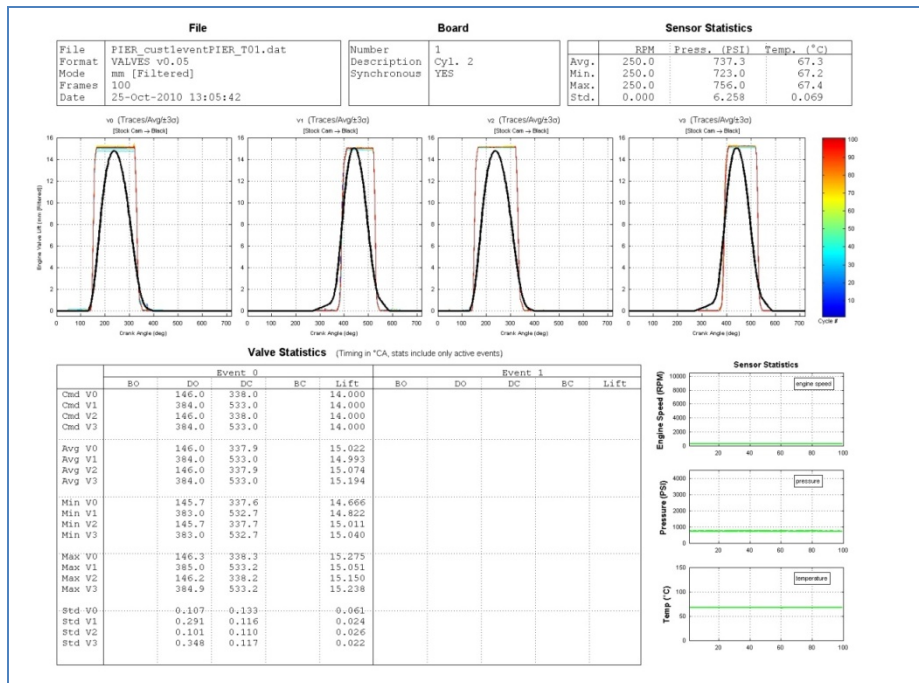
# Appendix A: Multi Cylinder Validation Test Results

## Figure 89: TP01 Cylinder 1 Overlay



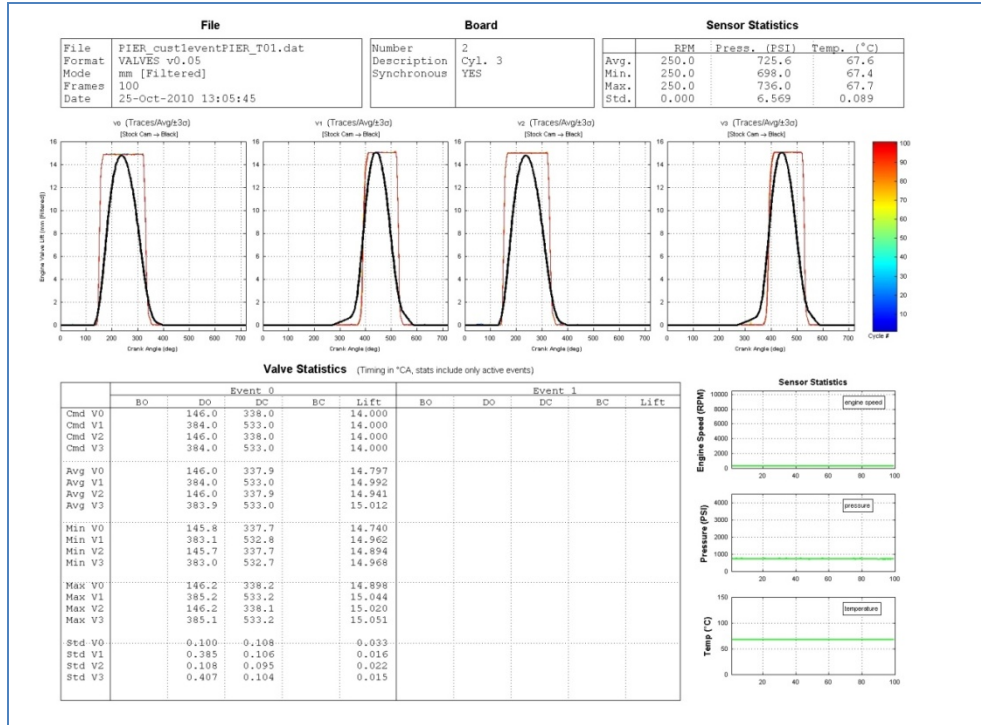
Source: Sturman Industries

## Figure 90: TP01 Cylinder 2 Overlay



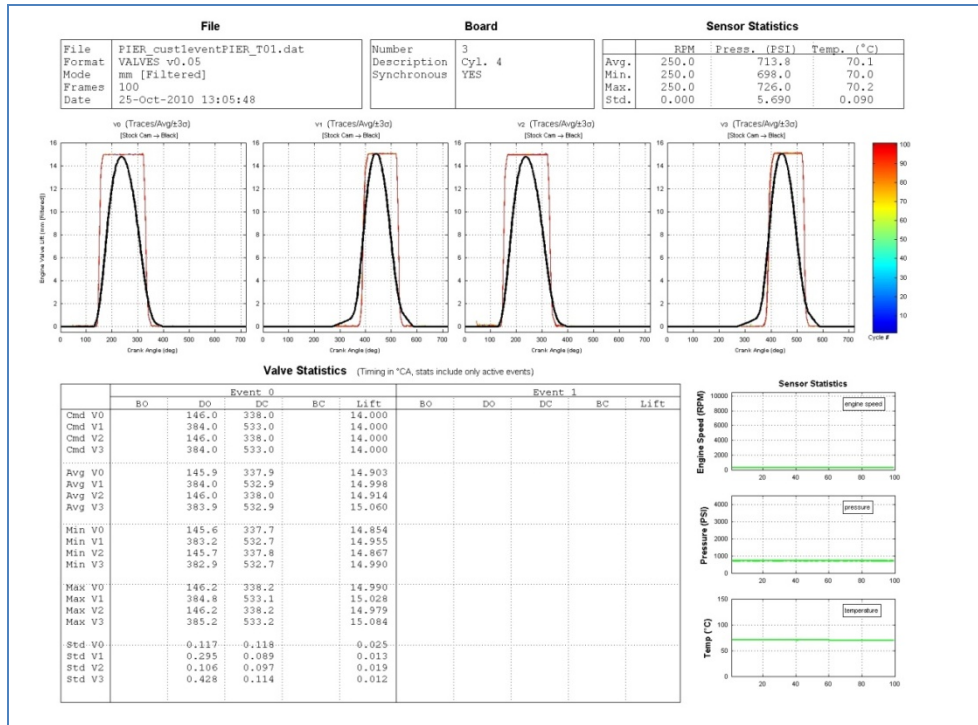
Source: Sturman Industries

## Figure 91: TP01 Cylinder 3 Overlay



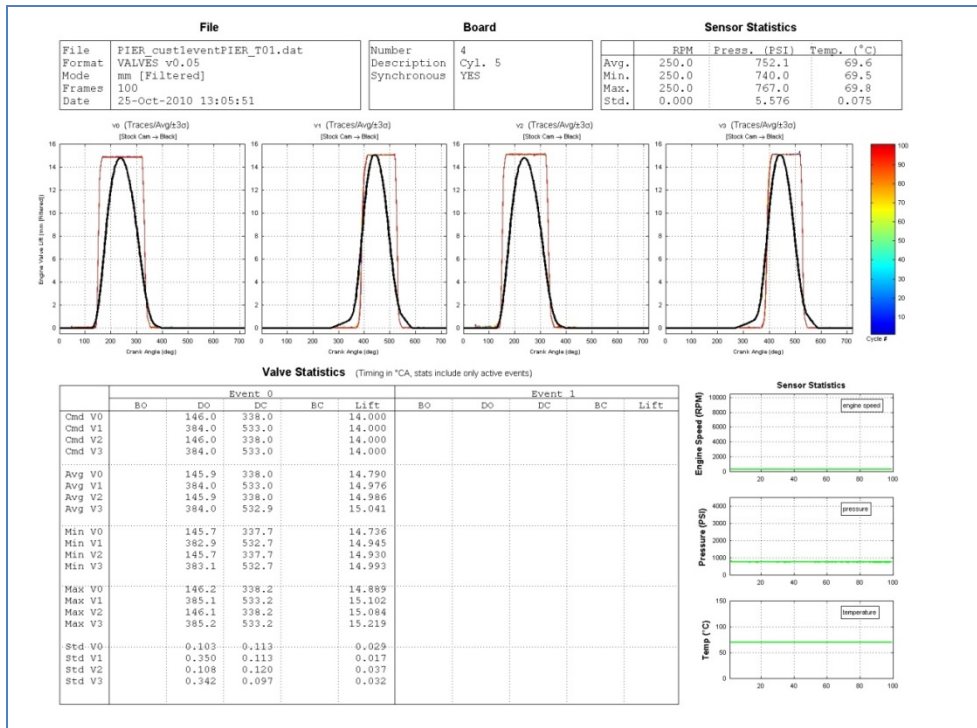
Source: Sturman Industries

Figure 92: TP01 Cylinder 4 Overlay



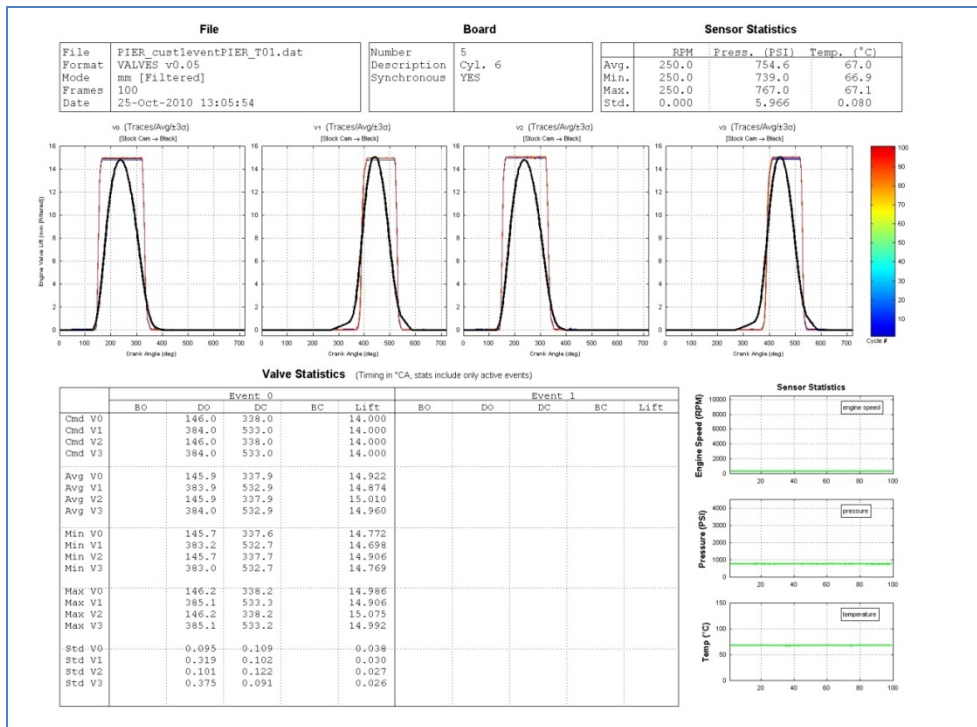
Source: Sturman Industries

Figure 93: TP01 Cylinder 5 Overlay



Source: Sturman Industries

Figure 94: TP01 Cylinder 6 Overlay



Source: Sturman Industries

Figure 95: TP01 Cylinder 1 by Cycle



Source: Sturman Industries

Figure 96: TP01 Cylinder 2 by Cycle



Source: Sturman Industries

Figure 97: TP01 Cylinder 3 by Cycle



Source: Sturman Industries

Figure 98: TP01 Cylinder 4 by Cycle



Source: Sturman Industries

Figure 99: TP01 Cylinder 5 by Cycle



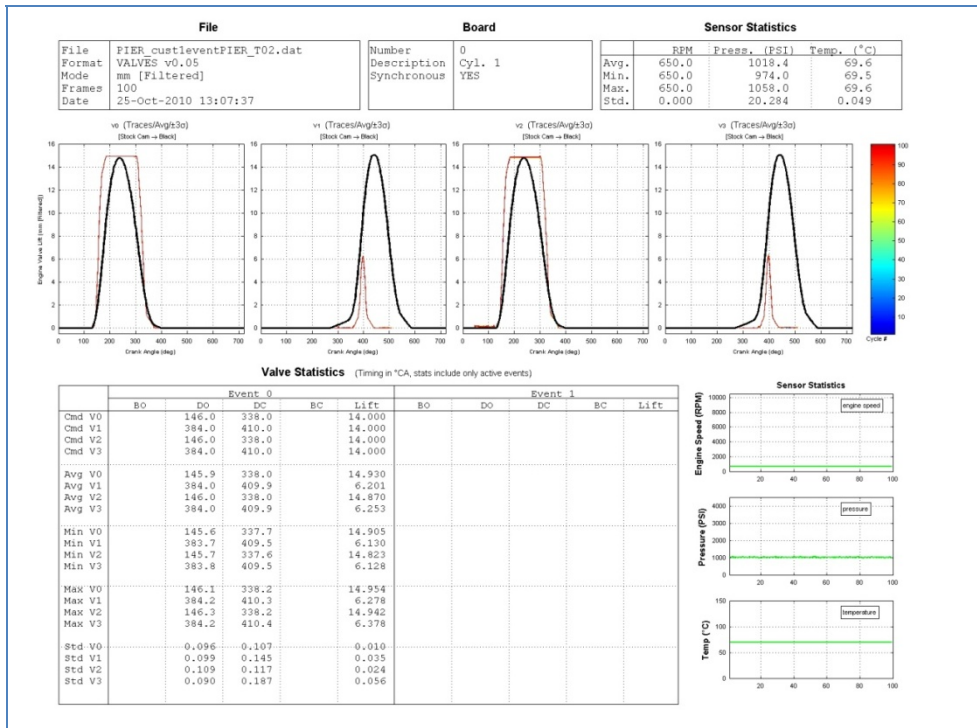
Source: Sturman Industries

Figure 100: TP01 Cylinder 6 by Cycle



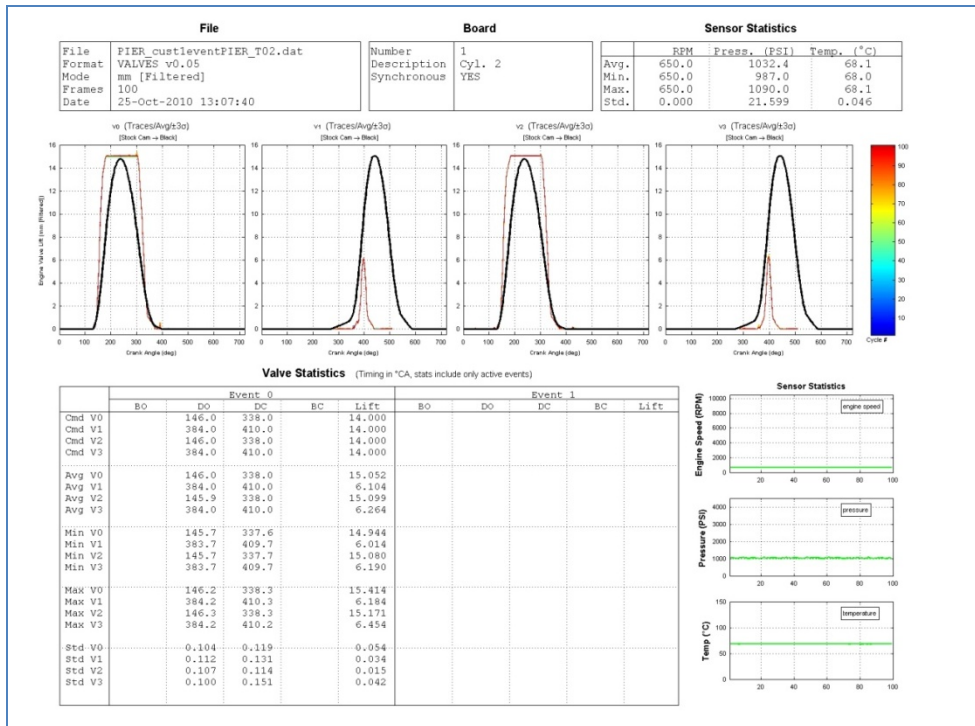
Source: Sturman Industries

Figure 101: TP02 Cylinder 1 Overlay



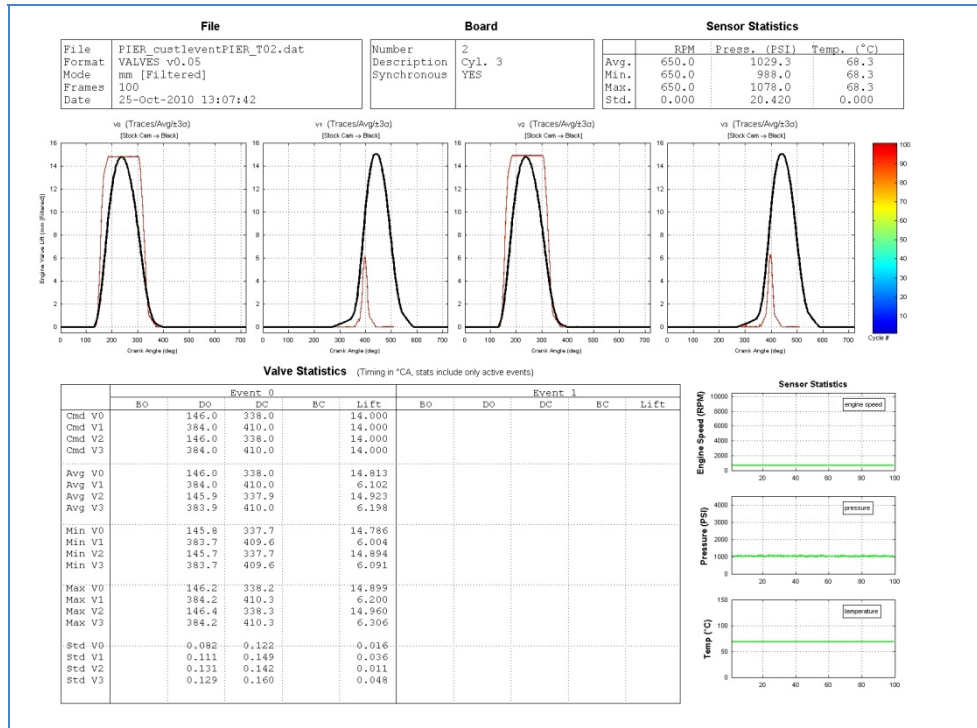
Source: Sturman Industries

Figure 102: TP02 Cylinder 2 Overlay



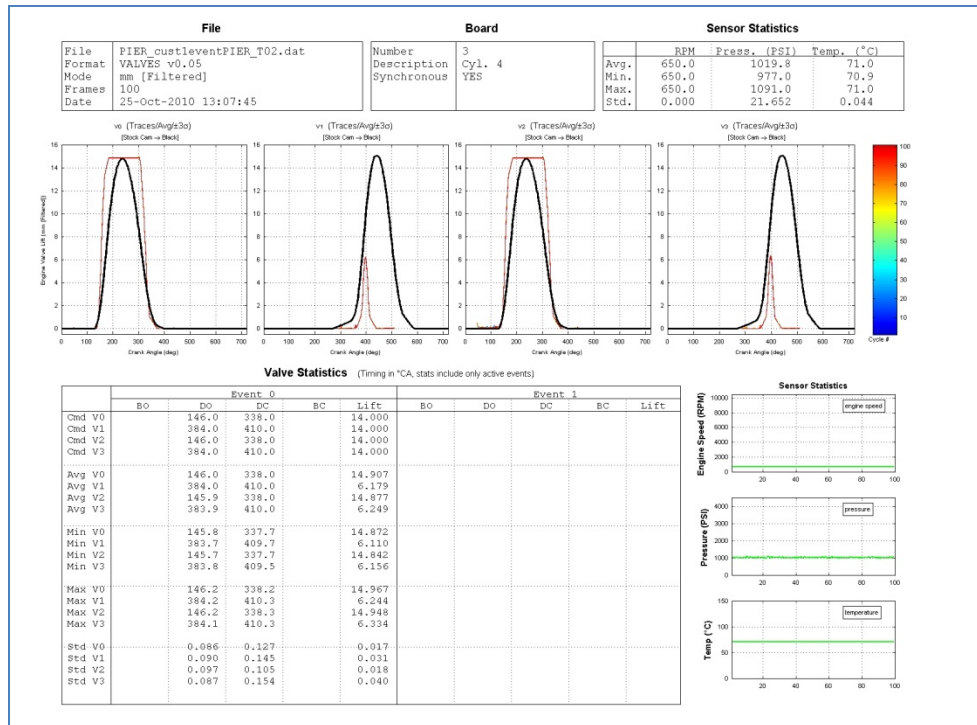
Source: Sturman Industries

Figure 103: TP02 Cylinder 3 Overlay



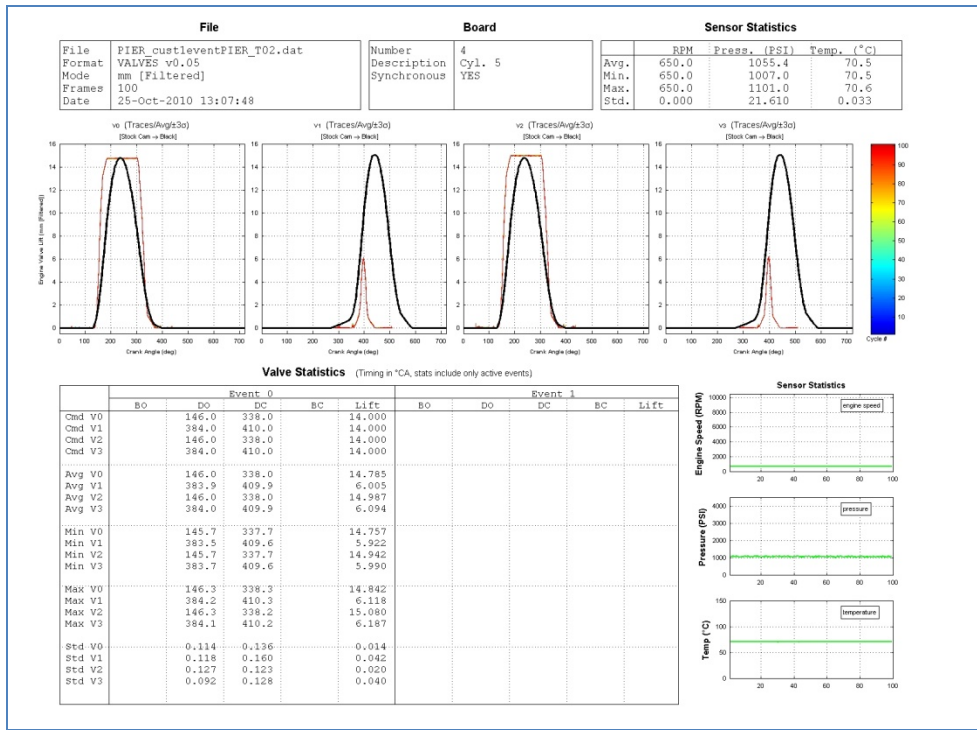
Source: Sturman Industries

Figure 104: TP02 Cylinder 4 Overlay



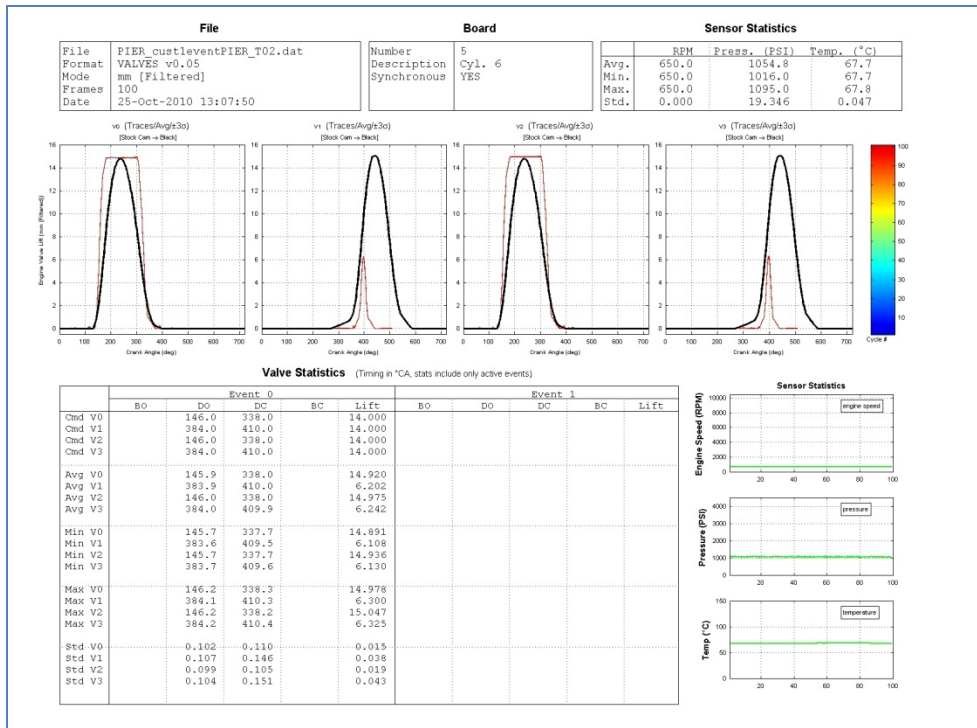
Source: Sturman Industries

Figure 105: TP02 Cylinder 5 Overlay



Source: Sturman Industries

Figure 106: TP02 Cylinder 6 Overlay



Source: Sturman Industries

Figure 107: TP02 Cylinder 1 by Cycle



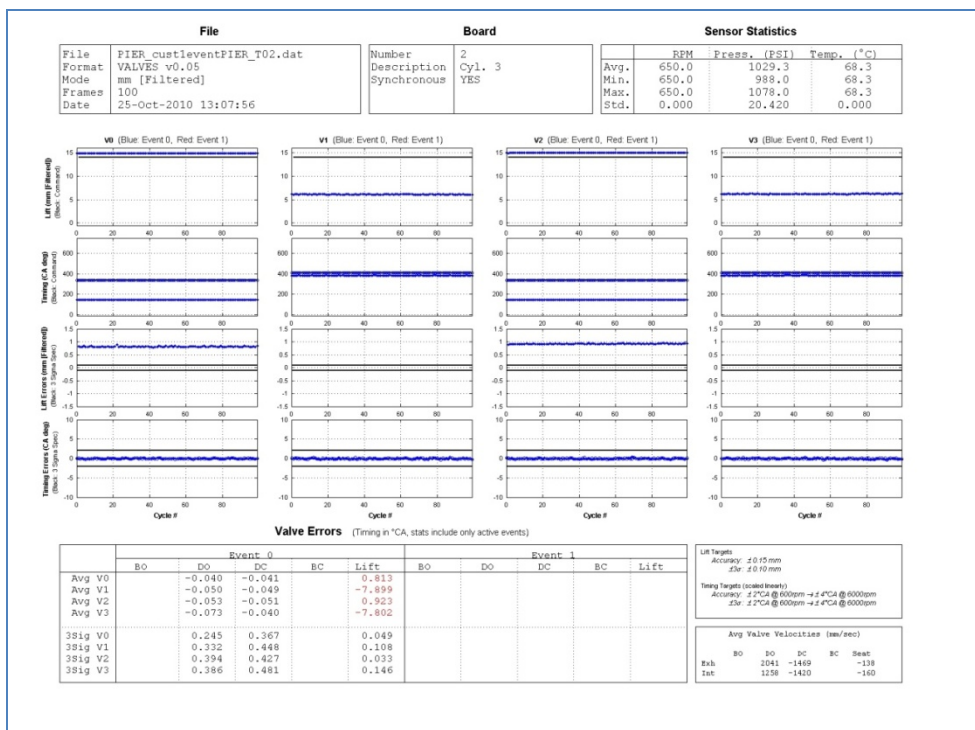
Source: Sturman Industries

Figure 108: TP02 Cylinder 2 by Cycle



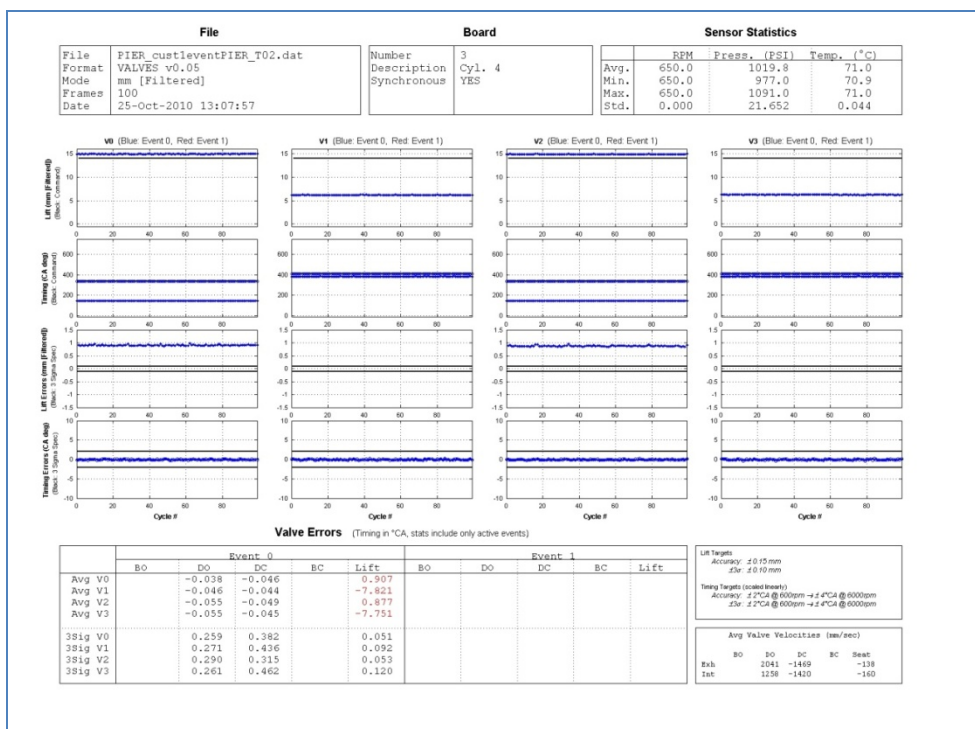
Source: Sturman Industries

Figure 109: TP02 Cylinder 3 by Cycle



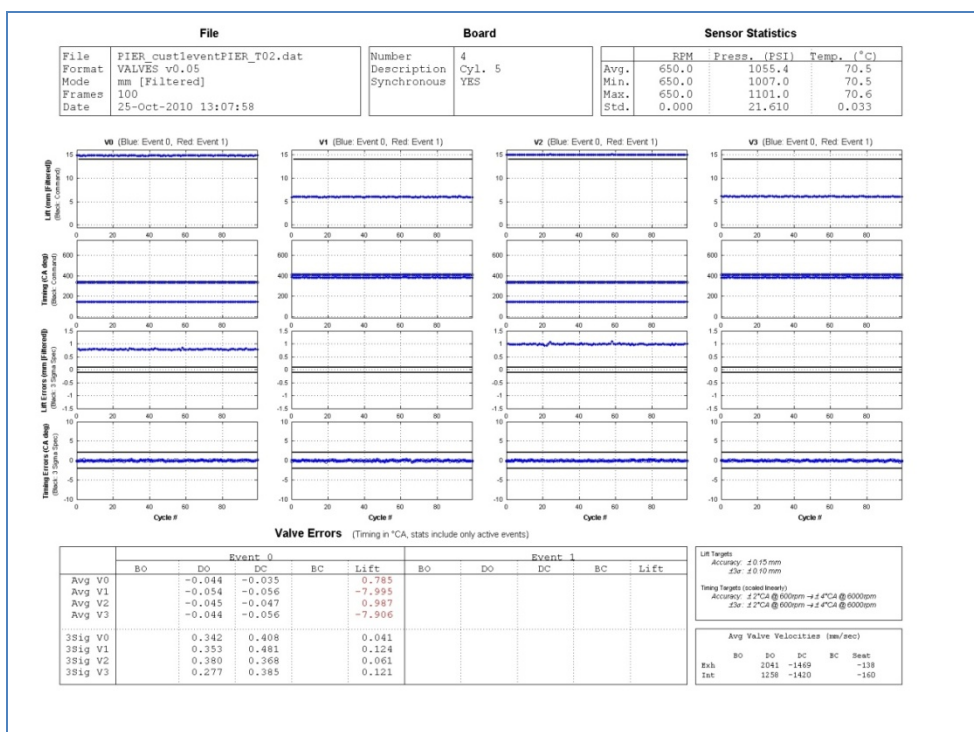
Source: Sturman Industries

Figure 110: TP02 Cylinder 4 by Cycle



Source: Sturman Industries

Figure 111: TP02 Cylinder 5 by Cycle



Source: Sturman Industries

Figure 112: TP02 Cylinder 6 by Cycle

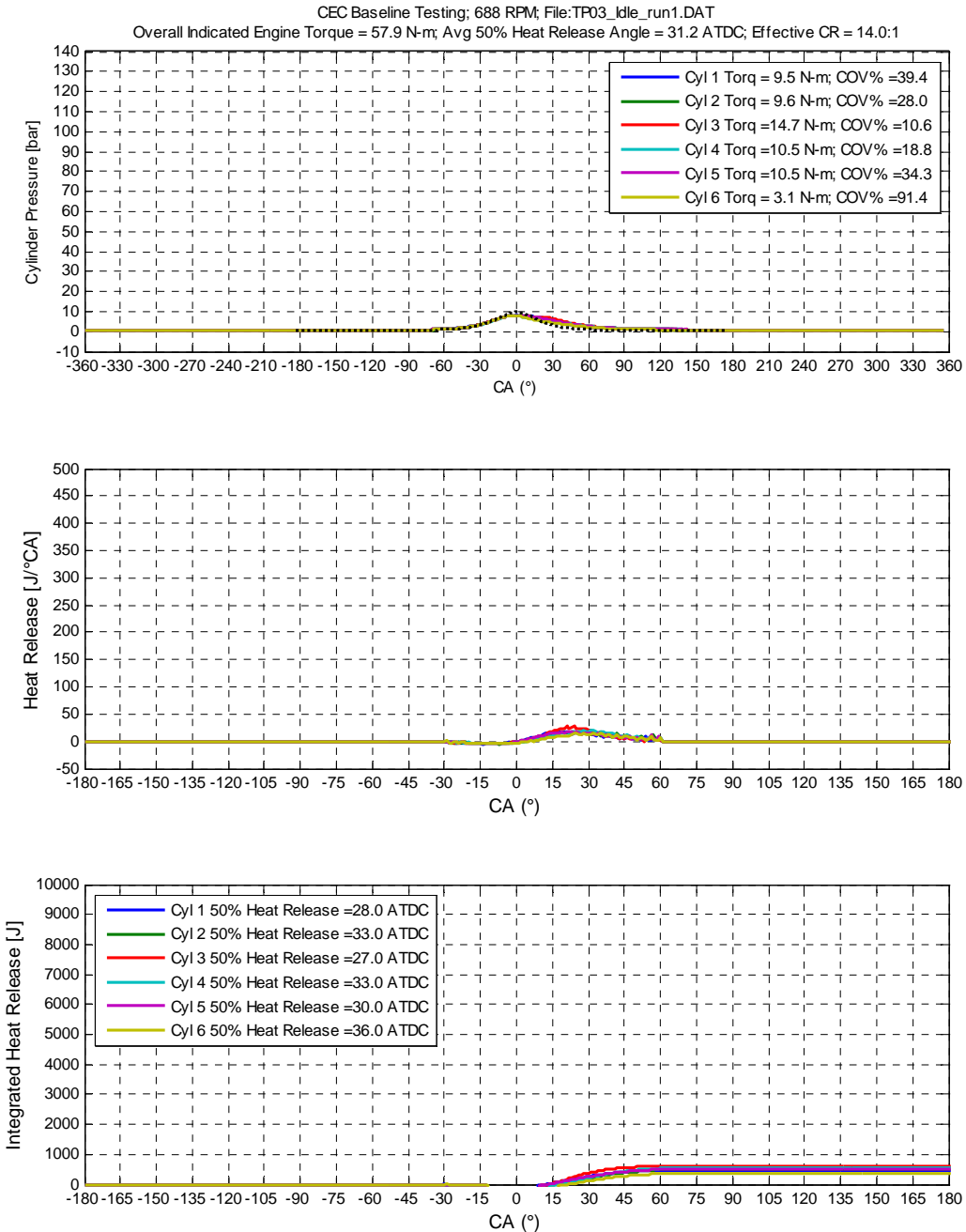


Source: Sturman Industries

# Appendix B: Dyno Testing Cylinder Pressure & Heat Release Results - Baseline

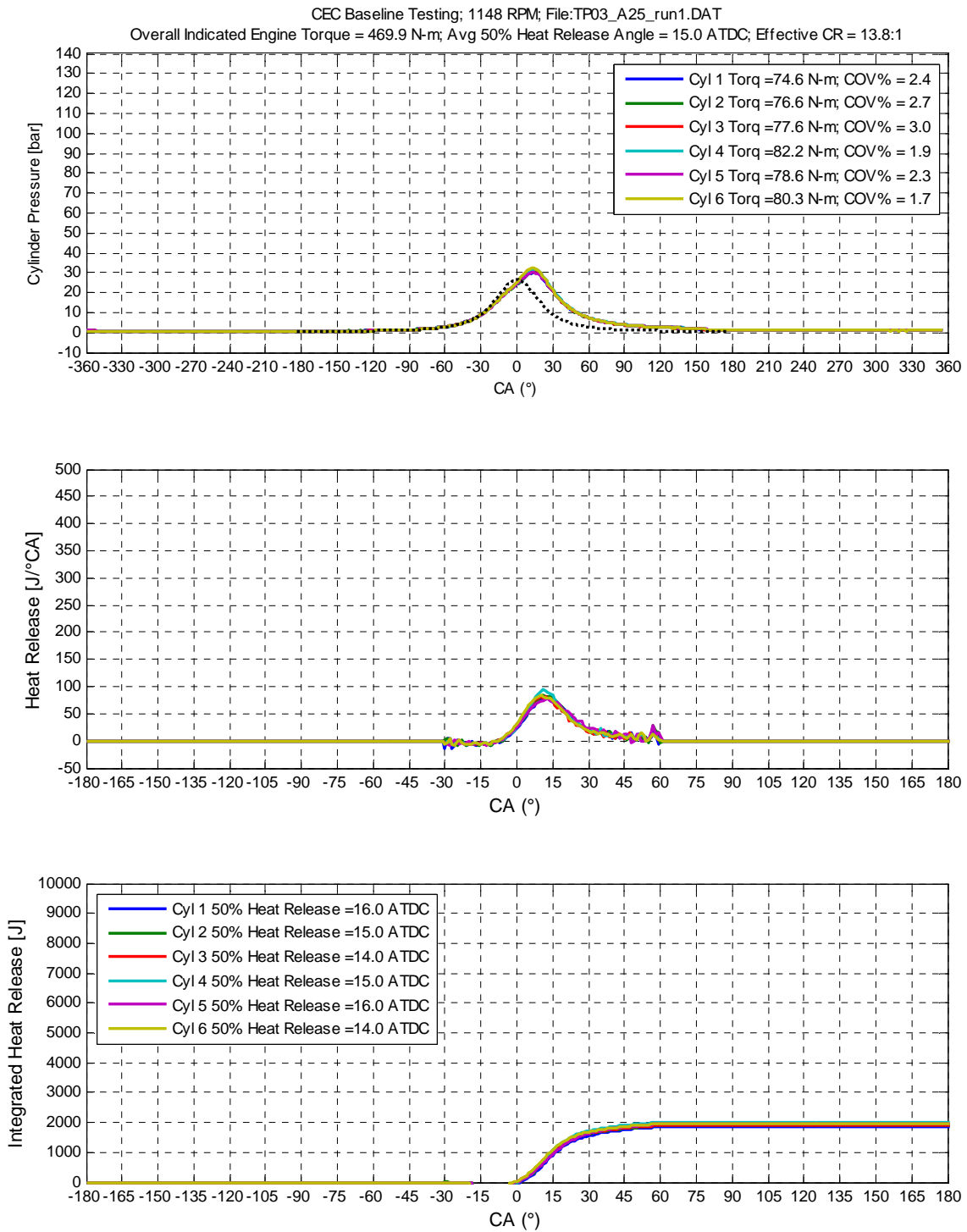
## Baseline 13-Mode Testing with Catalyst

Figure 113: Baseline – Idle Test Point



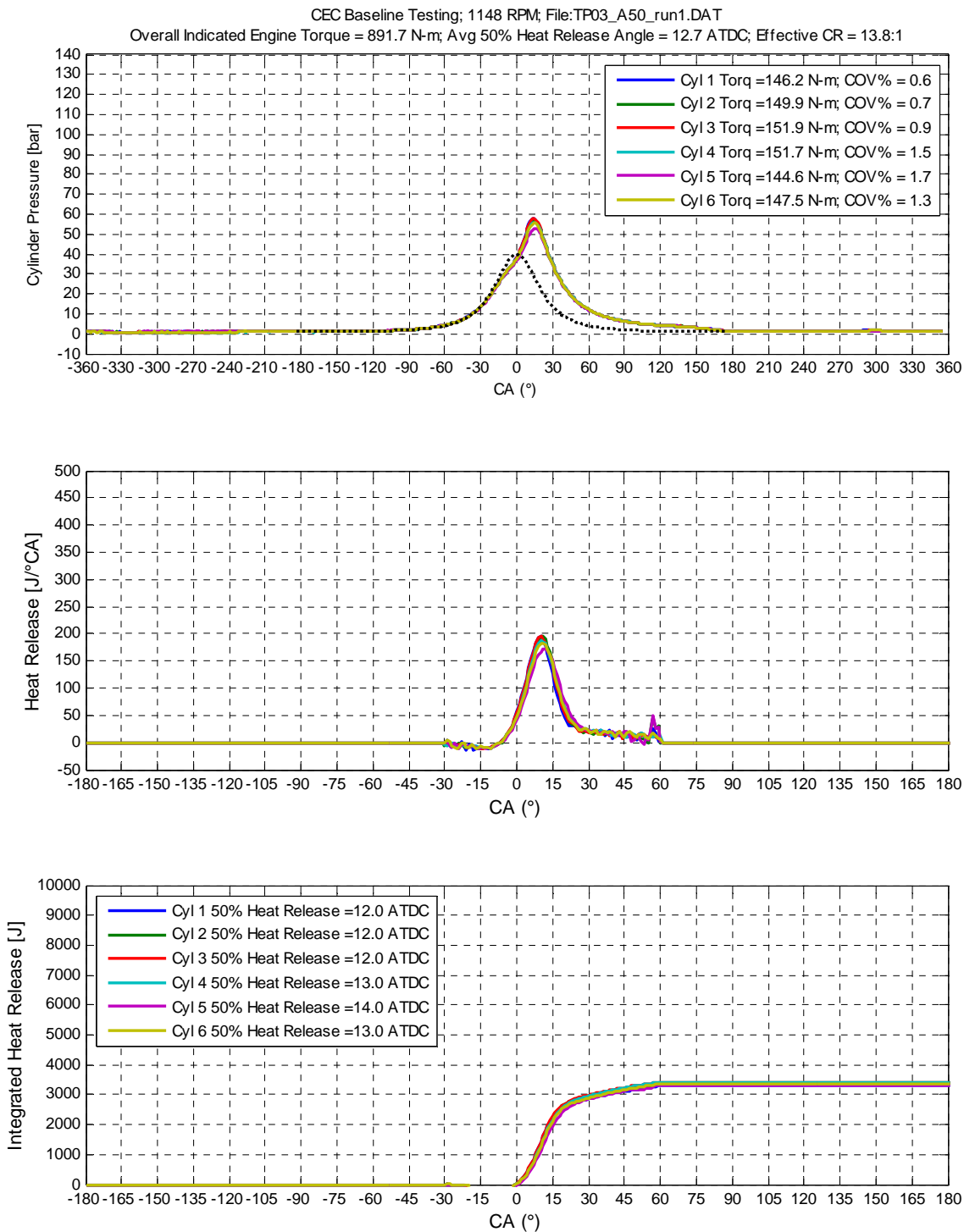
Source: Sturman Industries

**Figure 114: Baseline - A25 Test Point**



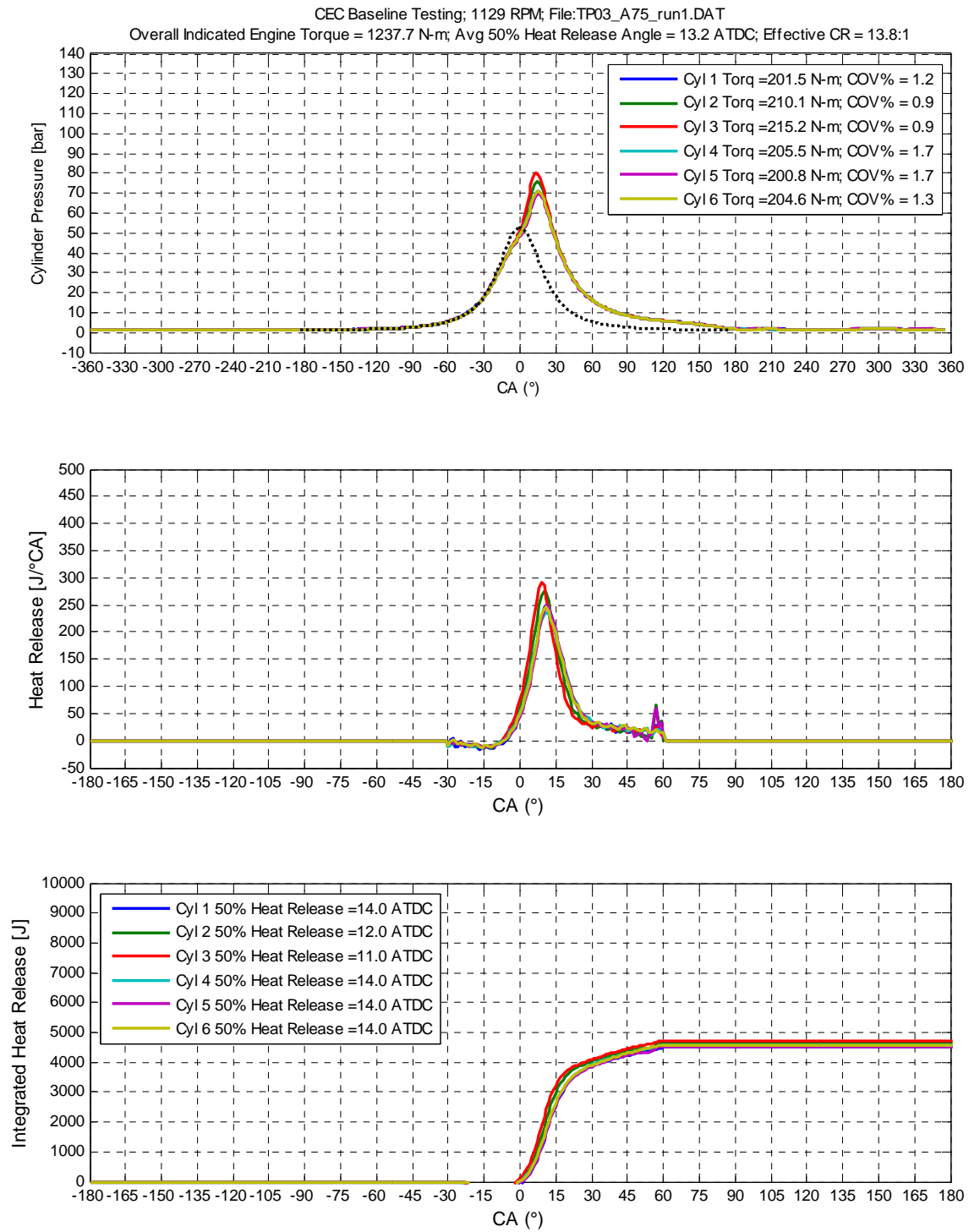
Source: Sturman Industries

**Figure 115: Baseline – A50 Test Point**



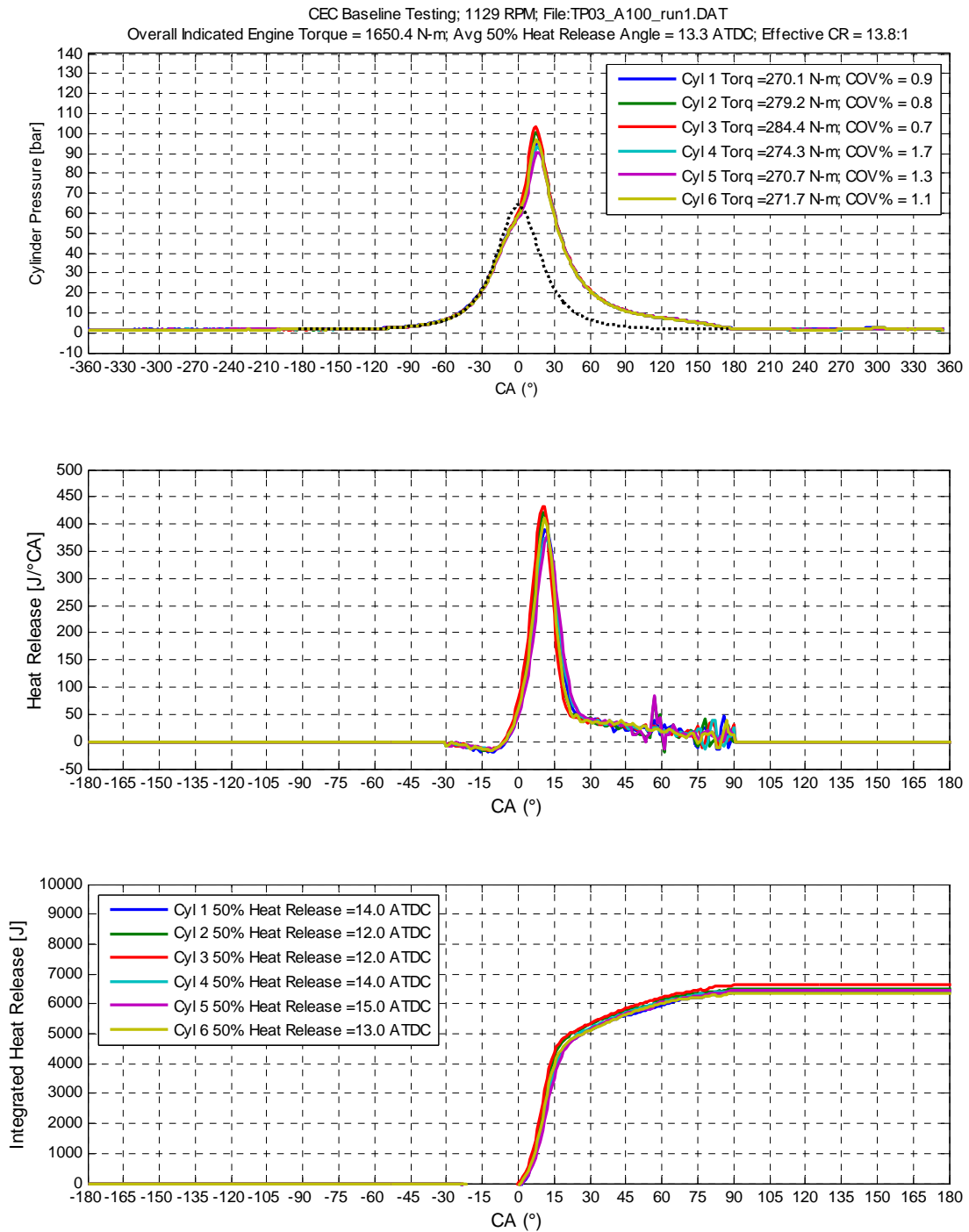
Source: Sturman Industries

**Figure 116: Baseline – A75 Test Point**



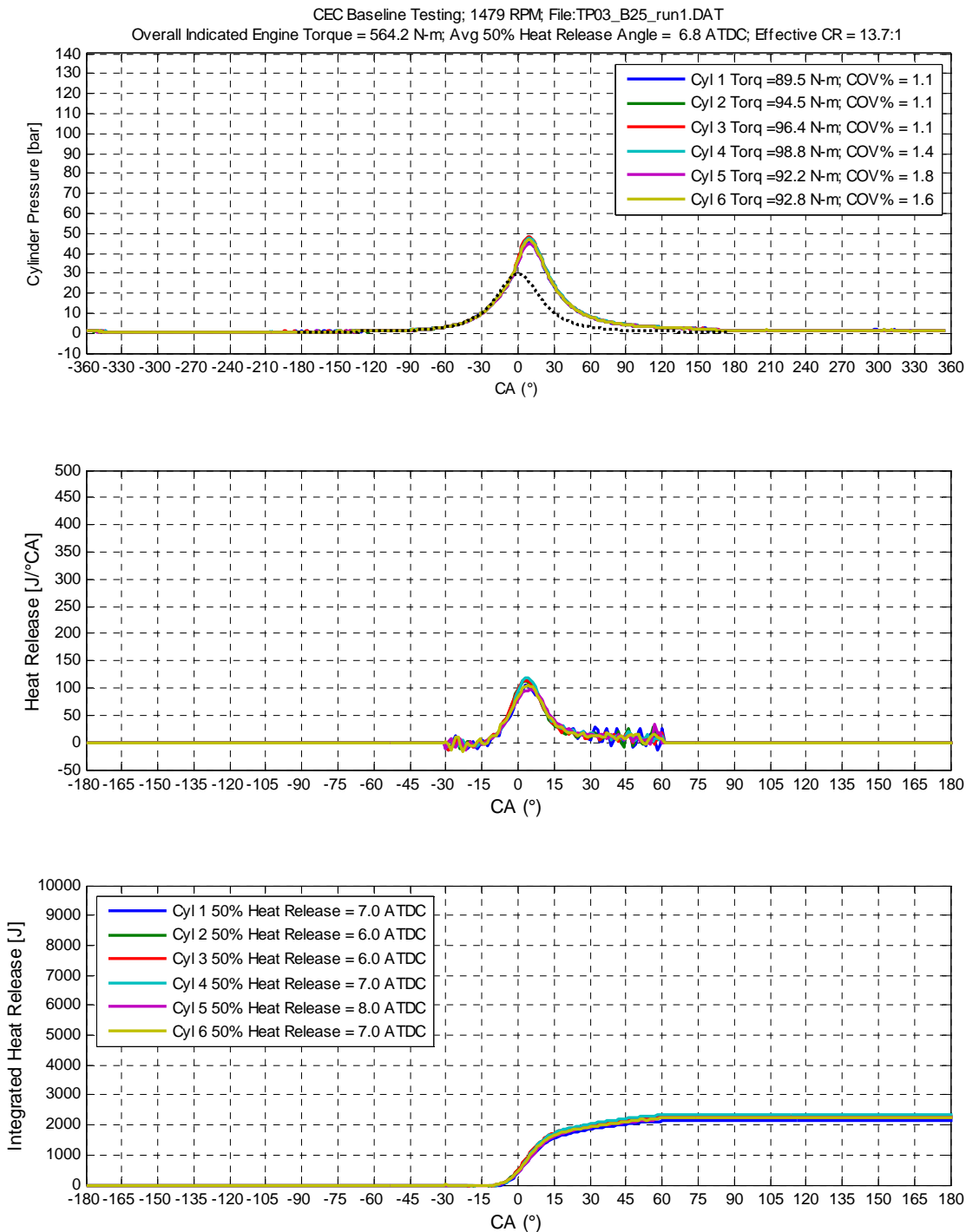
Source: Sturman Industries

**Figure 117: Baseline – A100 Test Point**



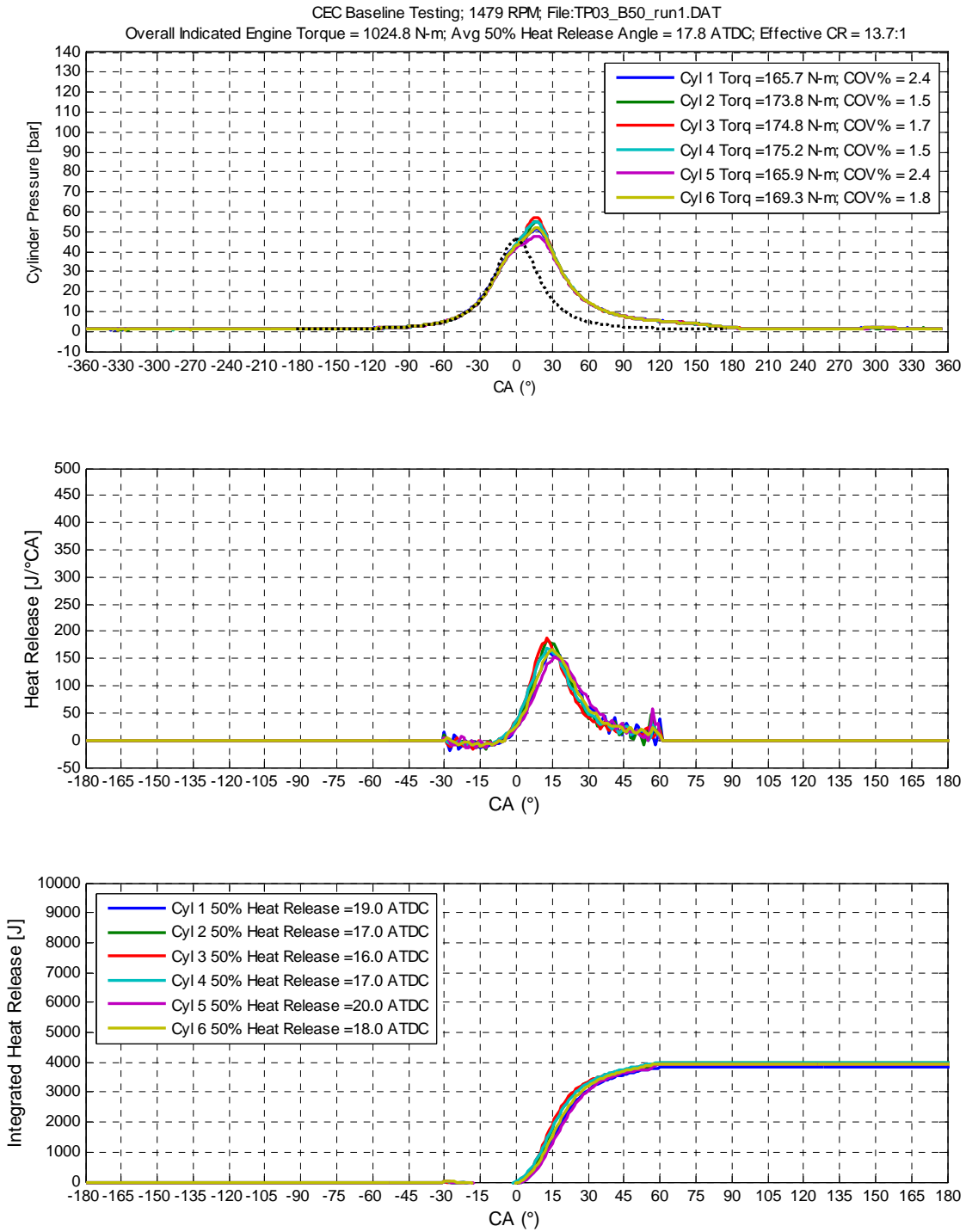
Source: Sturman Industries

**Figure 118: Baseline - B25 Test Point**



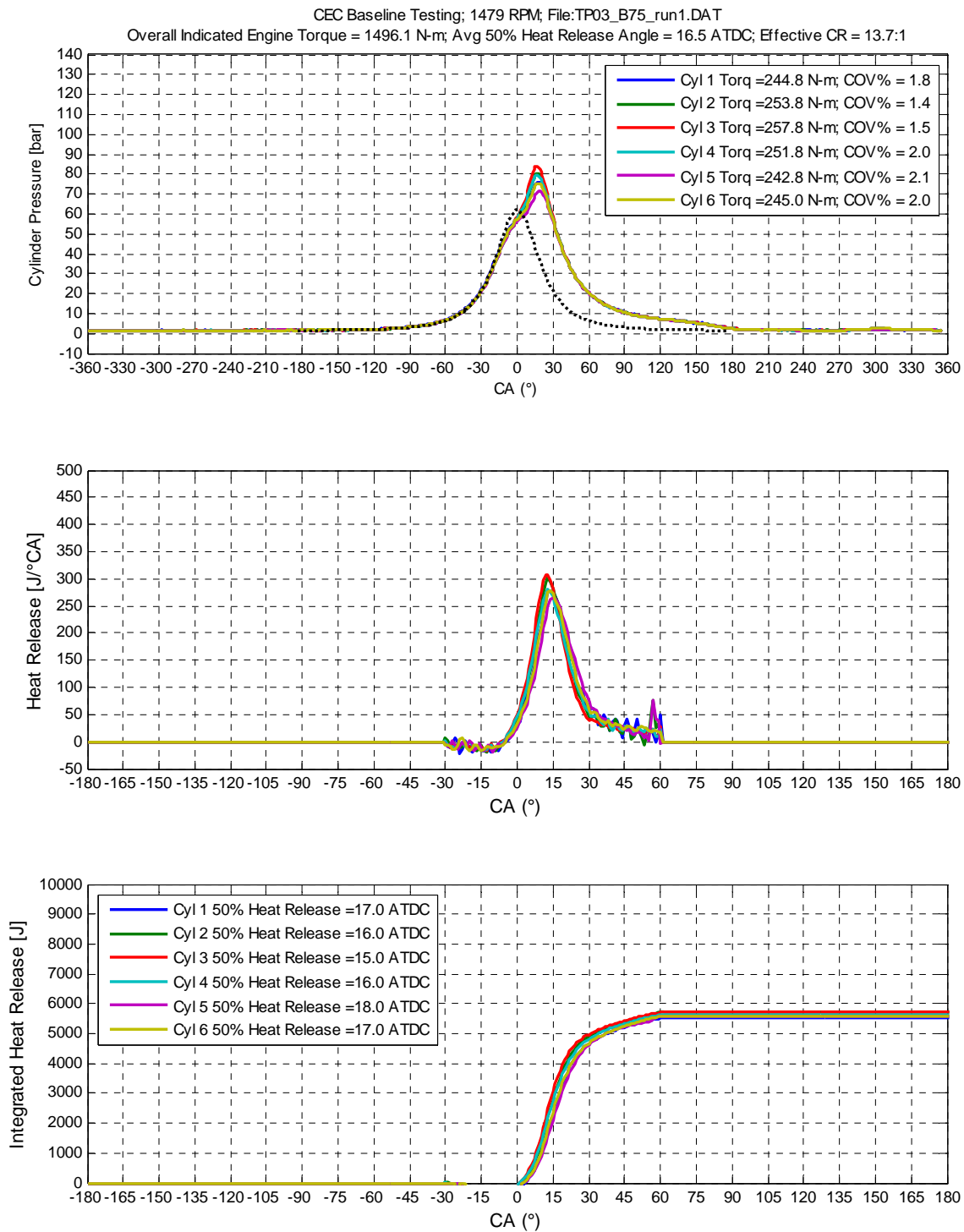
Source: Sturman Industries

**Figure 119: Baseline – B50 Test Point**



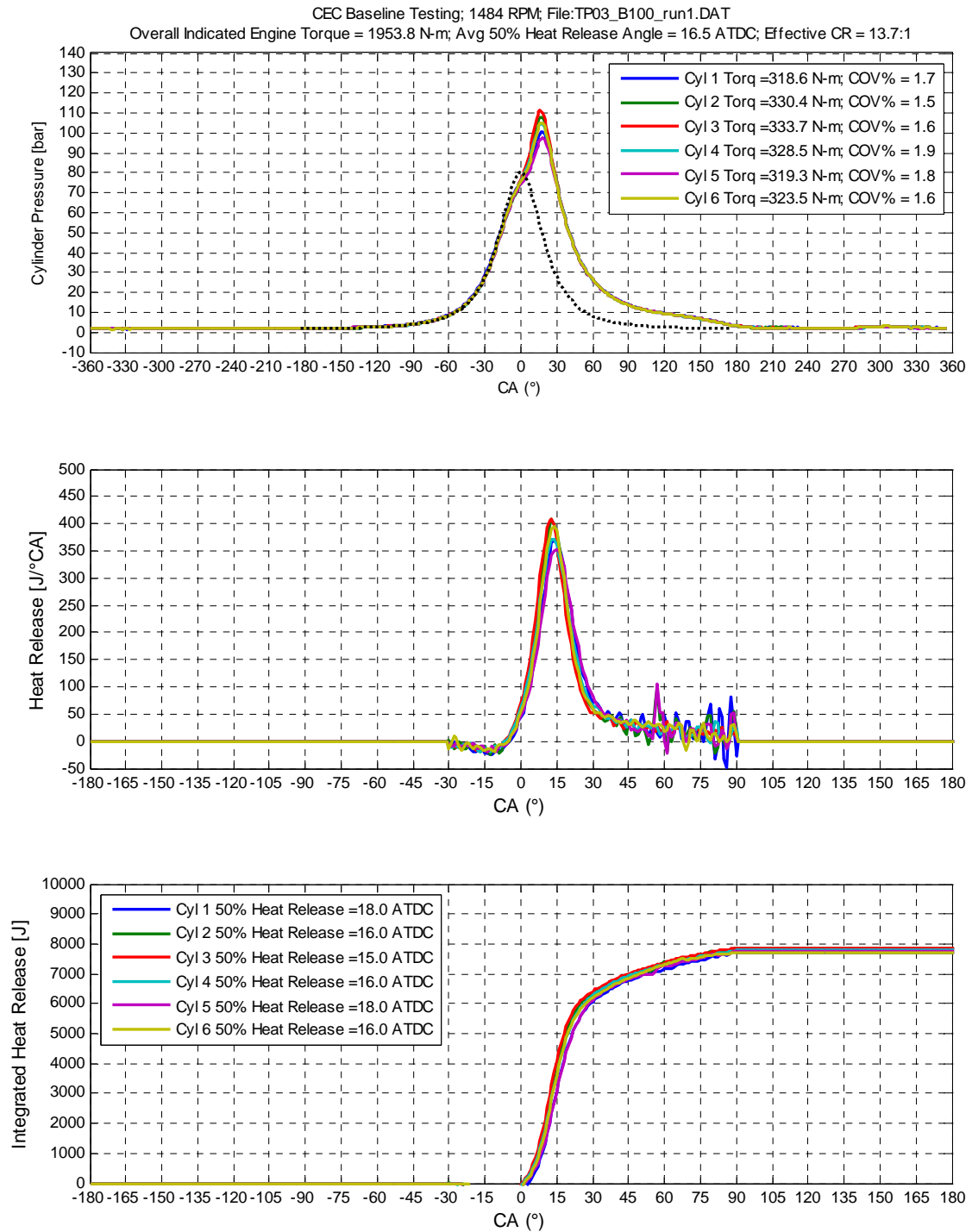
Source: Sturman Industries

**Figure 120: Baseline – B75 Test Point**



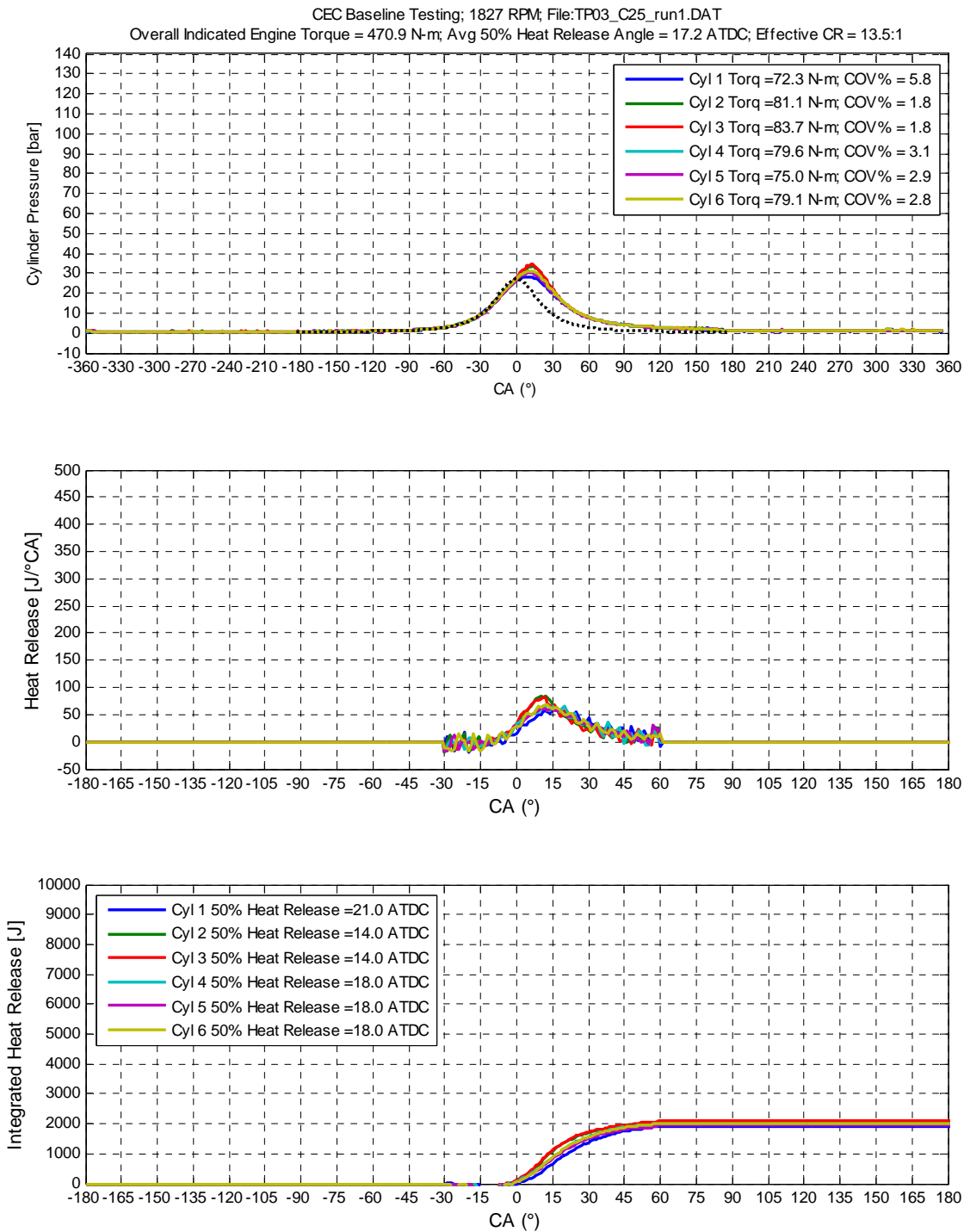
Source: Sturman Industries

**Figure 121: Baseline – B100 Test Point**



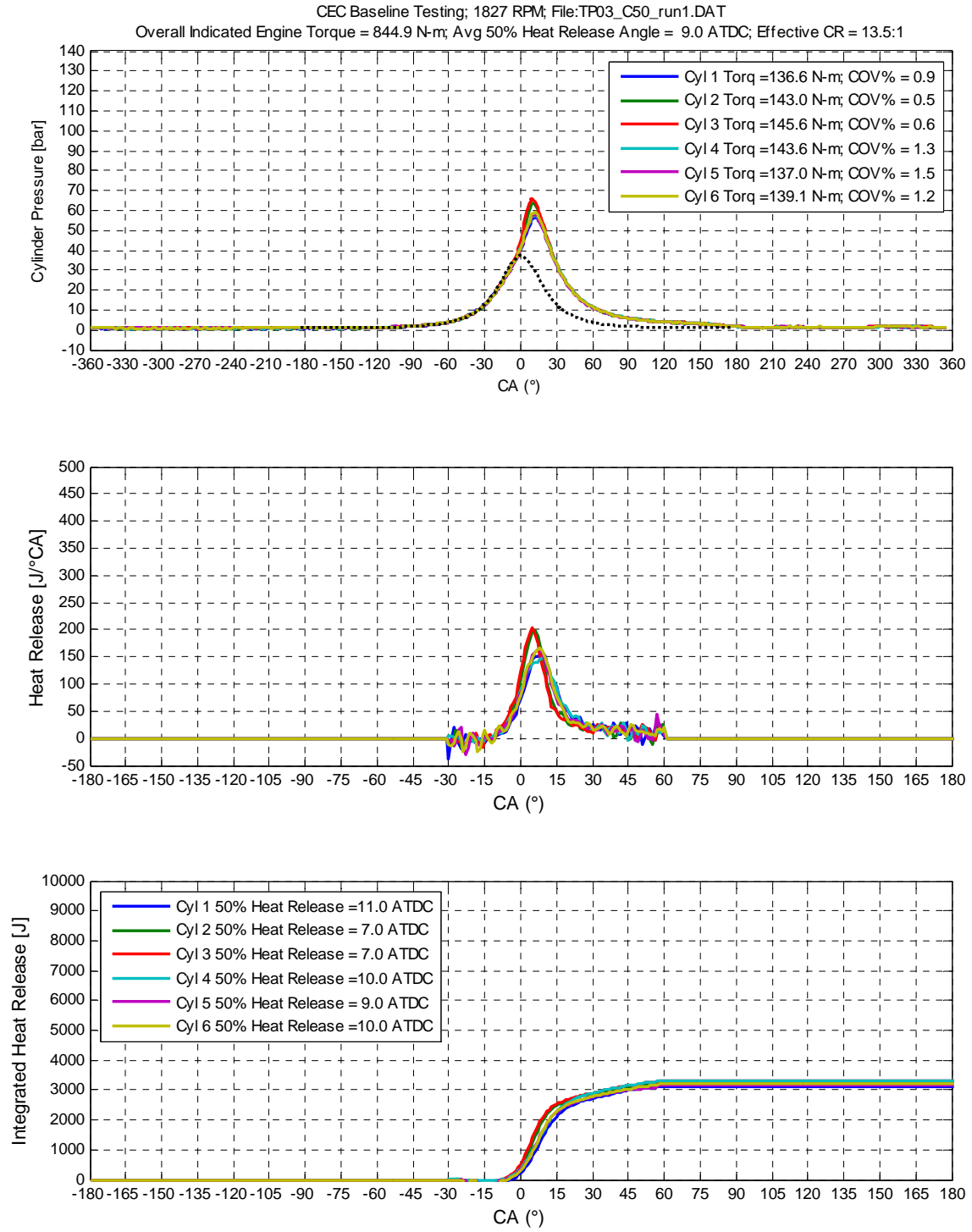
Source: Sturman Industries

**Figure 122: Baseline - C25 Test Point**



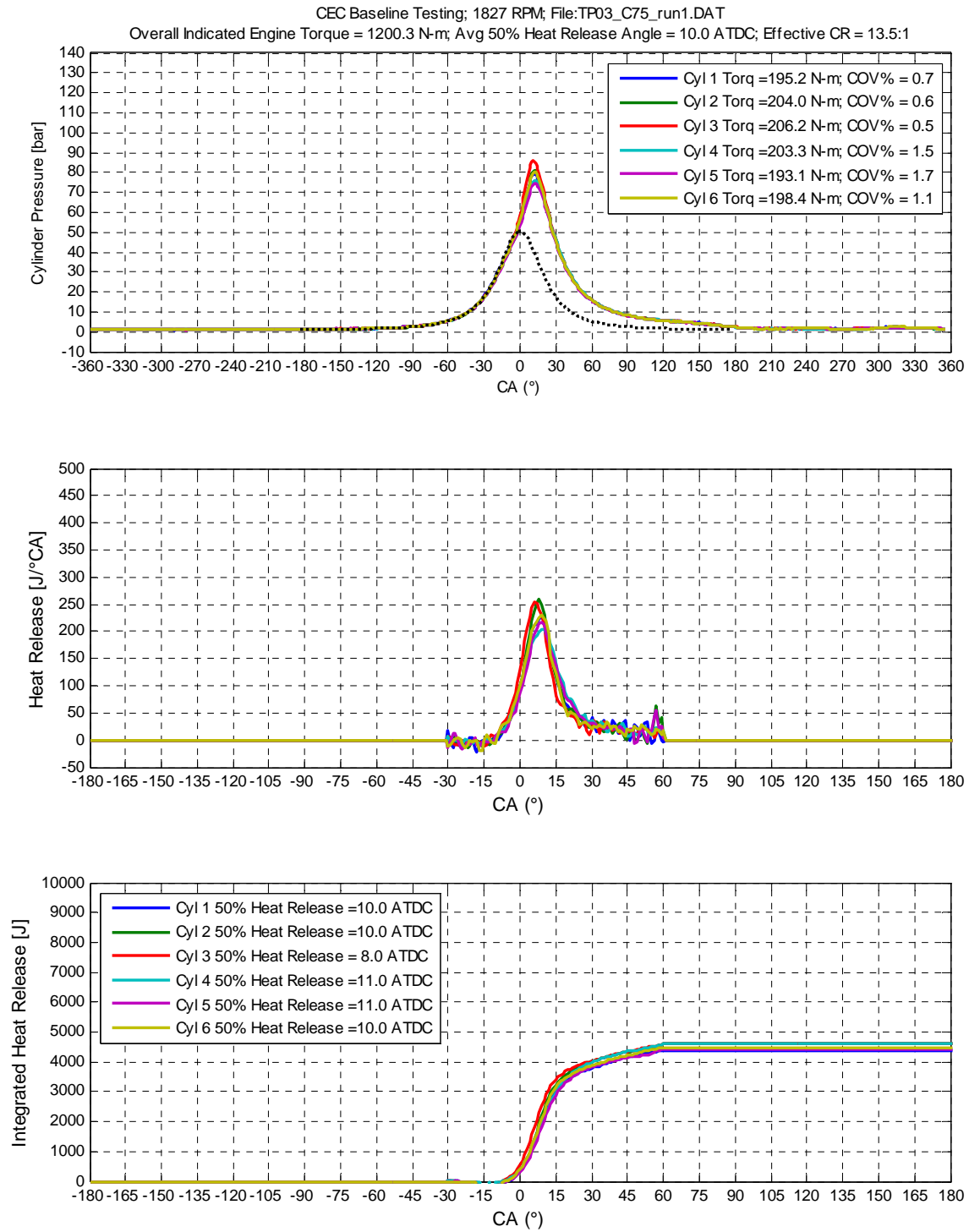
Source: Sturman Industries

**Figure 123: Baseline – C50 Test Point**



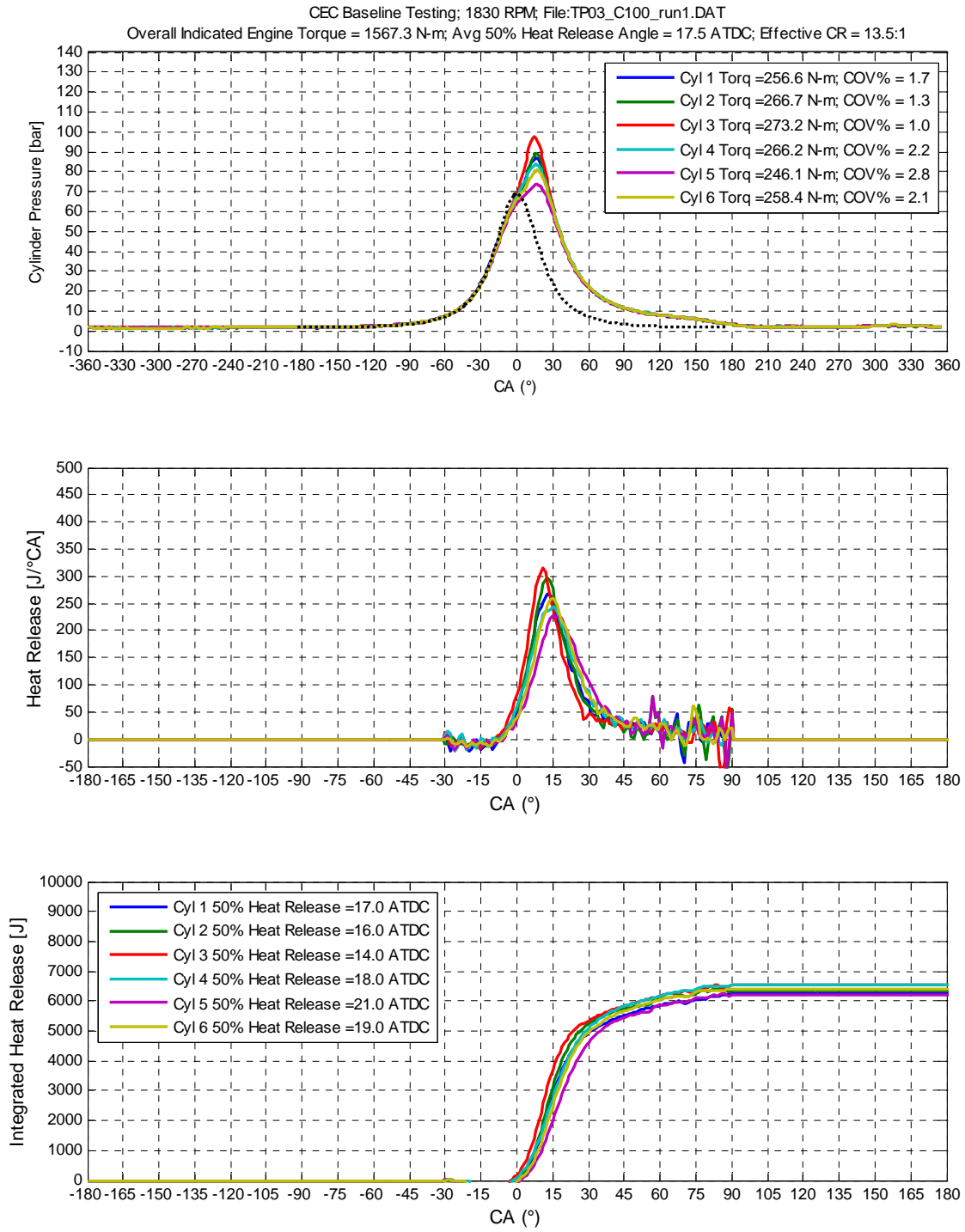
Source: Sturman Industries

**Figure 124: Baseline – C75 Test Point**



Source: Sturman Industries

**Figure 125: Baseline – C100 Test Point**

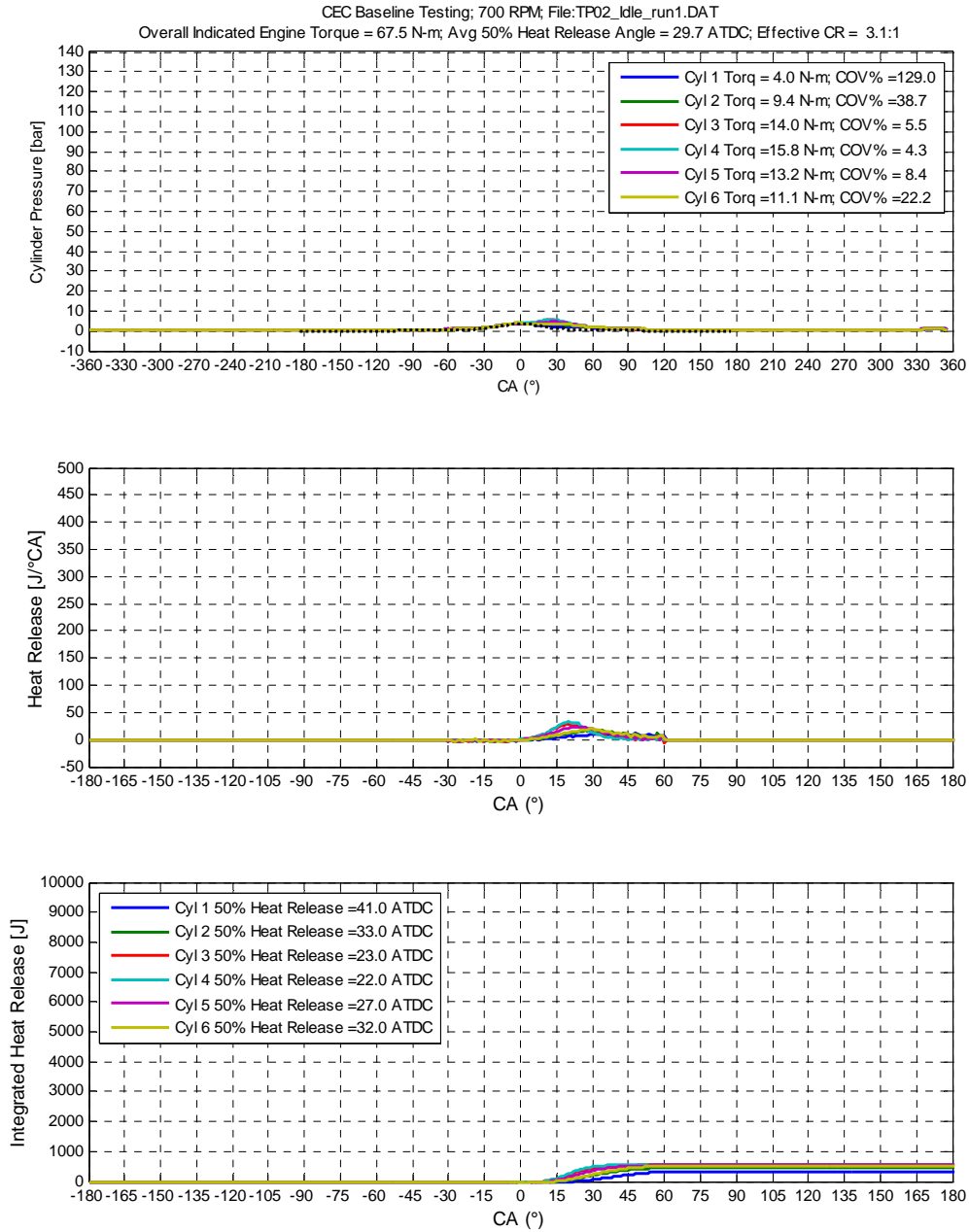


Source: Sturman Industries

# Appendix C: Dyno Testing Cylinder Pressure & Heat Release Results - Optimized

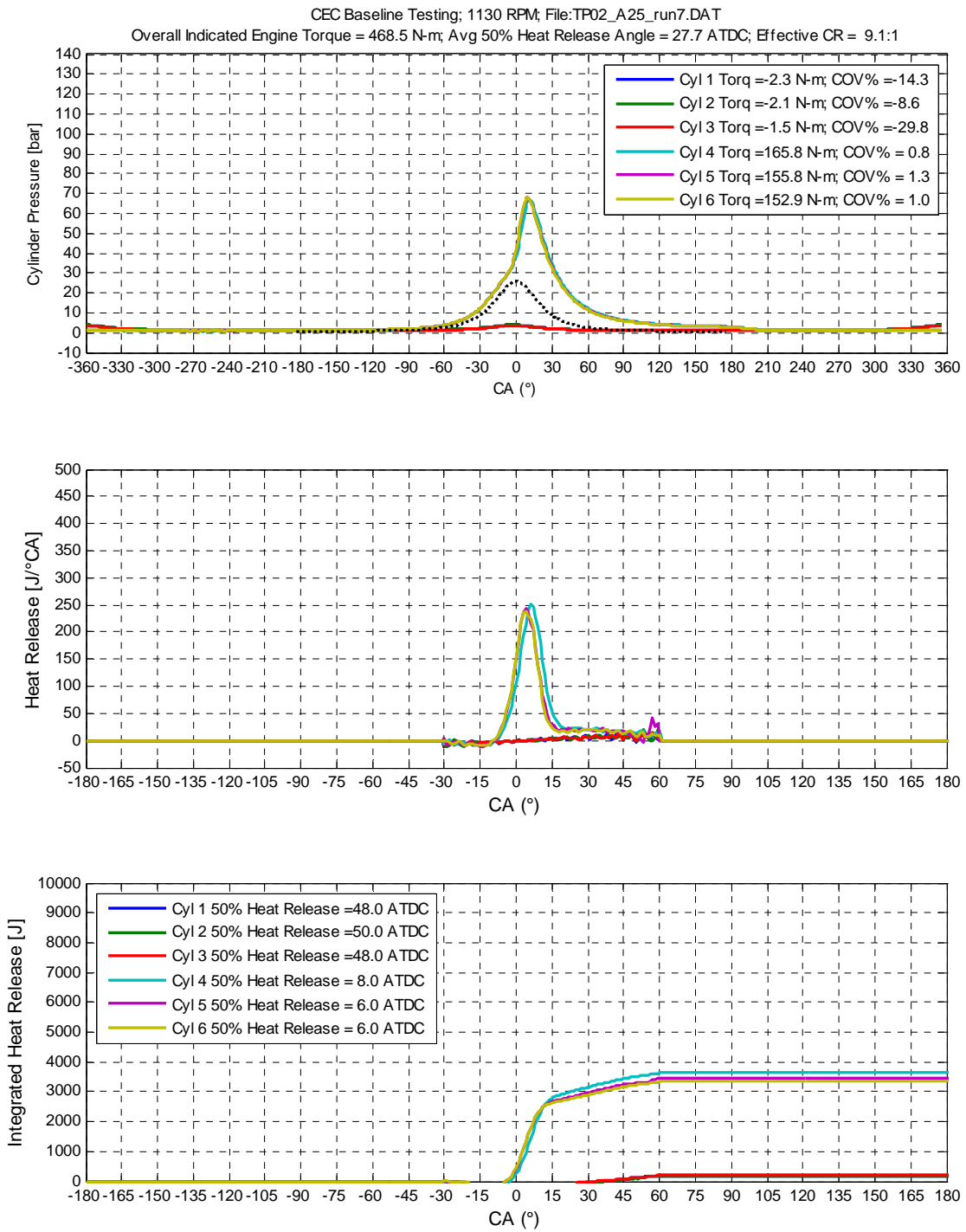
## Optimized 13-Mode Testing with Catalyst

Figure 126: Optimized – Idle Test Point



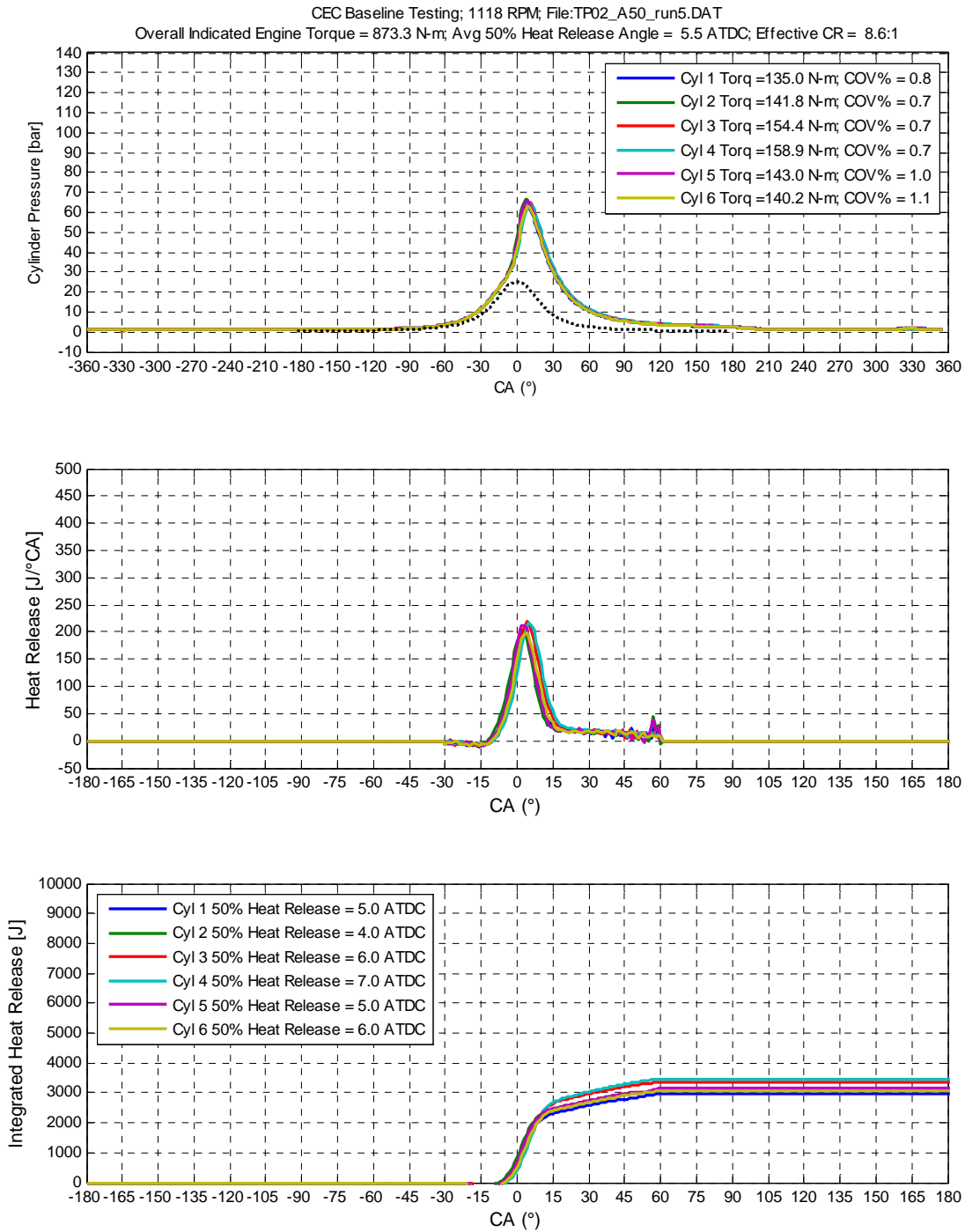
Source: Sturman Industries

**Figure 127: Optimized - A25 Test Point**



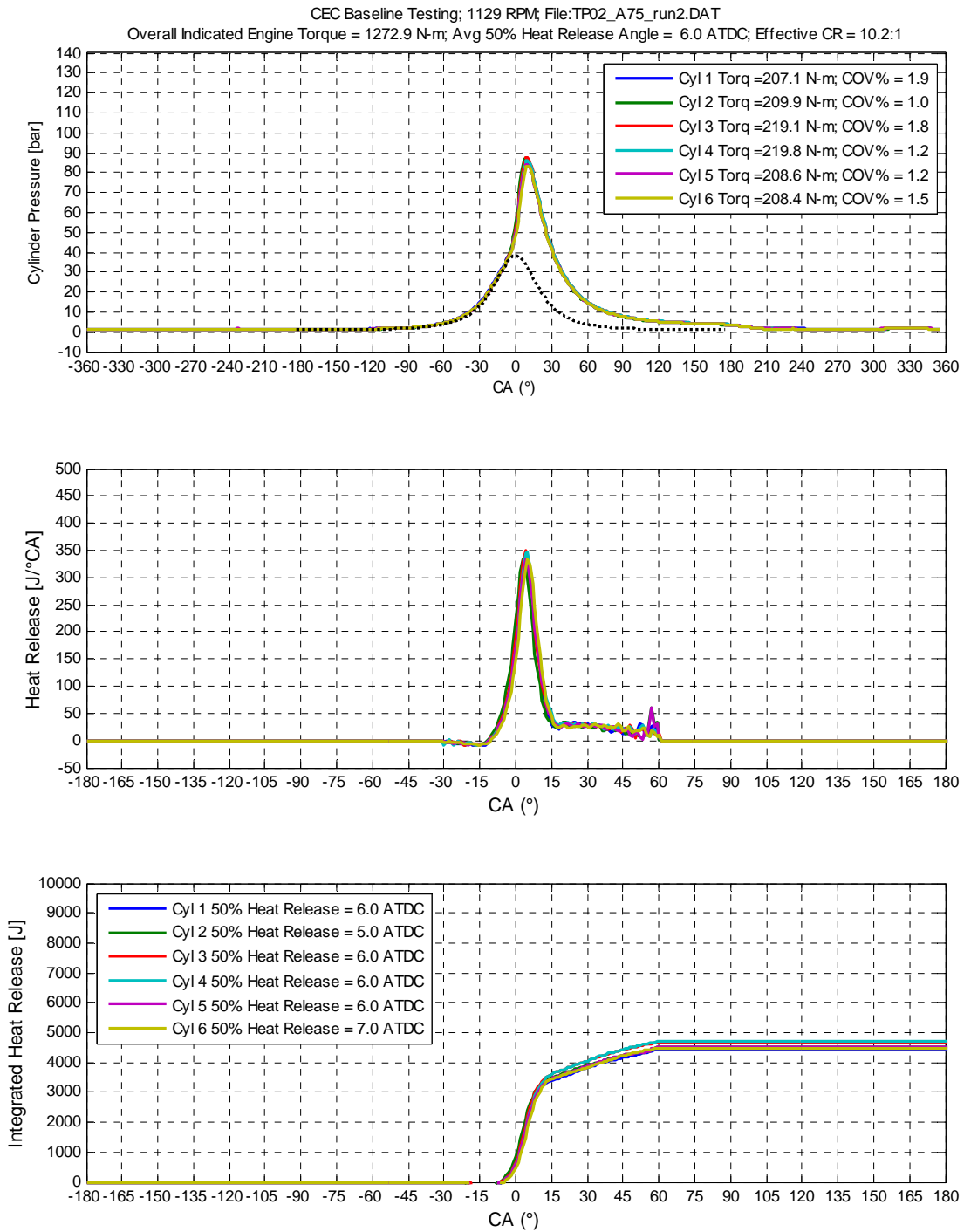
Source: Sturman Industries

**Figure 128: Optimized – A50 Test Point**



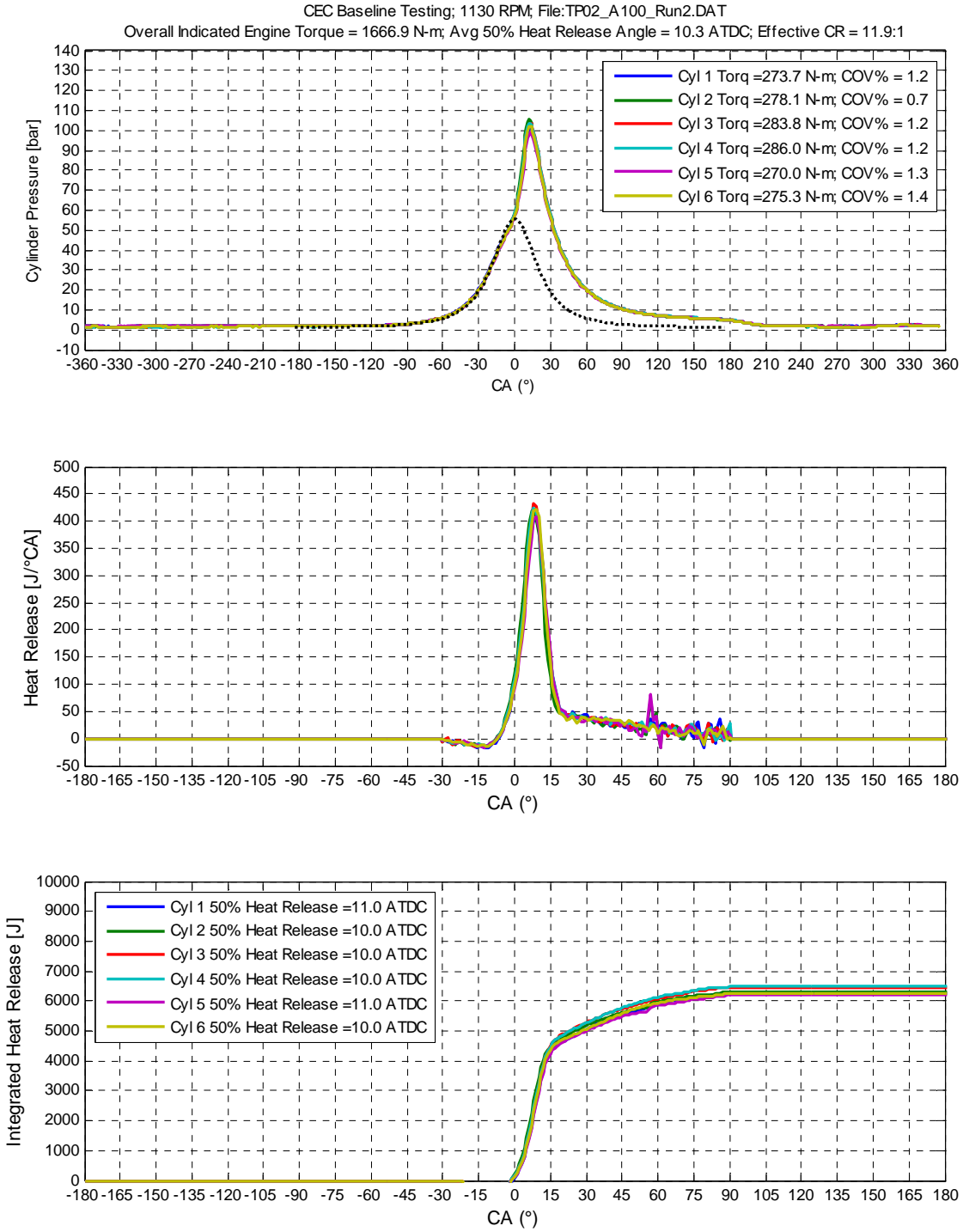
Source: Sturman Industries

**Figure 129: Optimized – A75 Test Point**



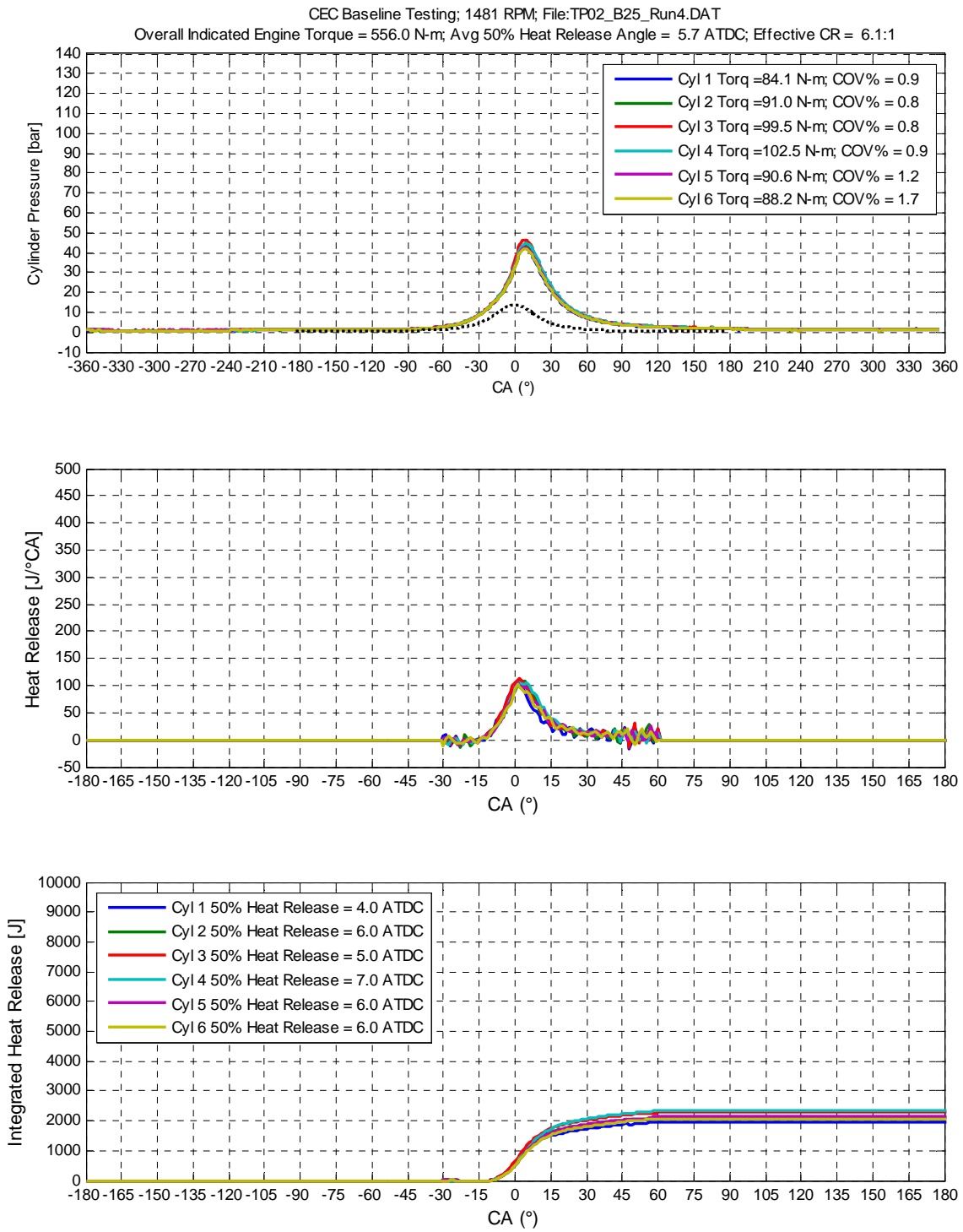
Source: Sturman Industries

**Figure 130: Optimized – A100 Test Point**



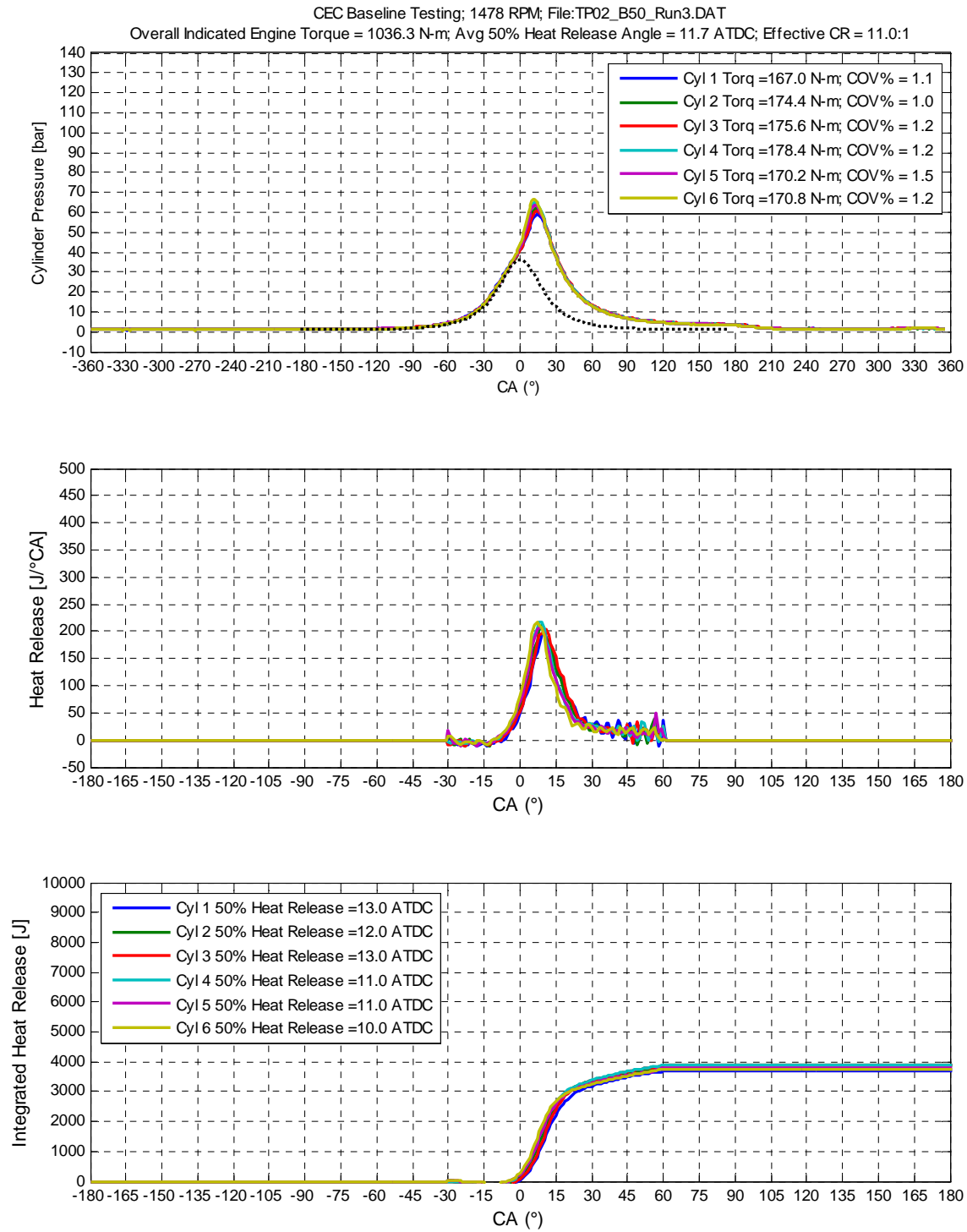
Source: Sturman Industries

**Figure 131: Optimized - B25 Test Point**



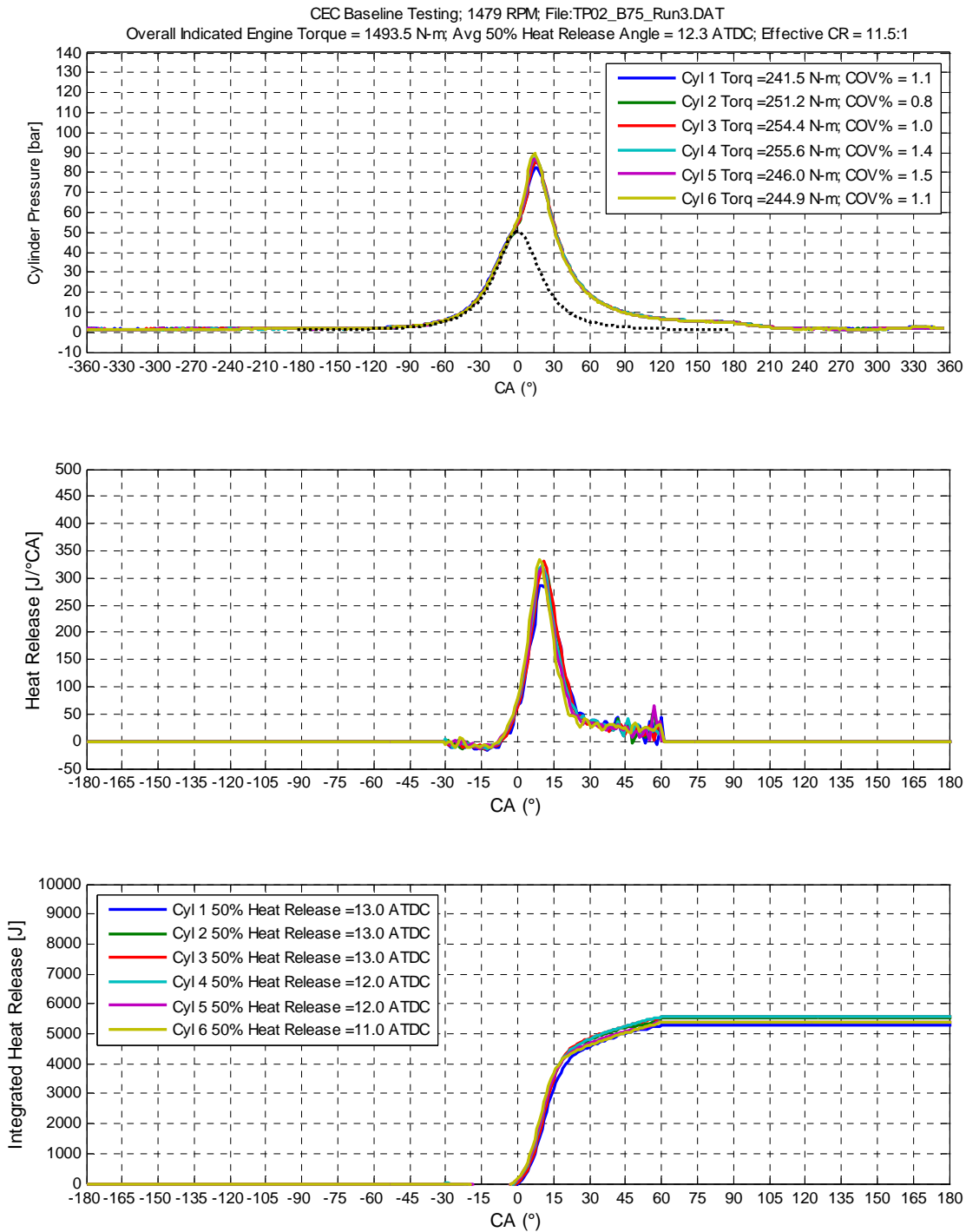
Source: Sturman Industries

**Figure 132: Optimized – B50 Test Point**



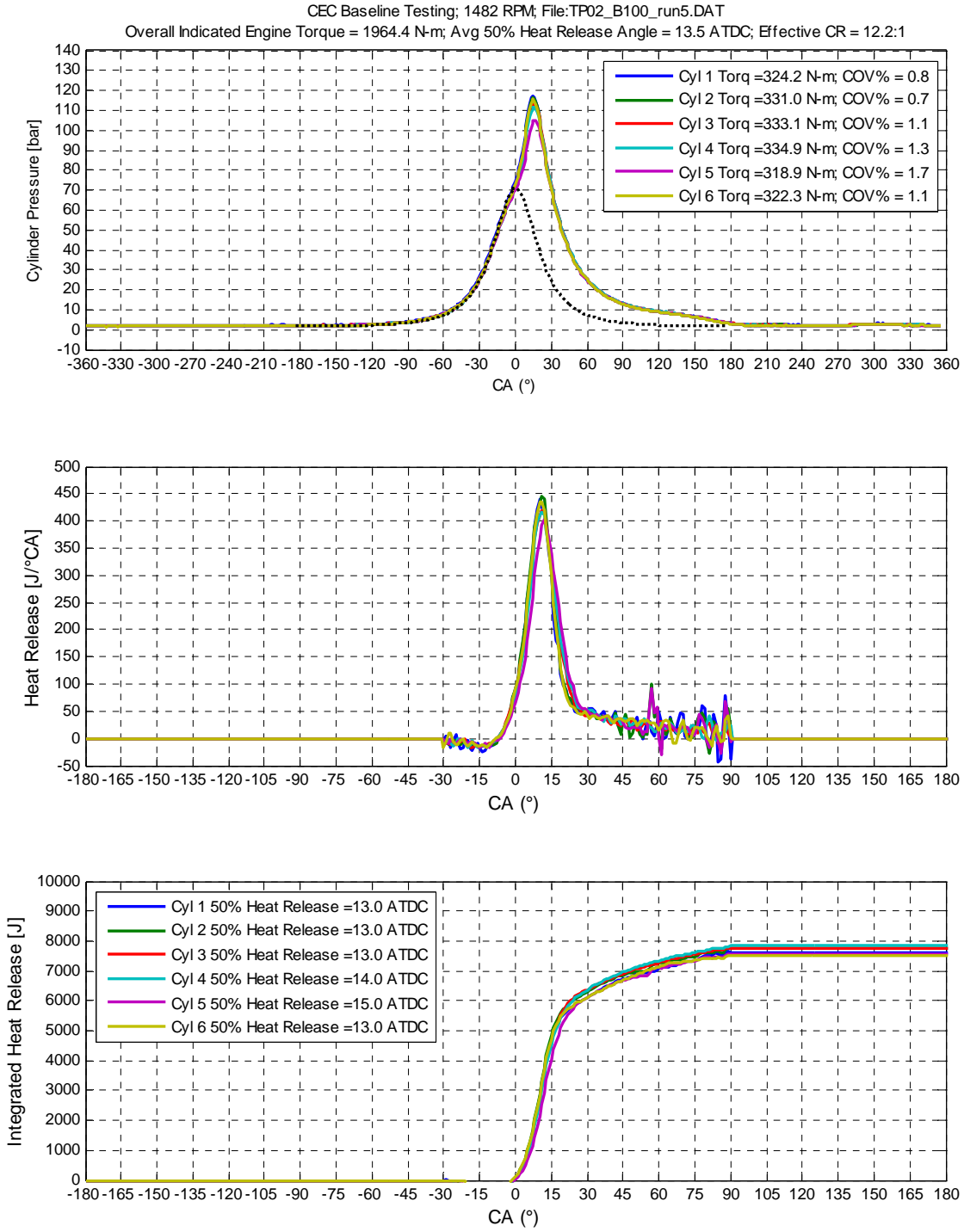
Source: Sturman Industries

**Figure 133: Optimized – B75 Test Point**



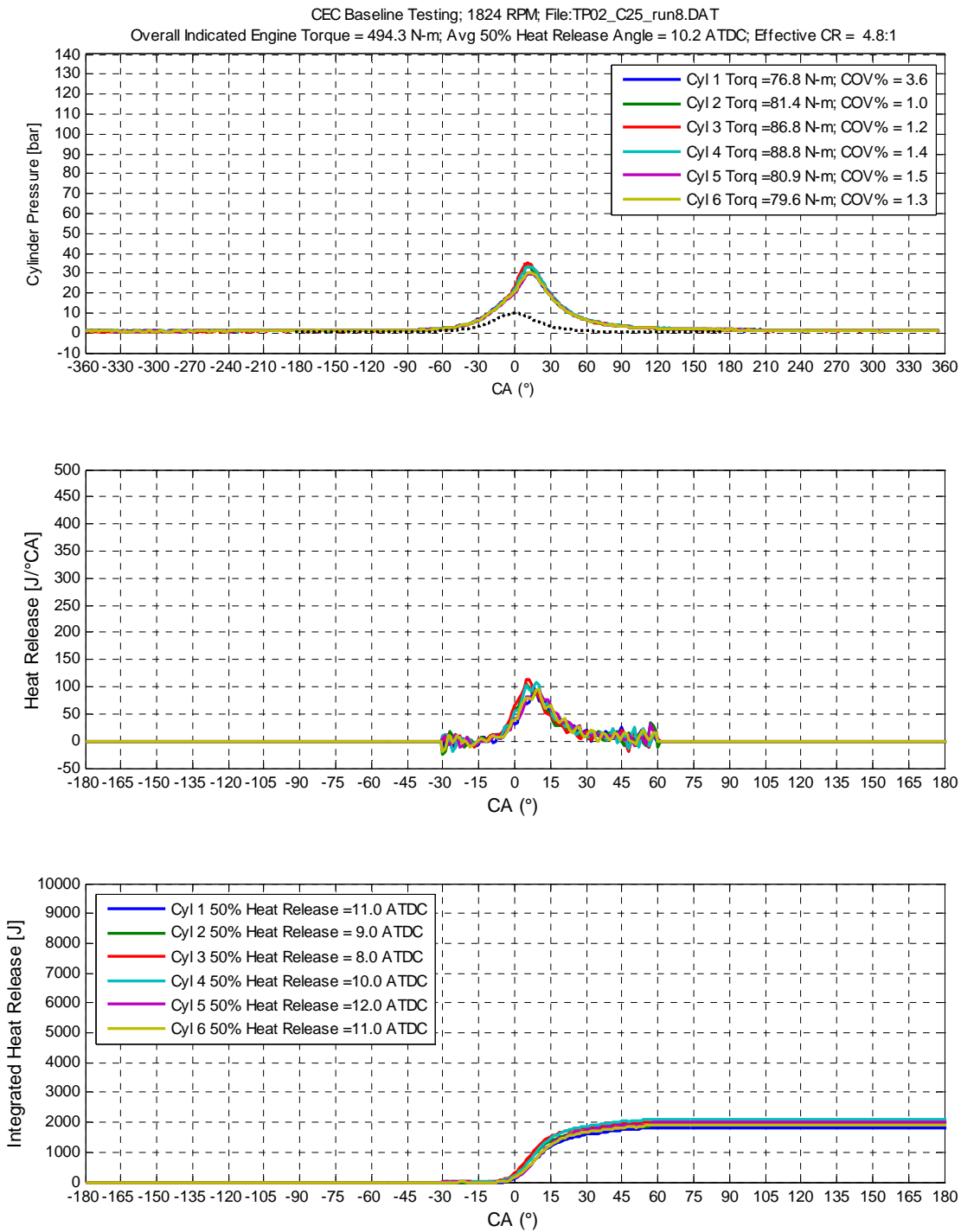
Source: Sturman Industries

**Figure 134: Optimized – B100 Test Point**



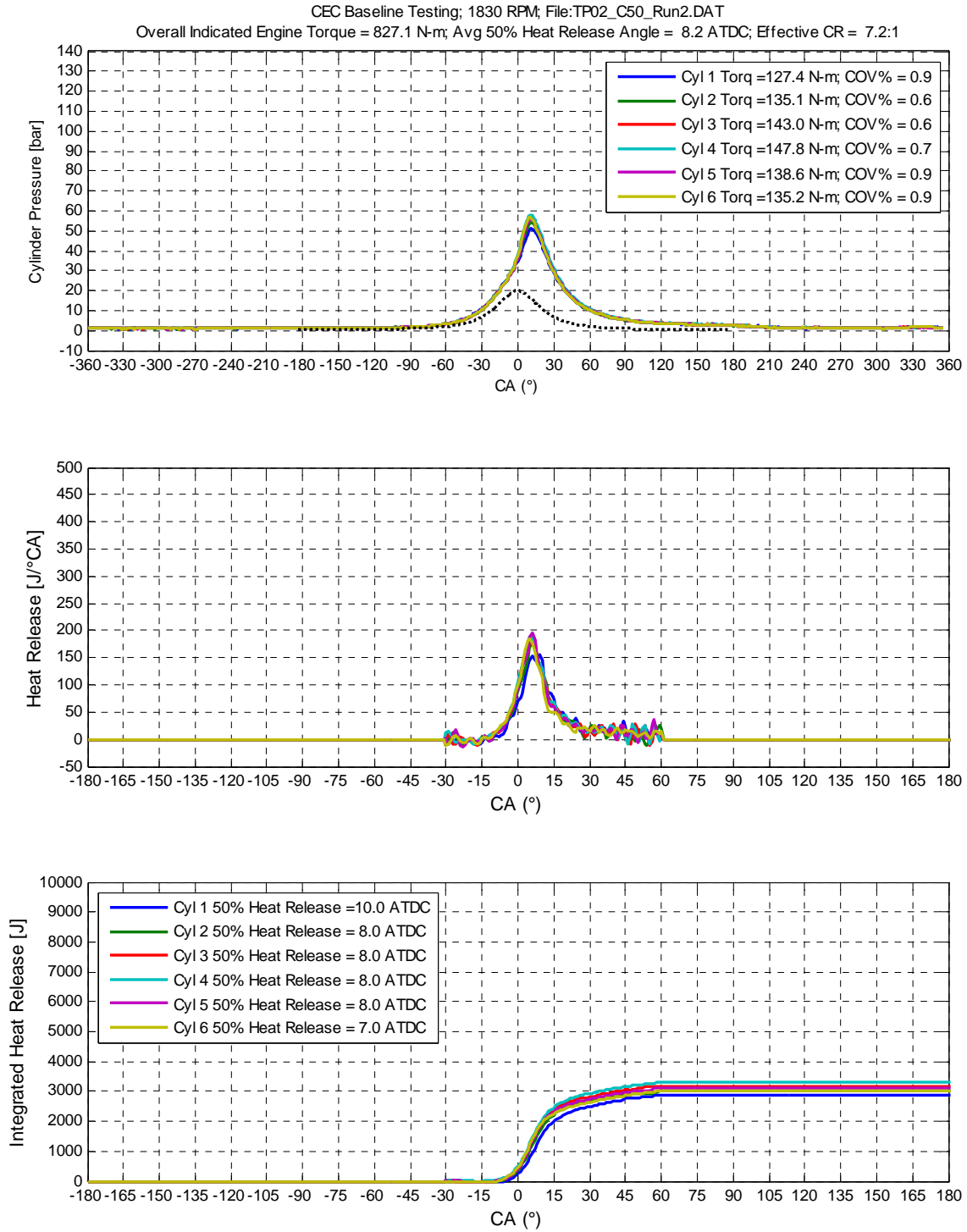
Source: Sturman Industries

**Figure 135: Optimized - C25 Test Point**



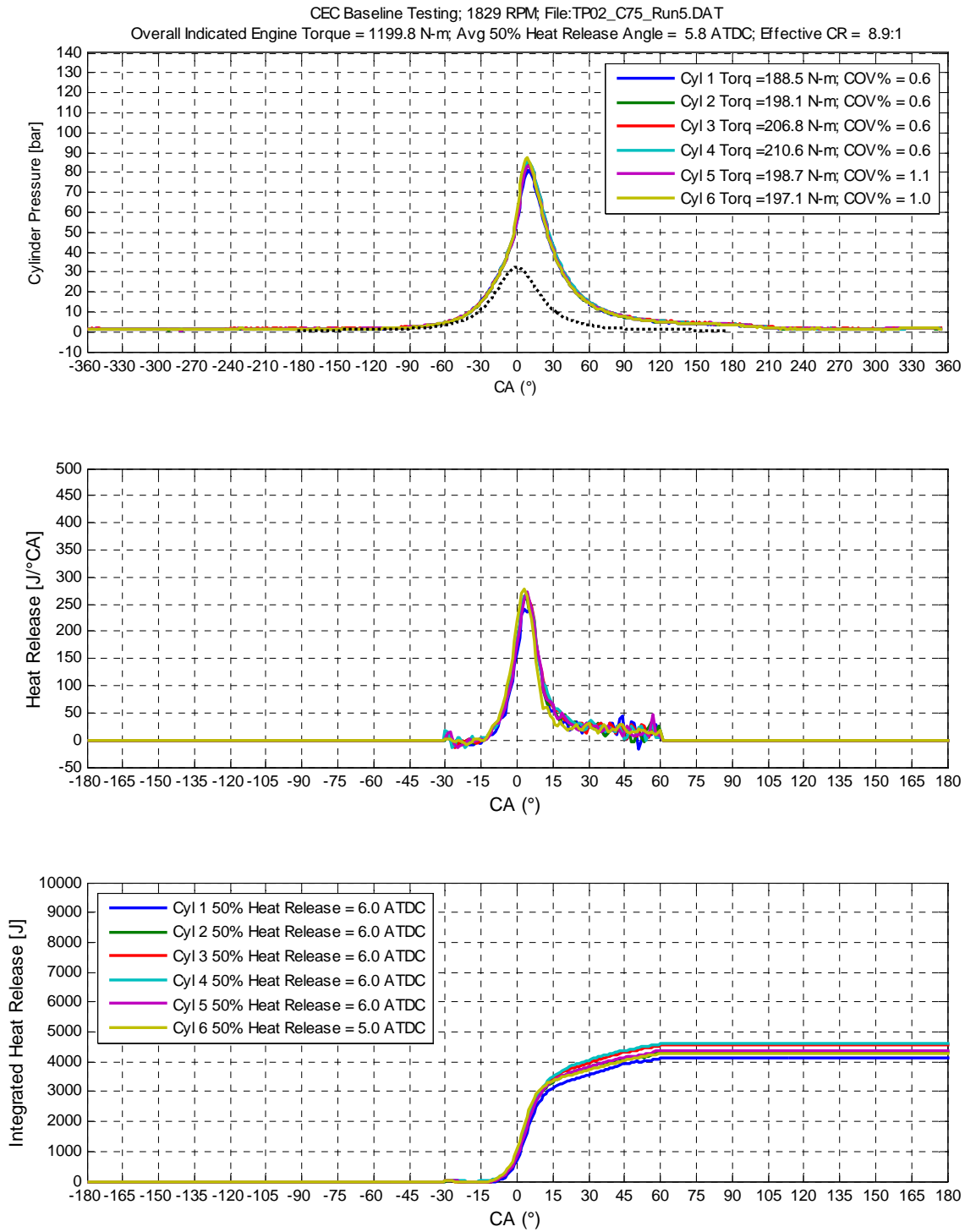
Source: Sturman Industries

**Figure 136: Optimized – C50 Test Point**



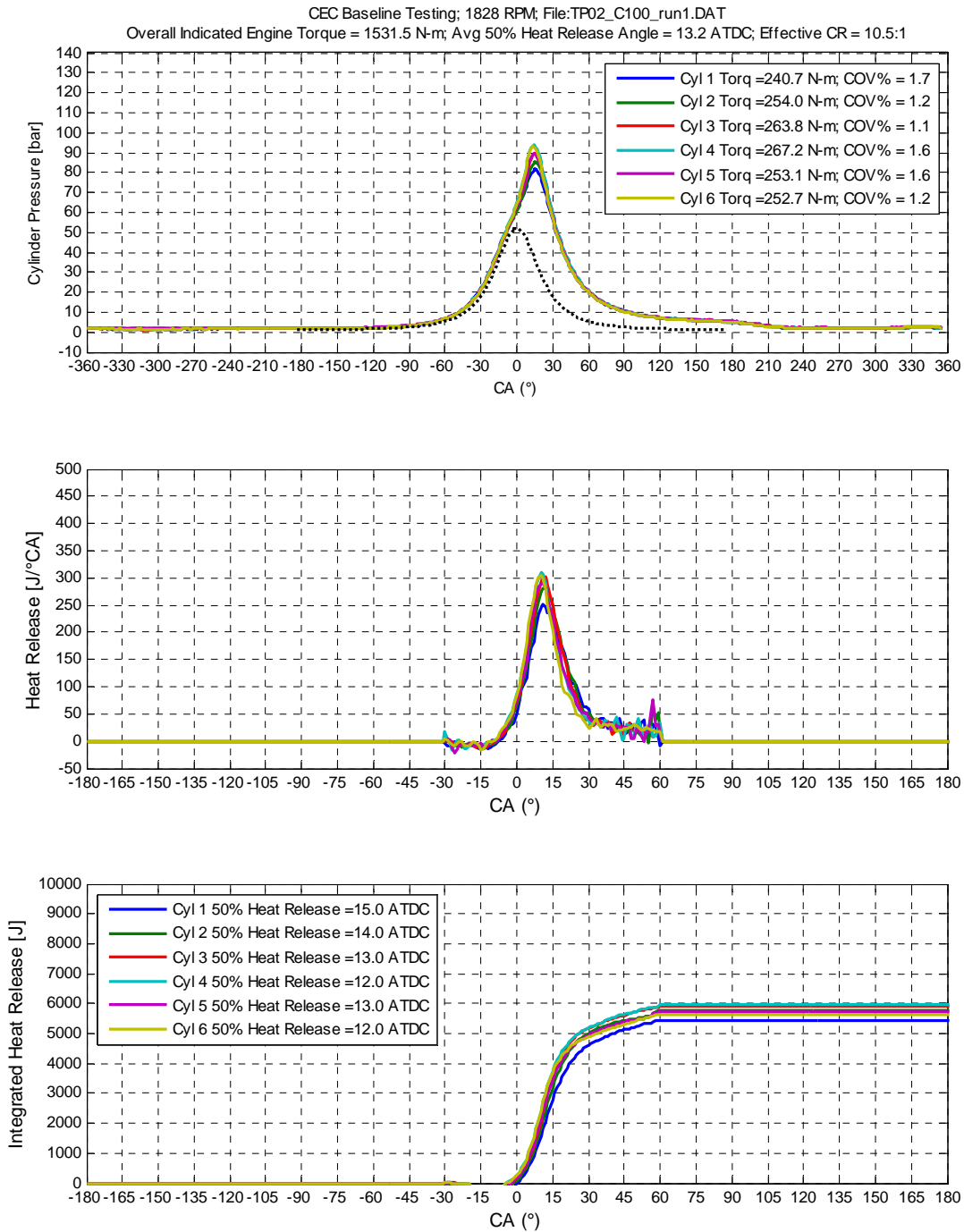
Source: Sturman Industries

**Figure 137: Optimized – C75 Test Point**



Source: Sturman Industries

**Figure 138: Optimized – C100 Test Point**



Source: Sturman Industries

# Appendix D: Peripheral Data for Baseline and Optimized Tests

Figure 139: Peripheral Data for Baseline and Optimized Tests

298 kW Cummins ISX, Omnitek Natural Gas System, Sturman HVA, Pump Cart, Optimized (Idle, A25, B26, C25 3-Qr) Mid-Loaded 3-Way Catalyst														
Mode	K/P (0/1)	W/a	W/a	W/a	W/a	W/a	W/a	W/a	W/a	W/a	W/a	W/a	W/a	W/a
Mode	W/a	W/a	W/a	W/a	W/a	W/a	W/a	W/a	W/a	W/a	W/a	W/a	W/a	W/a
A25	8.15	0.0	12	84.9	0.979	22.3	190	150	336	336	365	365	540	540
A75	8.15	0.0	18	9.3	0.981	16.8	190	150	336	336	365	365	540	540
A100	8.15	14.90	30	9.8	0.979	17.0	190	150	336	336	365	365	540	540
C25	8.15	176.1	25	7.9	0.979	13.0	190	150	336	336	365	365	540	540
C75	14.91	115.3	0.0	15	11.8	0.979	27.4	190	150	336	336	365	540	540
C100	14.91	203.2	0.0	10.6	0.984	21.0	190	150	336	336	365	365	540	540
B26	11.53	169.3	65	9.2	0.983	16.1	190	150	336	336	365	365	540	540
B75	11.53	220.1	70	9	0.981	16.2	190	150	336	336	365	365	540	540
C25	14.91	0.0	20	88.7	0.980	32.0	190	150	336	336	365	365	540	540
C50	14.91	132.1	18	10.3	0.982	32.0	190	150	336	336	365	365	540	540
C75	14.91	155.8	35	10.7	0.982	24.0	190	150	336	336	365	365	540	540
C100	14.91	203.2	65	11.1	0.982	24.0	190	150	336	336	365	365	540	540

298 kW Cummins ISX, Omnitek Natural Gas System, Sturman HVA, Pump Cart, Optimized (Idle, A25, B26, C25 3-Qr) Mid-Loaded 3-Way Catalyst														
Mode	K/P (0/1)	W/a	W/a	W/a	W/a	W/a	W/a	W/a	W/a	W/a	W/a	W/a	W/a	W/a
Mode	W/a	W/a	W/a	W/a	W/a	W/a	W/a	W/a	W/a	W/a	W/a	W/a	W/a	W/a
A25	8.15	115.1	65	11.6	0.954	21.8	180	180	336	336	365	-1	670.671	-1
A75	8.15	128.7	30	9.7	0.960	16.8	180	180	336	336	365	-1	615	-1
A100	8.15	149.0	30	3.8	0.960	17.0	180	180	336	336	365	600	600	600
B26	11.53	176.1	32	4.9	0.983	13.5	180	180	336	336	365	365	590	590
B75	11.53	105.0	60	16	0.972	27.0	180	180	336	336	365	-1	630	-1
C25	14.91	128.7	65	12.2	0.967	21.0	180	180	336	336	365	365	595	595
C50	14.91	169.3	65	9.2	0.978	16.3	180	180	336	336	365	365	590	590
C75	14.91	216.7	70	9.6	0.975	15.3	180	180	336	336	365	365	570	570
C100	14.91	270	27	9	0.983	21.8	180	180	336	336	365	365	635	635
B26	11.53	132.1	30	8.1	0.965	20.5	180	180	336	336	365	365	615	615
B75	11.53	155.8	55	9.8	0.985	25.8	180	180	336	336	365	365	600	600
C25	14.91	203.2	70	11.9	0.980	21.4	180	180	336	336	365	365	595	595

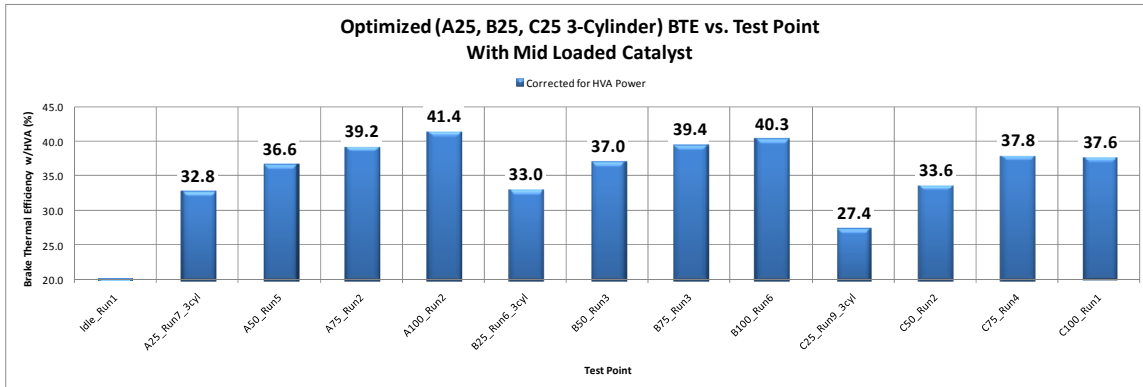
  

298 kW Cummins ISX, Omnitek Natural Gas System, Sturman HVA, Pump Cart, Optimized (Idle, A25, B26, C25 3-Qr) Mid-Loaded 3-Way Catalyst														
Mode	K/P (0/1)	W/a	W/a	W/a	W/a	W/a	W/a	W/a	W/a	W/a	W/a	W/a	W/a	W/a
Mode	W/a	W/a	W/a	W/a	W/a	W/a	W/a	W/a	W/a	W/a	W/a	W/a	W/a	W/a
A25	8.15	115.1	55	6.1	0.961	12.0	180	180	336	336	365	-1	610	-1
A75	8.15	128.7	30	3.8	0.960	16.8	180	180	336	336	365	-1	615	-1
A100	8.15	149.0	30	3.8	0.960	17.0	180	180	336	336	365	600	600	600
B26	11.53	176.1	32	4.9	0.983	13.5	180	180	336	336	365	365	590	590
B75	11.53	118.5	50	15.1	0.963	25.8	180	180	336	336	365	365	575	575
C25	14.91	128.7	65	12.2	0.967	21.0	180	180	336	336	365	365	595	595
C50	14.91	169.3	65	9.2	0.978	16.3	180	180	336	336	365	365	590	590
C75	14.91	216.7	70	9.6	0.975	15.3	180	180	336	336	365	365	570	570
C100	14.91	270	27	9	0.983	21.8	180	180	336	336	365	365	635	635
B26	11.53	132.1	30	8.1	0.965	20.5	180	180	336	336	365	365	615	615
B75	11.53	155.8	55	9.8	0.985	25.8	180	180	336	336	365	365	600	600
C25	14.91	203.2	70	11.9	0.980	21.4	180	180	336	336	365	365	595	595

Source: Sturman Industries

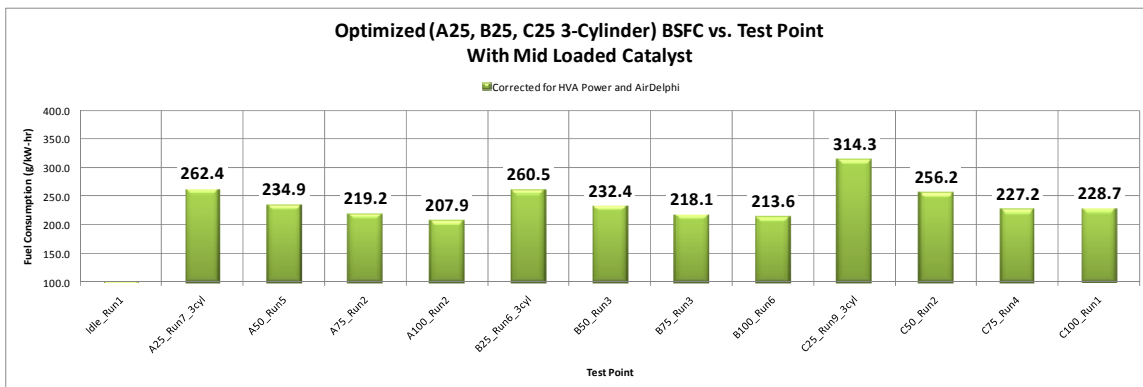
# Appendix E: Optimization Sweep Results

Figure 140: Optimized (A25, B25, C25 3-Cylinder) BTE vs. Test Point



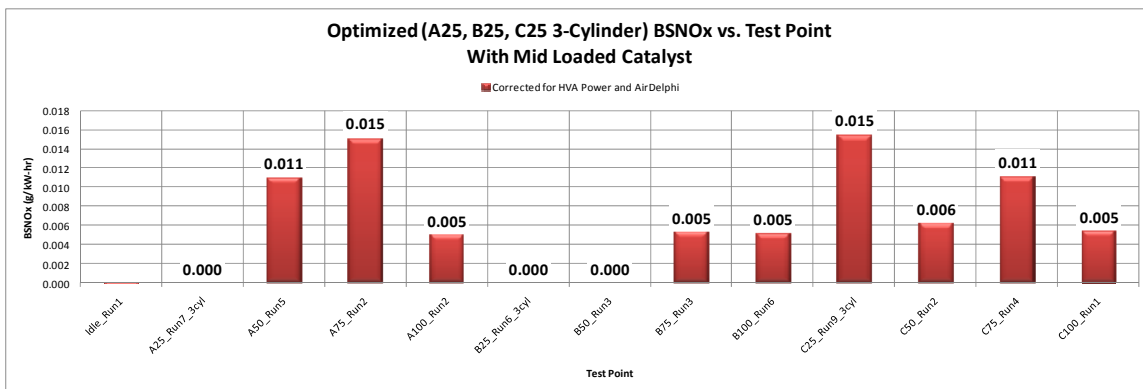
Source: Sturman Industries

Figure 141: Optimized (A25, B25, C25 3-Cylinder) BSFC vs. Test Point



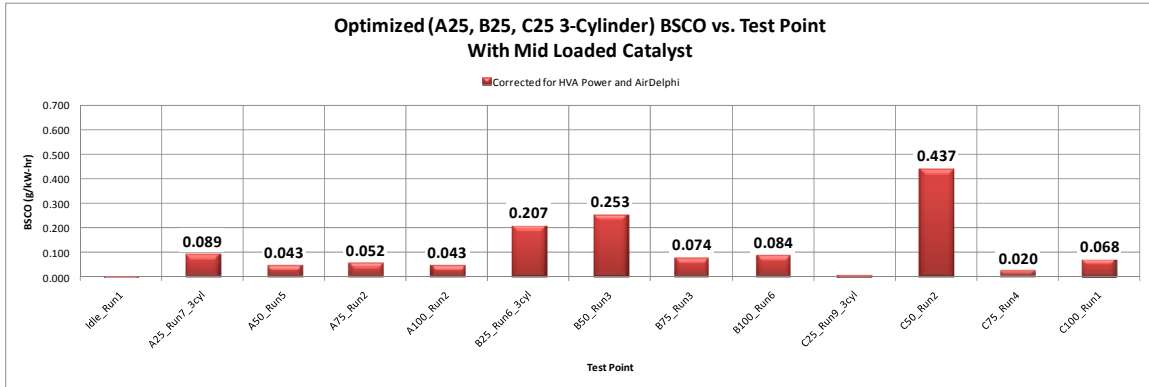
Source: Sturman Industries

Figure 142: Optimized (A25, B25, C25 3-Cylinder) BSNOx vs. Test Point



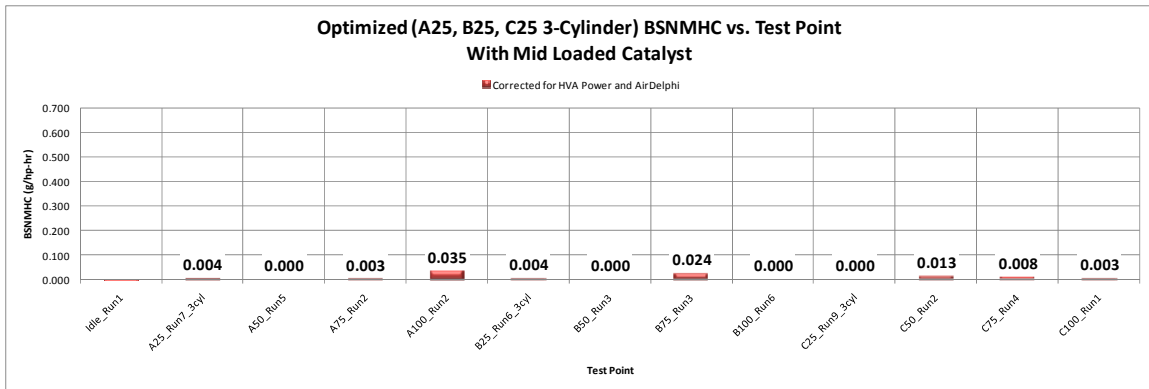
Source: Sturman Industries

**Figure 143: Optimized (A25, B25, C25 3-Cylinder) BSCO vs. Test Point**



Source: Sturman Industries

**Figure 144: Optimized (A25, B25, C25 3-Cylinder) BSNMHC vs. Test Point**



Source: Sturman Industries